AD-A091 025 NOTRE DAME UNIV IN DEPT OF ELECTRICAL ENGINEERING F/G 11/4
MODELING AND MODIFICATION OF THE ELECTROMAGNETIC PROPERTIES OF --ETC(U)
1980 W J GAJDA, P K AJMERA, W C STRIEDER AFOSR-77-3453

UNCLASSIFIED AFOSR-TR-80-1071 NL

1 . 2

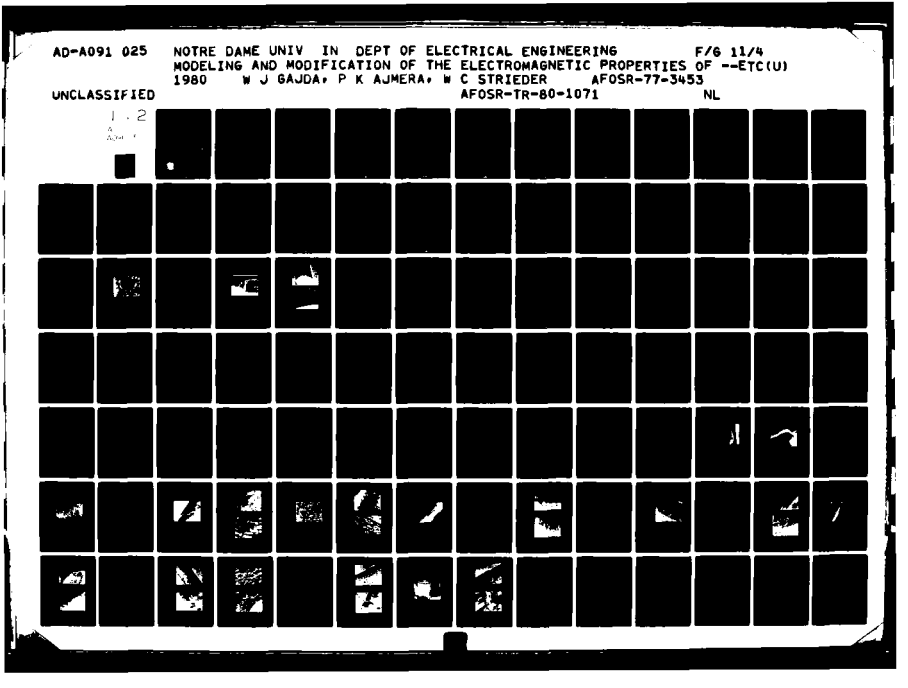

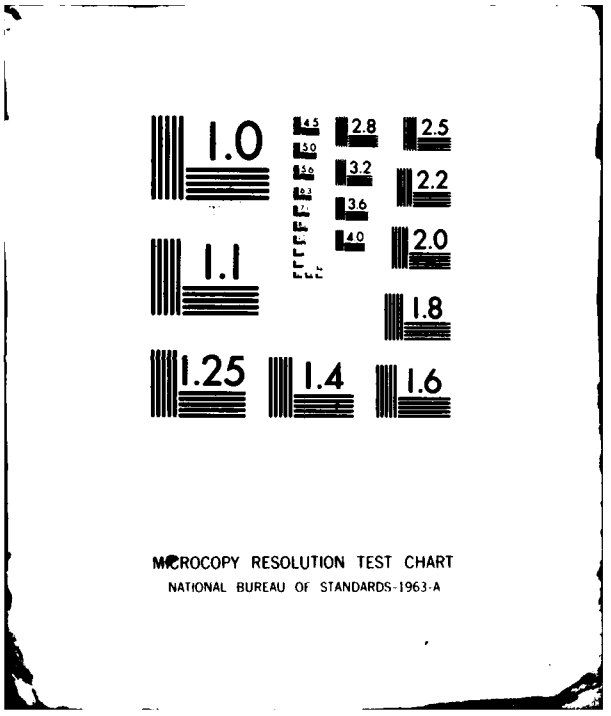
1.0
1.1
1.25
1.4
1.6
1.8
2.0
2.2
2.5
2.8
3.2
3.6
4.0
4.5
5.0
5.6
6.3
7.1
8.0
9.0
MICROCOPY RESOLUTION TEST CHART
NATIONAL BUREAU OF STANDARDS-1963-A

AFOSR-TR- 80 - 1071

LEVEL II

12

4w

AD A091025

DDC FILE COPY

DTIC
ELECTE
OCT 30 1980
S D
E

Department of

ELECTRICAL ENGINEERING

UNIVERSITY OF NOTRE DAME, NOTRE DAME, INDIANA

...release;
distribution unlimited.

80 10 21 053

LEVEL II (12)

MODELING AND MODIFICATION OF THE ELECTROMAGNETIC PROPERTIES OF ADVANCED COMPOSITE MATERIALS

Final Report - AFOSR 77-3453

Project Director - W. J. Gajda, Jr.

(6)

MODELING AND MODIFICATION OF THE ELECTROMAGNETIC PROPERTIES OF ADVANCED COMPOSITE MATERIALS.

(10) W. J./Gajda, Jr.
P. K./Ajmera

Department of ~~Electrical Engineering~~

W. C./Strieder Richard/Knorr C./Araujo

Department of Chemical Engineering

(11) 1984 (12) 153

(11)

AFOSR/TR-84-1471

University of Notre Dame
Notre Dame, IN 46556

Final Report
prepared for
Air Force Office of Scientific Research
Grant No.
(15) AFOSR-77-3453

TABLE OF CONTENTS

LIST OF ILLUSTRATIONS

ACKNOWLEDGEMENTS

In addition to the co-principal investigators named on the cover sheet of this report, the following individuals associated with the Department of Electrical Engineering of the University of Notre Dame contributed to this report: Professor Richard Kwor, C. Araujo, T. Joy and L. Scruggs.

Further, the assistance of T. Schoenberg (AVCO), S. Cross (Hercules) and D. Black (Narmco) is gratefully acknowledged.

ABSTRACT

The electromagnetic hazards involved in using composite materials in aircraft are considered. Attention is focused on the problems associated with the lower conductivities of composites in comparison to those of metals. The concept of a high conductivity composite is advanced as a solution to the electromagnetic problems associated with presently available composites.

The electrical properties of available advanced composite materials, primarily graphite/epoxy and boron/epoxy, are presented. Basic deterministic models relating the electrical conductivities (D.C. to 50 MHz) of composites to the fiber conductivity, the matrix conductivity and the volume fraction of the fibers are developed. The electrical behavior of as-manufactured graphite and boron fibers is also detailed.

The possibility of 'doping' fibers with suitable impurities to increase conductivity without an associated decrease in specific strength is explored. Boron fibers undergo a recrystallization when heated above 800°C and have, as a consequence, significantly reduced strengths. Since thermal diffusion of impurities requires temperatures above 800°C, significant effort was devoted to inhibiting this recrystallization. Diffusion of nickel impurities inhibited this process and resulted in increased conductivities.

To add impurities to boron while avoiding recrystallization, it is necessary to add the impurity species while boron fiber growth is underway. A boron growth apparatus which produces fibers similar (under optical microscopy) to commercial fibers was used to introduce impurities into the chemical vapor deposition growth process in an attempt to increase the conductivity of boron fibers. Parallel efforts involving graphite fibers were also carried out. Results of these experiments are detailed.

Models of charge flow in composites are developed based upon effective medium theory. Extensions to finite thickness samples are presented. Comparison between theory and experiment is shown to be excellent. The existence of a 'thickness effect' was predicted theoretically and confirmed by experiment.

1. MODELING AND MODIFICATION OF THE ELECTROMAGNETIC PROPERTIES OF ADVANCED COMPOSITE MATERIALS

1.1 Introduction

As the use of fiber reinforced composite materials has increased in aircraft, the assessment of the associated electromagnetic hazards has drawn increasing attention. Immediate questions arise concerning the effects of lightning upon composite structures, the shielding effectiveness of these materials against electromagnetic interference (EMI) and electromagnetic pulse effects (EMP), radar cross-section and power supply grounding. In addition, the build-up of precipitation static on an aircraft is an area of concern. At the present time, there is information available concerning the electrical properties of the more widely used composites (graphite/epoxy, boron/epoxy and Kevlar/epoxy) and available experimental results indicate that the issues raised above may involve some operational problems.

For example, an all composite aircraft would not be able to withstand a direct lightning strike. Laboratory experiments have shown that charge relaxation through the composite material is not sufficiently rapid and the resultant local heating and stress cause delamination[1-1]. Other research has shown that the shielding effectiveness of graphite/epoxy and boron/epoxy is lower than that of the metals which are presently used in aircraft[1-2]. The decrease in shielding is significant at low frequencies. Published data indicates that graphite/epoxy shields more effectively than does boron/epoxy although questions have been raised concerning the validity of the shielding experiments involving boron/epoxy[1-3].

The introduction of these materials causes significant problems for

individuals concerned with the electromagnetic compatibility and survivability of defense systems[1-4]. A great amount of effort has been expended to predict electromagnetic scattering and penetration for all metallic structures (with and without openings) but the applicability of this research to composite structures is not clear at the present time. If fundamental physical changes in the composites can be made so that their electrical properties more closely approach those of metals, all scattering and penetration algorithms can be applied directly to composite systems. This is the ultimate goal of the research described in this report.

The first goal is the development of suitable low-level (in the sense of weight per-cent) doping techniques to allow significant increases in the conductivity of graphite and boron fibers used in the fabrication of advanced composites. The second goal is to develop suitable models based on the statistical theory of random media to allow the prediction of the overall electrical conductivity of fiber reinforced materials based only upon a knowledge of conductivities of the fibers and the matrix materials as well as the statistical arrangement of the fibers in the matrix. As will be discussed later in section 4, graphite/epoxy conductivities could only be modeled by including the mechanism of electrical conduction between fibers in contact. The third goal, which supports the first two, is to develop a suitable laboratory facility to allow the production of reinforcing fibers of graphite and boron under carefully controlled conditions in which electronic grade gases are used to introduce impurities into the fibers. The purpose of this work was to examine the most useful ways in which doping techniques could be carried out on a production-line basis. The successful completion of this third task will insure the rapid dissemination of this new technology throughout the production facilities presently manufacturing advanced composites. In

addition, this in-house processing capability will allow the background impurity contents of the fibers to be carefully controlled so that the effects of intentionally added impurities are not masked by impurities present as a result of earlier processing. This cannot be achieved by using samples provided by manufacturers because, although the manufacturers have been most cooperative in providing such samples, they are not willing, for understandable reasons, to release proprietary information concerning the precise conditions under which the fibers are manufactured. For example, detailed information concerning growth rates, temperatures and ambient gases is not available. Some information is available through government supported research reports but this data does not necessarily correspond to the conditions presently being used by various manufacturers in their production facilities. For these reasons, it was felt that an independent processing facility aimed at the production of graphite and boron fibers under highly controlled conditions was of value.

The modeling and modification of the electrical conductivity of graphite/epoxy and boron/epoxy is the focus of this research. No detailed investigations of the permeability or permittivity of these materials was carried out because earlier work in this laboratory[1-5] has shown that the relative permeability of these materials is essentially unity and there are no readily apparent ways to increase this value without accompanying increases in mass density and associated decreases in specific strength (i.e., strength/mass ratio). The permittivity of boron/epoxy is primarily related to the permittivity of the epoxy resin and the details of its cure during the fabrication of the composite part. Although it is conceivable that the permitivity could be increased and thus yield improvements in shielding, such efforts are beyond the scope of the proposed research. The permittivity

of graphite/epoxy is indeterminant because these materials do not show any capacitive effects even at frequencies as high as 50 MHz. Since this work is aimed at low frequency improvements in the properties of advanced composites, there was no point in investigating permittivity modification in graphite/epoxy.

Successful experiments were performed in which the conductivities of manufactured graphite and boron fibers were increased by adding small amounts (parts per million to parts per billion) of impurity atoms via high temperatures diffusion. The initial boron experiments produced positive results but, when samples were acquired from the Avco Corporation (the only company presently manufacturing boron/epoxy composites), we encountered a surface defect situation which prevented successful reheating of these samples to the temperatures required to allow impurity diffusion. A detailed investigation of this behavior of boron fibers was carried out and is described in the body of the report. Nickel diffusion was found to inhibit the surface defect nucleation and increase conductivity of the boron fibers.

Successful models to predict the conductivity of advanced composite materials based upon the conductivities of the fibers and matrix, the degree of fiber-to-fiber contact and the volume fraction of fibers were formulated by suitable extensions of effective medium theory.

Furnaces for the growth of boron and graphite fibers were designed and fabricated. Boron and graphite fiber growth experiments were conducted and several in-situ doping processes were investigated.

1.2 Review of Previous Work

This section reviews earlier work conducted under the sponsorship of the Rome Air Development Center at the University of Notre Dame and the results are essential to an understanding of the research results presented in this report.

The materials of interest are inhomogeneous, consisting of arrays of fibers (each fiber, in general, electrically anisotropic) dispersed in an insulating (electrically isotropic for all materials presently under investigation) matrix. The theoretical situation is worsened by the lack of spatial periodicity which precludes the use of translational invariance symmetry as commonly applied in the theory of crystalline solids. In order to develop some starting concepts about the nature of electrical current in composites, it is necessary to use statistical theories of inhomogenous materials which were developed primarily to examine problems of heat flow in disordered media (for example, the thermal insulation problem). The basic method is to determine upper and lower bounds of the transport coefficients (thermal conductivity, electrical conductivity, ...) in terms of the properties of the two phases and the volume fractions of each phase. Although such models have been primarily for solids consisting of spheres dispersed in a matrix, extensions[1-6] have been published for dispersions of fibers. The published theoretical analysis does not assume any touching between the fibers but rather assert that each fiber is surrounded by matrix material.

We begin by examining the applicability of these bounds to the case of graphite fibers in an insulating matrix. It is most convenient to examine the ratio of the upper bound (σ_U) of the electrical conductivity to the lower bound (σ_L).

The general expression takes the form[1-6]

$$\sigma_U/\sigma_L = \alpha^{-1}[1 + \alpha f - A]/[f + \alpha(1-f) + B] \qquad (1\text{-}1)$$

with

$$A = .5\alpha f(1-f)/[f + 2G_1(1-f)^2 - 2G_2 f^2]$$

$$B = .25\alpha f(1-f)/[f^2 G_2 - (1-f)^2 G_1]$$

where α is the ratio of fiber to matrix conductivities, f the volume fraction of the fibers and G_1, G_2 are empirical shape factors.

In writing equation (1-1), available experimental evidence[1-5] indicating that fiber conductivities are several orders of magnitude greater than matrix conductivities was invoked. As long as neither f nor $1-f$ closely approaches zero (a condition which is satisfied in both typical graphite/epoxy and boron/epoxy samples), the bounds ratio (σ_U/σ_L) simplifies further and numerical values for the shape factors may also be substituted[1-7].

$$G_1 = G_2 = 0.25$$

For a sample of graphite/epoxy representative of the materials used in aircraft, the following approximate numerical values apply.

$$f = 0.7,\ \sigma_1 = 10^4 \text{ mhos/meter},\ \sigma_2 = 10^{-8} \text{ mhos/meter}$$

The bounds may be evaluated directly as

$$\sigma_U/\sigma_L = 4.41(10^{10})$$

This value is significantly greater than the experimentally measured values[1-5] which yield a ratio

$$\sigma_U/\sigma_L = 200$$

It follows that these bounds are not sufficiently tight to realistically predict the electrical properties of graphite/epoxy composites. Although the bounds are valid, they are more than ten orders of magnitude apart and are of little value in predicting the conductivities to be expected in a given composite system. These results imply that the basic divergence between theory and experiment is caused by the theoretical neglect of fiber-to-fiber contact. This contact is a dominant feature in configurations in which current is directed orthogonal to the fiber axis (in single ply samples) and cannot be ignored if useful bounds are to be derived theoretically.

A second approach to the analysis of the electrical properties of composites rests upon deterministic models in which attempts are made to solve for the precise distributions of currents in a sample excited by an externally applied voltage and, in this way, determine an effective conductivity for the material. Such models become intractable when large numbers of fibers must be considered but insight can be obtained into the elctrical behavior of composites by examining a few simple cases.

We begin our development of such models of electrical conductivity in advanced composites by considering the unidirectional, single-ply system. If care is taken to abrade any epoxy-rich regions from the upper and lower surfaces of such a sample, experiments indicate that the conductivity may be characterized by two quantities: σ_L, the value associated with current along the fiber axis and σ_T, the value associated with current orthogonal to the fiber axis (either from top to bottom or in the sample plane at right angles to the fibers).

The symbol f denotes the volume fraction of fibers in the unidirectional sample while σ_1, σ_2 denote the fiber, epoxy conductivities respectively. For current in the longitudinal direction (along the fibers), the total sample conductance is simply the summation of the conductances of the individual fibers

plus the conductance of the epoxy. Figure 1-1 shows the sample geometry. This may be written as

$$G = \frac{\sigma_1 fA}{L} + \frac{\sigma_2(1-f)A}{L} \qquad (1\text{-}2)$$

from which it follows that the longitudinal conductivity may be written as

$$\sigma_L = \sigma_1 f + \sigma_2(1-f) \qquad (1\text{-}3)$$

Although minor deviations from this result are observed in some unidirectional samples as a result of breaks in fibers and skewing of fibers from the longitudinal axis, it is in acceptable agreement with experimental results. For unidirectional samples with a fiber volume fraction of 0.6, the above equation predicts the longitudinal conductivity to be

$$\sigma_L = 2(10^4)(0.6) + \sigma_2(0.4) \qquad (1\text{-}4)$$
$$= 1.2(10^4) \text{ mhos/m.}$$

The second term is, of course, negligible when the matrix is epoxy. This value agrees with low frequency measurements[1-5] (DC to 50 MHz), which have been in the range of $1\text{-}2(10^4)$ mhos/m for unidirectional samples.

The calculation of the transverse conductivity σ_T is more difficult. In order to develop insight into this problem, consider a simple composite composed of two fibers with rectangular cross-sections, which touch each other via a rectangular "neck".

Consider a slab (Δx thick, depth W and length L) of this sample as sketched in Figure 1-2. The conductance of this segment can be calculated directly as

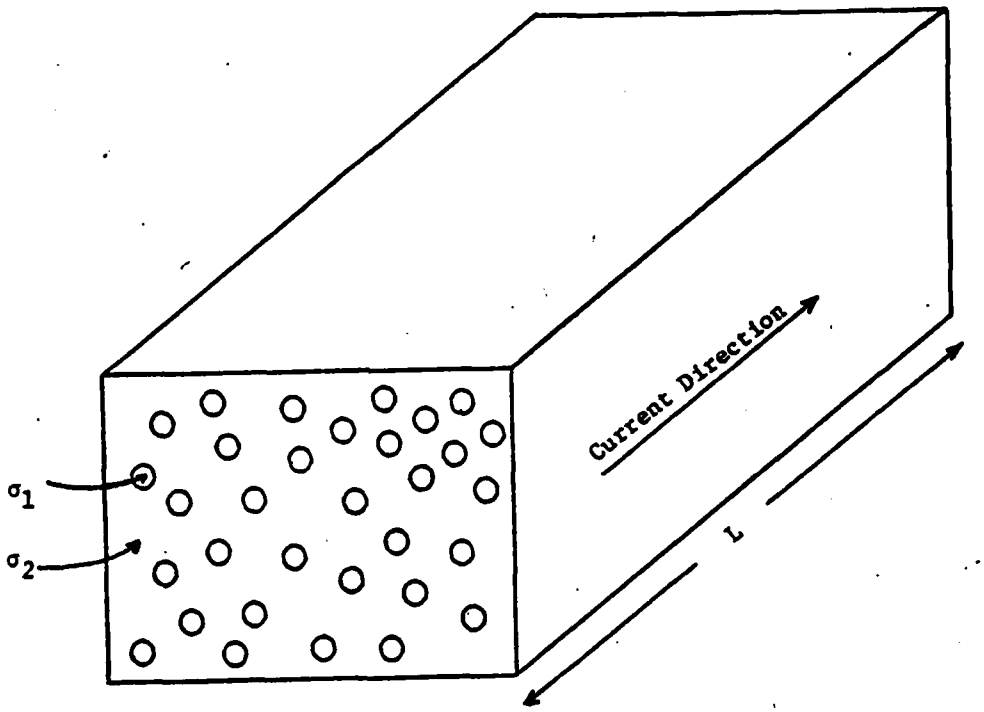

LONGITUDINAL CONDUCTIVITY MODEL

FIGURE 1-1

$$\Delta G = \sigma_1 W \Delta x / L \quad \text{for} \quad -\frac{t}{2} + \beta < x < \frac{t}{2} - \beta$$

$$\Delta G = \sigma_1 \sigma_2 W \Delta x / (\sigma_1 \alpha + \sigma_2 (L - \alpha)) \text{ for other values of } x.$$

The quantities α, β are used to define the 'neck' connecting the two fibers and are defined in Figure 1-2.

The total conductance may be found directly.

$$G = \int_{-t/2}^{t/2} dG = \frac{\sigma_1 W t}{L} + \left[\frac{\sigma_1 \sigma_2 W}{\sigma_1 \alpha + \sigma_2 (L - \alpha)} - \frac{\sigma_1 W}{L} \right] (2\beta)$$

This result may be expressed in terms of a transverse conductivity, σ_T, defined as

$$G = \sigma_T t W / L,$$

which implies that

$$\sigma_T = \sigma_1 (1 - 2\beta/t) + \frac{\sigma_1 \sigma_2 (2\beta/t)}{\sigma_1 (\alpha/L) + \sigma_2 (1 - \alpha/L)}$$

The general expression for σ_T is of interest because of the information it contains about the situation in which the fibers do not touch. This is described by the geometric condition $\beta = t/2$ and the equation for transverse conductivity reduces to

$$\sigma_T = \sigma_2 (L/\alpha)$$

The existence of touching fibers in graphite/epoxy materials is demonstrated by experimental results. The transverse conductivity for graphite/epoxy has been measured[1-5] to have a value of 200 mhos/m., while the quantity W is approximately $2(10^{-5})$m. The conductivity of the epoxy matrix is 10^{-8} mhos/m.

and substitution of these values yields

$$\alpha = 1(10^{-19})\text{m}.$$

Such a small separation is equivalent to contact between fibers and it may be concluded that, in a transverse sample of graphite/epoxy, fiber-to-fiber contact is essential to describe the conduction of charge in directions orthogonal to the fiber axis.

It is important to note that such fiber contact does not occur in boron/epoxy and, in these materials, the flow of charge across fibers is limited by the conductivity of the epoxy matrix. In unidirectional samples of boron/epoxy[1-3], $\sigma_L = 30$ mhos/m and $\sigma_T = 2(10^{-8})$ mhos/m.

All of these results pertain to cases in which current is moving between opposite faces of rectangular slabs of the material. Physical situations of interest often display, of course, more complex geometries. In the case of lightning attachments or precipitation static, the charge is injected into a series of points along the surface and then distributes itself (via a relaxation process) through the three-dimensional aircraft fuselage. Although detailed modeling of such processes is difficult, the above description will hold qualitatively. There will be significant differences as a result of the geometric complexity but the basic conclusion that fiber contact dominates the observed graphite/epoxy conductivity will hold.

The models developed above indicate that composite conductivities could be increased in one of two ways: either increase the conductivity of the fibers or increase the fiber contact. The second path is ruled out by mechanical requirements. The resistance of composites to microbuckling decreases as fiber contact increases. Attempts to increase conductivities by

increasing such contact would lead to an unacceptable degradation in mechanical behavior.

The only viable approach is to develop techniques for increasing the conductivities without an accompanying decrease in specific strengths. This implies that the basic mechanical strengths of the fibers must be unchanged and, at the same time, their densities should not increase. These requirements, in conjunction with processing difficulties, make coating the fibers with metallic sheaths an unattractive approach.

To gain insight into possible methods for increasing fiber conductivity the transport equations for the conductivity σ of a solid provide a starting point.

$$\sigma = q(\mu_e n + \mu_h p)$$

where

$$q = 1.6(10^{-19}) \text{ coulombs},$$

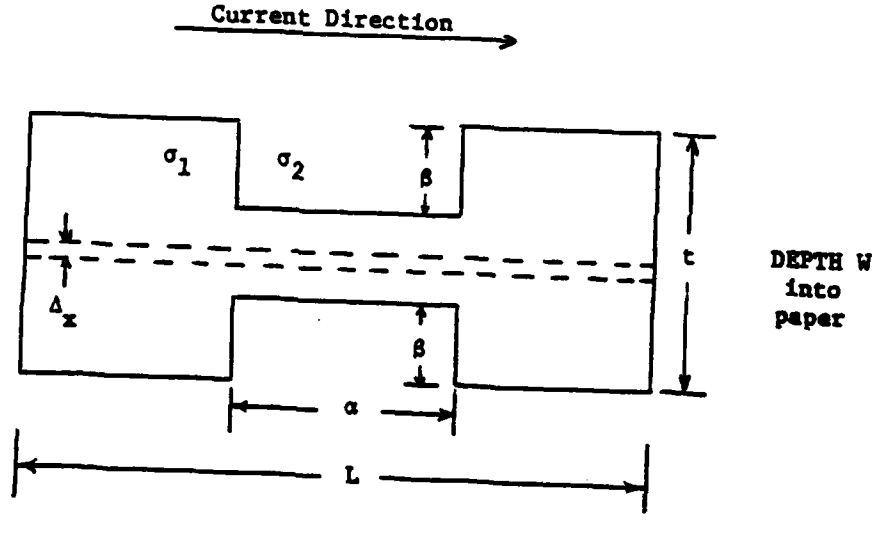

TRANSVERSE CONDUCTIVITY MODEL

FIGURE 1-2

μ_e, μ_h are the electron, hole mobilities and

n, p are the densities of "free" electrons, holes per unit volume.

In the case of a metal, the hole concentration is, of course, zero.

The electron and hole mobilities essentially measure the ease with which charged particles move through the material under the influence of an external electric field. The mobilities depend primarily upon the atomic species of which the solid is composed as well as the crystalline perfection. In general, a higher degree of crystalline order implies a larger value of mobility. While mobility increases could result from changes in the structure of the fibers, decreases in specific strengths are quite likely. Experimental efforts along these lines are not anticipated.

Increases in electron and hole densities can result in large increases in conductivities and orders of magnitude increases result from relatively small additions of the proper impurity atoms. In a typical semiconductor, an addition of 0.1 parts per million of a donor impurity increases the conductivity by over five orders of magnitude[1-8].

Although future confirming experiments will be necessary, it seems likely that such a small impurity addition to the fibers will not have a major effect upon either the mechanical strength or the mass density. This process of adding small amounts of electrically active impurity atoms (either donors or acceptors) to semiconductors is known as "doping". It is widely used in fabricating solid state devices in silicon, germanium and compound semiconductors.

The next germane question is "Are graphite and boron fibers semiconductors?". Available evidence indicates that both materials are semiconductors in their normal composite forms. Semiconductor behavior has been observed

in polycrystalline specimens of both graphite[1-9] and boron[1-10].

One caveat is essential at this point. As impurity atoms are introduced into a host solid, their degree of electrical activity depends upon the crystalline perfection of the host medium. Given the high degree of atomic disorder present in the fibers used in advanced composite materials, it is highly probable that the doping process will not be as efficient as it is in, for example, single crystal silicon. This inefficiency will lead to limits upon the amounts of conductivity enhancement attainable in both graphite and boron fibers.

The most natural method of adding impurities to fibers utilizes the thermal diffusion of impurity atoms under the influence of a concentration gradient[1-11]. This is the method used in the research described in this report. This process is well characterized theoretically and has been widely used. For these reasons, high temperature diffusion has been chosen as the method to add selected impurities to graphite and boron fibers.

In the next sections, the physical and electrical properties of as-grown fibers are examined. In addition, techniques used to make repeatable, electrical contacts to both graphite and boron fibers are discussed in detail.

1.3 Properties of As-Grown Fibers

1.3.1 Graphite

Preliminary investigation revealed that fibers produced by various companies had different conductivities. To simplify the following discussions, the work reported involved only one fiber type--Thornel T300 as used in Narmco 5208 pre-preg tapes.

Individual graphite fibers have radii on the order of a few micrometers and are difficult to handle. In general, it was convenient to immerse a segment of graphite tow in methanol and use teflon coated tweezers to separate

individual fibers from the bundle. The fibers, in lengths from two to four centimeters, were mounted on pre-cleaned glass microscope slides. This was accomplished by applying electrically conductive silver paint to the ends of the fibers. When dry, this paint holds the fiber to the glass slide and provides an ohmic electrical contact.

The fibers measured had an average DC conductivity of 20,000 mhos/m with a range of 14,000 to 30,000 mhos/m. All of the fibers displayed linear electrical responses up to maximum electric fields of approximately 4000 volts/m. Thirty percent of the samples broke at electric fields below this value.

1.3.2 Boron Fibers

Boron fibers were supplied by Avco in different diameters: 4, 5.6 and 8 mils (0.01, 0.14 and 0.02 cm). These fibers are produced by chemically depositing boron on a heated tungsten wire of 0.0018 cm. diameter in an atmosphere of $H_2 + BCl_3$. A reduction reaction occurs.

$$3H_2 + 2BCl_3 \rightarrow 2B + 6HCl$$

The boron is deposited on the heated tungsten wire and complete reaction of the tungsten occurs. The remaining core consists of a mixture of WB_4 and W_2B_5. The core diameter is unchanged and is essentially coated with pure boron[1-12].

Electroplated nickel was used to make ohmic electrical contact to the boron fibers. These contacts proved quite satisfactory from both mechanical and electrical viewpoints. Although formal tests of the mechanical adhesion of the electroplated nickel to the boron were not conducted, no separation

during routine laboratory handling of the fibers was observed. In addition, the current-voltage characteristics of the boron fibers, with and without electrical isolation of the tungsten boride core, have been linear.

The geometry used in the current-voltage measurements is shown in Figure 1-3. In order to relate the measured conductance to the boron conductivity, the conductive core was isolated from the nickel plating using a suitable wax. To model current flow in the fibers, it is assumed initially that the core conductance is large compared to that associated with the boron and voltage drops along the boride core are neglected. Further, the contacts are circularly symmetric and this implies a circularly symmetric electrostatic potential[1-13].

The following results were obtained for boron sheath and core conductivities.

$$\sigma_{BORON} = 0.25 \text{ mhos/m}$$

$$\sigma_{CORE} = 3(10^5) \text{ mhos/m}$$

An overall effective conductivity for the fiber may also be determined.

$$\sigma_{eff} = 2.3(10^3) \text{ mhos/m.}$$

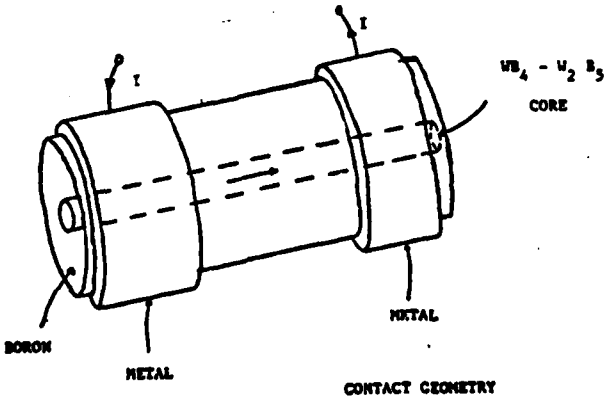

CONTACT GEOMETRY

FIGURE 1-3

CHAPTER ONE REFERENCES

1-1 F.A. Fisher and W.M. Fassell, "Lightning Effects Relating to Aircraft," Technical Report AFAL-TR-72-5, (1972).

1-2 C.D Skouby, "Electromagnetic Effects of Advanced Composites," Final Report N00014-74-C-0200 (1975).

1-3 J.L. Allen, W.J. Gajda, Jr. et al. "Electromagnetic Properties and Effects of Advanced Composite Materials," Final Report RADC-TR-78-156 (1978).

1-4 J.L. Allen, W.J. Gajda, Jr., et al. "A Technology Plan for Electromagnetic Characteristics of Advanced Composites," Final Report RADC-TR-76-206 (1976).

1-5 W.J. Gajda, Jr., et al. "Electromagnetic Properties of Graphite/Epoxy Composites over the Frequency Range of DC to 30 MHz," to be published in the Journal of Composite Materials.

1-6 M. Beran and N. Silnutzer, "Effective Electrical, Thermal and Magnetic Properties of Fiber Reinforced Materials," J. Composite Materials, 5, p. 246-249 (1971).

1-7 M. Beran, "Use of Variational Methods to Determine Bounds for the Effective Permittivity in Random Media," Nuovo Cimento, 38, p. 771 (1965).

1-8 R.B. Adler, et al. "Introduction to Semiconductor Physics," J. Wiley and Sons, New York p. 17 et seq. (1974).

1-9 A. Marchand, "Chemistry and Physics of Carbon," 7, Marcel Dekker, New York (1971).

1-10 W. Neff and K. Seiler, "Boron" 2, Plenum Press, New York (1965).

1-11 W.J. Gajda, Jr., "On Solutions to the Diffusion Equation," Solid State Electronics, 13 p. 1427 (1970).

1-12 T. Schoenberg, (Private Communication), Avco Corporation, Lowell, MA (1977).

1-13 W.J. Gajda, Jr., "A Fundamental Study of the Electromagnetic Properties of Advanced Composite Materials," Final Report, RADC-TR-78-158 (1978).

CHAPTER II

INTRINSIC PROPERTIES OF BORON FIBERS

2.1 Major Characteristics of Boron Fibers

Boron fibers have generally been produced by the method of Chemical Vapor Deposition (CVD). The nature of the CVD process requires a heated substrate such as Ta, W, Mo or SiO_2 in an evacuated chamber where hydrogen reduction of a reactant gas such as BCl_3, BBr_3 or BI_3 is accomplished. The deposition of boron in this method follows the general equation

$$2BX_3 + 3H_2 \quad 2B + 6HX \qquad (1)$$

where X is Cl, Br or I [1].

Commercially available boron fibers are generally produced by depositing boron from a Boron Trichloride source on a heated tungsten wire of 0.018 cm diameter, in the manner described by equation 1 [1,2]. Complete reaction of the tungsten with boron occurs and a highly conductive region of tungsten-rich material, a mixture of W_2B_5 and WB_4, forms the inner core [1]. Figure 2.1 shows this core region to be roughly 20μm in diameter.

Bulk boron from the core region up to the surface of the fiber is understood to be essentially amorphous. This is based on the interpretation of x-ray patterns that consist of four broad diffuse halos at 4.3, 2.5, 1.5 and 1.4 Å [1]. However, there is considerable controversy in the current literature about the structure of the boron in the fibers. In the next section, the amorphous character of boron in the fiber configuration is discussed in more detail.

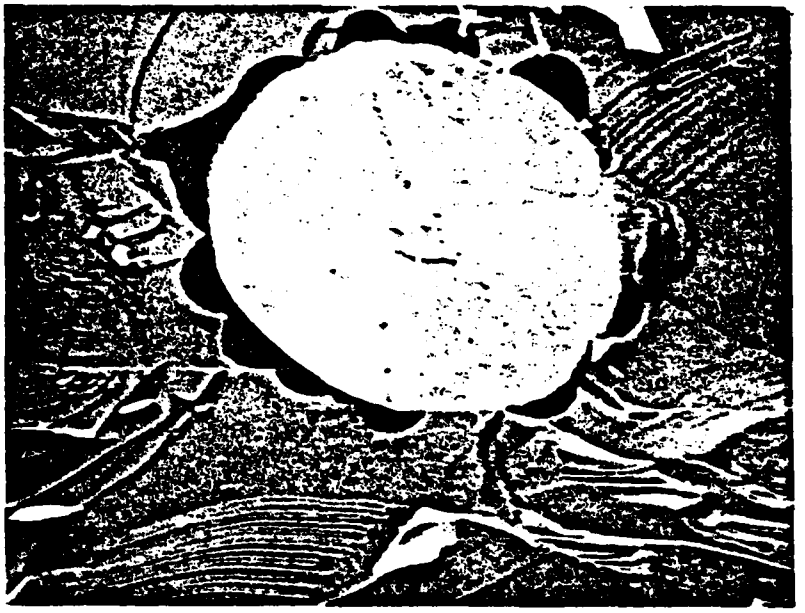

Fig. 2.1 - Tungsten rich inner core region of a typical boron fiber. (SEM micrograph, 2000X, 81° angle)

Boron grows on the top of the tungsten wire in the form of cones. These cones terminate at the surface giving rise to the "orange peel" (nodules) appearance of the fibers. These nodules are only found on the surface and although they vary in diameter they are well ordered. Figure 2.2 shows a split fiber where the orange-peel appearance of the surface of the fiber, the transverse side of cones and the absence of nodules inside the bulk region can be easily identified. The inclination of the cones may be due to the tungsten wire being constantly pulled out of the reaction chamber where the residence time for boron growth is only a few minutes. As the boron fiber leaves the reaction chamber, it cools rapidly due to its small thermal mass. This, together with the constant pulling, may be the cause of the circular orientation of the nodules as shown in Figures 2.3a and 2.3b. The basic outline of the major physical characteristics of the fibers is shown in Figure 2.4. These fibers are made commercially by AVCO in diameters of 4, 5.6, and 8 mils (102, 142 and 203μm).

2.2 The Crystalline Structure of CVD Boron

The wealth of literature on the crystalline structure of boron makes a synthesis of relevant information difficult. One such synthesis is accomplished in a paper by Hoard and Hughes [3]. Information from over 250 references covering roughly 150 polymorphs of boron is presented. This section attempts to focus on the proper classification of the crystalline structure of boron fibers. Three possibilities for the crystalline structure of CVD boron are discussed: heavily faulted polycrystalline, microcrystalline and massive amorphous.

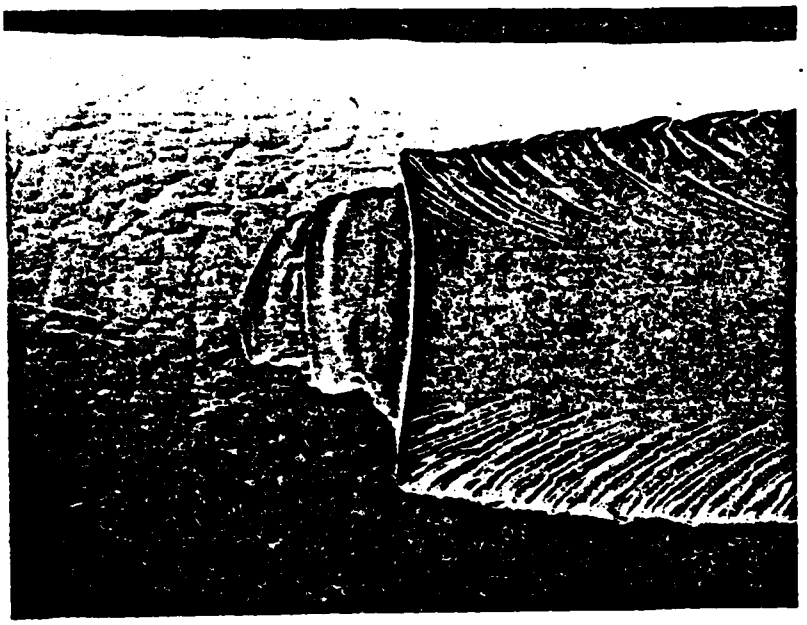

Fig. 2.2 - Micrograph of transverse side of an 8 mil diameter boron fiber showing cones and surface nodules. (500X, 0° angle)

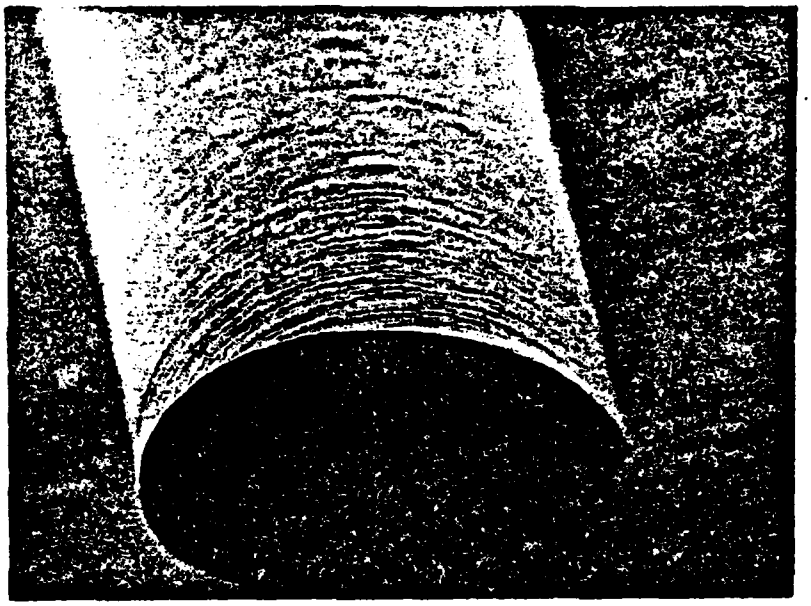

(a)

(b)

Fig. 2.3 - (a) Micrograph showing the circular orientation of surface nodules (200X, 69° angle); (b) Same as (a) at higher magnification (2000X, 69° angle).

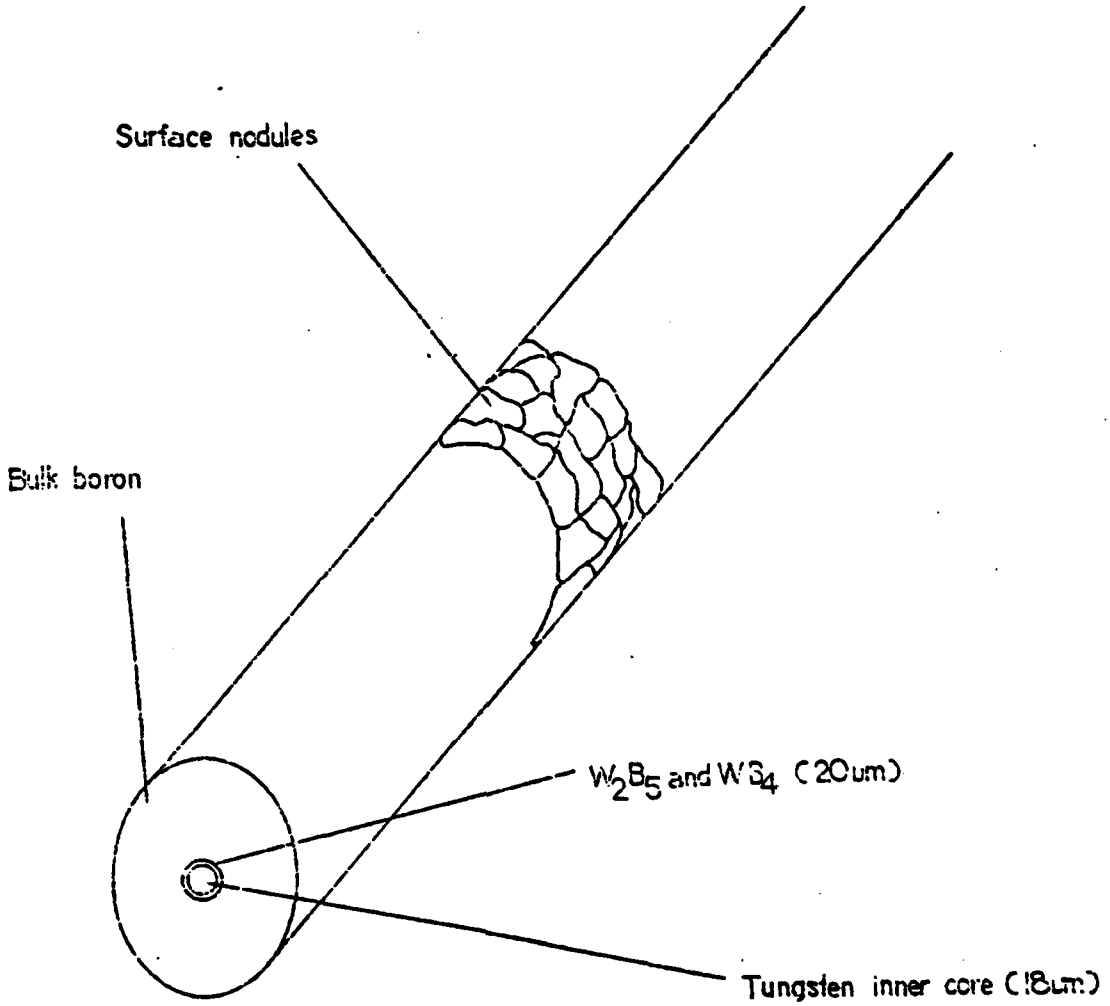

FIG. 2.4

SCHEMATIC DIAGRAM OF A BORON FIBER

The growth temperature of the CVD boron is an important parameter for initial classification. According to Hoard and Hughes [3], at preparative temperatures below about 1000°C the α-rhombohedral is the only crystalline form of boron. Below 800°C the product is amorphous, and above 1500°C only β-rhombohedral is formed.

In the temperature range of most CVD processes - between 1000°C to 1200°C - a variety of powder diffraction patterns appears throughout the literature. Wawner [1] uses the term "amorphous" and "microcrystalline" interchangeably based on the interpretation of the diffused maxima of the x-ray patterns quoted in the last section. The values of the d-spacings found in Wawner's paper are similar to those found in the paper by Otte and Lipsitt [4] were CVD grown on tungsten of 12μm diameter. The boron source is not revealed in their paper.

Otte and Lipsitt report diffuse maxima at d-spacings of 4.4, 2.5, 1.75 and 1.4Å. Spot patterns were also observed but were attributed to the tungsten borides of the inner core. Both relrod extension and diffuse rings were used as evidence of a heavily faulted structure and the material was understood to be "amorphous".

Otte and Lipsitt [4] also reported that the "amorphous" structure remained even after the sample was heat treated in vacuum up to 1000°C over extended periods. In the range between 1000°C - 1200°C, rapid transformation to the β-rhombohedral structure was also reported. The deposited "amorphous" boron was modeled as a heavily faulted f.c.c. structure. When heated, the structure "recrystallizes" to the β-rhombohedral form. This result does not agree with the thermodynamical considerations discussed by Hoard and Hughes [3].

Linquist, Hammond and Bragg [5] dispute several results reported by Otte and Lipsitt [4]. One of the conclusions of [5] is to characterize CVD boron as a collection of small crystallites of the α-rhombohedral form ranging from 10 to 10000 Å (average size 30 Å). Boron samples used in [5] were grown on a tungsten substrate as in [4], but in several different temperatures ranging from 670° to 1260°. Also, the substrate speed was varied from 2/3 to 6 ft/sec. It was found that there were no differences in the locations or intensities of the x-ray diffraction rings. Finally, [5] concludes that the presence of β-rhombohedral in boron fibers is highly doubtful because this form is only thermodynamically stable above 1500°C. Gillespie [6], however, confirms the findings of [4] on the existence of β-rhombohedral boron in the range of 1000° - 1200°C. A comparison of the data of both groups [4] and [5] is found in [7] where the disagreements are resolved.

The massive amorphous or glassy form of boron is described by Talley [8]. This material displays special mechanical properties such as extreme hardness, high tensile strength ($\sim 3 \times 10^5$ lb/in^2) and high Young's modules ($\sim 64 \times 10^6$ lb/in^2). Also, it is extremely flexible material. The CVD process was slightly changed to produce this kind of boron. Growth temperatures were maintained in the range 800 - 1200°C. By maintaining a sufficiently high deposition rate of boron; crystallization of boron could be prevented below 1200°C. X-ray diffraction yielded only two diffuse rings corresponding to d-spacings of 2.5 and 4.3 Å. The presence of the low temperature α-rhombohedral form was detected in very small quantities (1% by weight) embedded in the amorphous material. With these properties plus a lack of ductility, this material appeared to be a well formed glass. These properties of the amorphous

boron are common features of what is understood as a "fiber".

We now come to a point where it is necessary to distinguish between a "boron fiber" and CVD boron grown without specific interest in having a material with the mechanical properties of a boron fiber. The x-ray data available in the literature is of many different types of CVD boron, and that is why there is so much controversy regarding the proper classification of the crystal structure of CVD boron. Because the material is not the same for different processes of fabrication, the x-ray data is not conclusive and cannot be applied to all boron samples grown by vapor deposition. The "boron fiber" is a type of CVD boron which is probably grown in a manner similar to the "Talley-boron". In the present work, the AVCO boron fiber is assumed to be similar to the "Taley boron". Whether the AVCO fibers are truly "amorphous" is questionable because x-ray data of the AVCO fibers is not available and deviation from Mott's law (cf. Chapter III) indicates a possible polycrystalline structure. A fine line exists between what is considered amorphous and what is considered polycrystalline. One way to solve this dilemma is to accept the microcrystalline idea proposed by Linquist et al., but this conflicts with Talley's report. X-ray analysis should be done with the AVCO fibers to clarify these issues. There is only the possibility of analogy with the "Talley boron" based on the idea that the massive amorphous quality is responsible for the mechanical qualities observed by Talley and common to AVCO fibers.

CHAPTER III

ELECTRICAL CONDUCTIVITY

3.1 Nickel Ohmic Contacts

Linear electrical contact to boron fibers was accomplished by electroplating nickel on the surface of the fiber. The electroplating solution and process characterization are described in Appendix A.

Electroplated nickel adheres strongly to the surface of boron and to the tungsten inner core. All three materials have similar work potentials ($\phi_m \tilde{=} 4.5$ volts [9]). Boron and nickel form several compounds at temperatures above 1000°C and there is some evidence of low temperature (from room temperature to 500°C) nickel borides - probably Ni_2B or Ni_3B [10]. Another advantage of the plating process is that the geometry of the contact area could be controlled by changing the lengths of the cathodes in the solution. The thickness of the nickel sheath was contro-led by the plating time and plating current. Scanning electron microscope measurements of the nickel sheaths gave an average thickness of 12μm for 6 minutes of plating time at 6 ma plating current. The standards for solution temperature, acidity(pH), plating current and sample preparation described in Appendix A. (These standards were maintained throughout this work to assure proper characterization of the process and repeatable results).

It is difficult to make ohmic contact to boron fibers. Earlier work [1] using 99.999% pure molten indium yielded non-satisfactory contact from both electrical and mechanical points of view. Severe nonlinearities of the voltage-current relationship were observed along with instabilities and hysteresis.

Another important factor for repeatable and reliable measurements of conductivity, especially in the electroplating technique, is a clean boron surface. When the surface of the fiber was covered with foreign particles, measurements were not reproducible and the nickel sheath did not adhere strongly to the fiber. Surface preparation is described in Appendix A and a more detailed study of the chemical etching of boron fibers is included in Chapter IV. Hot sulfuric acid in the temperature range of 80° - 110°C was used as the standard cleaning procedure for all samples unless otherwise stated. Dipping samples of boron fibers in the H_2SO_4 bath for 10 minutes removed 2-3μm of the surface. Also, the sulfuric acid bath is appropriate to remove boron oxides that may have developed after exposure of the fibers to air and humidity. This technique removed uncertainties from the electrical measurements and proved vital to the repeatability of results.

3.2 Conductivity Model

In order to relate the measured conductance to the conductivity of boron, the conductive core was isolated from the nickel plating using Apiezon-W wax in the way shown in Fig. 3.1a. A first order model of current flow in the fibers, assumes initially that the core conductance is large compared to that associated with the boron and voltage drops along the boride core are neglected. Figure 3.1b shows the geometry used to develop this model [1,11]. The contacts are circularly symmetric and this implies similar symmetry in the electrostatic potential. For the geometry shown in Figure 3.1b the potential is written as

$$\phi(r) = B \ln(a/r) \qquad (1)$$

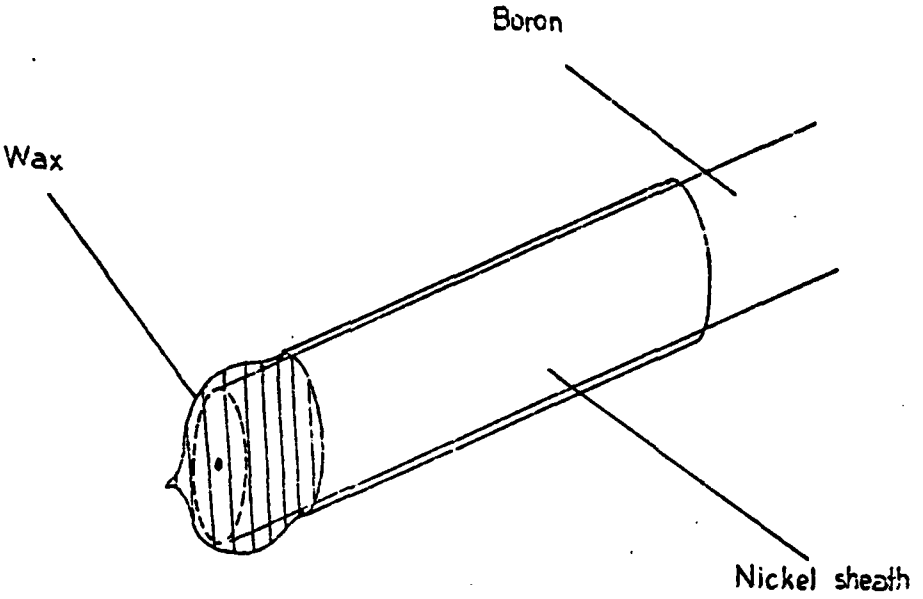

FIG. 3.1(A)

ISOLATION OF THE TUNGSTEN-BORIDE CORE

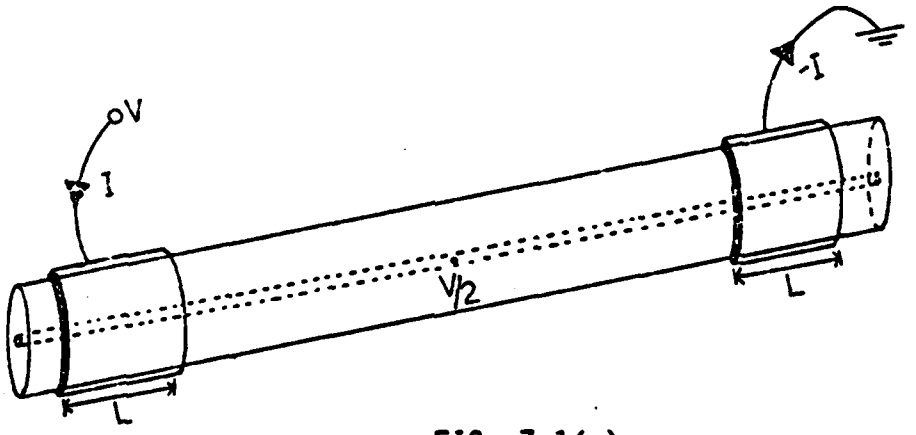

FIG. 3.1(B)

GEOMETRY OF CONTACTS

where a is the radius of the core, and

B is a constant fixed by the boundary conditions.

By symmetry, a voltage drop of V/2 will appear across each nickel coated boron segment when a voltage V is applied across the entire fiber. Using this fact, the constant B in the above equation can be evaluated. The total potential takes the form:

$$\phi(r) = \frac{V \ell n(a/r)}{2 \ell n(a/R)} \tag{2}$$

where R is the outer radius of the boron fiber.

The current (I) is related to the current density (J) in this geometry by the equation

$$I = -2\pi r L J \tag{3}$$

where L is the length of one of the nickel sheaths. (The minus sign is needed on the right hand side since positive J implies current flowing out).

The electric field is related to the static potential by the equation:

$$E = -\bar{\nabla}\phi(r) \tag{4}$$

assuming only radial variation we can write

$$E = \frac{-\partial\phi(r)}{\partial r} = \frac{v/2}{\ell n(a/R)} \left(\frac{1}{r}\right) \tag{5}$$

relating this to the current density by using

$$J = \sigma E \tag{6}$$

we can get the following expression for the current

$$I = -2\pi r L J = \frac{\pi\sigma V L}{-\ell n(a/R)} \tag{7}$$

and finally arrive at the expression for the conductivity of the boron:

$$\sigma = \left(\frac{I}{V}\right)\left(\frac{\ell n(R/a)}{\pi L}\right) \qquad (8)$$

3.3 Characterization of Fiber Conductivity at 300K

Measurements of current-voltage characteristics allows calculation of the conductivity of AVCO fibers with diameters 4, 5.6 and 8 mils. The samples were contacted using the procedure described above and mounted on glass slides. Silver conductive paint was used to contact the nickel sheath. Fibers that were contacted without the use of silver paint yielded the same results. Probes for contacting were regular aluminum or copper clips, although point contacts were used sporadically to check the quality of the clip contact. A Tektronix curve tracer (type 576) was used to determine the current-voltage characteristics.

The first measurements were made on samples with 8 mils diameter and standard 9 cm length. The plated length (L), also standard in these nearly d.c. (400Hz) conductivity characterization measurements, was 1 cm.

The results of these measurements are shown below.

Table 3.3.1

Sample Number	Conductivity (mhos/m)
AA-6	.0837
AA-7	.0814
AA-8	.0814
AA-9	.0814
AA-10	.0814
AA-11	.0814
AA-12	.0814

In cases, the current-voltage curve was linear for both polarities of applied voltage and displayed no evidence of any rectifying behavior at the nickel-boron interface. The average value for the conductivity of the 8 mil diameter boron fibers is then

$$\bar{\sigma} = 0.0817 \text{ mhos/m}$$

standard deviation of the data: $s = 8.69(10^{-4})$

For 5.6 mil fibers, the values shown in the table below were measured.

Table 3.3.2

Sample Number	(mhos/m)
BB-1	0.1
BB-2	0.155
BB-3	0.097
BB-4	0.1

$\sigma = 0.113$ mhos/m $(s = 2.80 \times 10^{-2})$

Although there is more scatter in these values than the corresponding 8 mil diameter fiber values, the cluster is good and yields a comparable value for the average conductivity of the boron sheath.

For boron fibers of 4 mils diameter, the results of conductivity measurements are summarized below. (For the data shown σ=0.1412mhos/m (s=0.0)

Table 3.3.3

Sample Number	σ(mhos/m)
CC-1	0.1412
CC-2	0.1412
CC-3	0.1412
CC-4	0.1412

3.4 Circuit Analogs

The above set of experiments provided initial electrical characterization of boron fibers. In order to more fully understand the mechanism of current flow in these fibers, a series of electrical measurements were made on fibers in which nickel contacts were plated directly to the tungsten boride core as well as the boron sheath. The plated length was varied as well as the total length of the fibers. However, only 8 mil diameter fibers were used in this series of experiments. Figure 3.2a shows the different geometries of these samples and Figure 3.2b indicates electrical d.c. circuit analogs. From these, circuit equations were derived.

The results of the electrical measurements are summarized below:

Table 3.4.1

Sample	Total length(cm)	L(cm)	Contact with the core	DC Resistance (ohms)
(1)	9.0	1.0	No	800
(2)	9.0	1.0	Yes	300
(3)	16.0	1.0	No	1120
(4)	16.0	1.0	Yes	500
(5)	2.8	1.0	No	714

The equations derived from the circuits of Fig. 3.2b are shown in Table 3.4.2.

Table 3.4.2

Sample	Expressions for total Resistance
(1)	$8R_W + 2R_B$
(2)	$9R_B$
(3)	$15R_W + 2R_B$
(4)	$16R_W$
(5)	$1.8R_W + 2R_B$

where R_W is the tungsten core resistance per unit length.

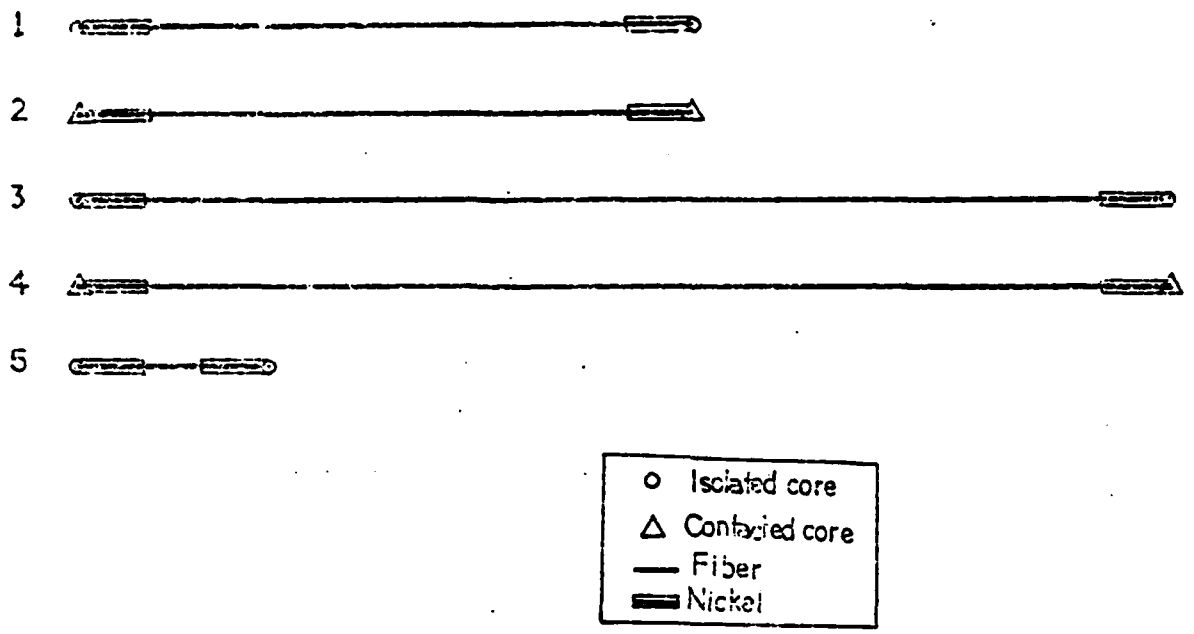

FIG. 3.2(A)

DIFFERENT CONTACT GEOMETRIES

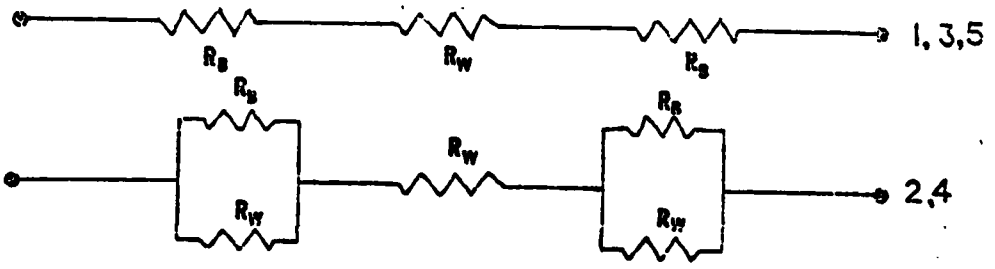

FIG. 3.2(B)

CIRCUIT ANALOGS FOR GEOMETRIES SHOWN IN FIG. 3.2(a)

The quantity R_B (resistance of the boron sheath) does not appear in the expressions for samples (2) and (4) because the resistance of the boron sheath is shorted by the direct contact between the nickel sheath and the core.

Using these five expressions and the measured values of resistance, values for R_W and R_B can be obtained. The measured values of resistance for samples (2) and (4) lead directly to the results shown in Table 3.4.3.

Table 3.4.3

Sample	Resistance R_W
(2)-(9cm.)	33.3 ohms/cm
(4)-(16cm.)	31.3 ohms/cm

The average value of the core resistance obtained for all of the samples measured during this research was 32 ohms/cm. Using this average value, the quantity R_B may be calculated using the experimental results from samples (1), (3) and (5). These calculations are shown below

Sample (1) (9 cm.) $\quad R_B = \frac{800 - (7)(32)}{2} = 288$ ohms

Sample (3) (16 cm.) $\quad R_B = \frac{1120 - (14)(32)}{2} = 336$ ohms

Sample (5) (2.8 cm.) $\quad R_B = \frac{714 - (0.8)(32)}{2} = 344$ ohms.

There are, of course, variations in this value caused by differences in the "as grown" fibers as well as uncontrollable variations in the total length of the plated electrodes. The averaging of all available data yields a value of 300 ohms for R_B .

This result allows a more accurate calculation of the boron conductivity than was possible earlier when the resistance of the tungsten

boride core was assumed to be zero. The value obtained for the boron conductivity when the finite conductance of the core is also included is

$$\sigma_{BORON} = 0.25 \text{ mhos/m.}$$

In order to assess the contact resistance involved in the nickel plating procedure, a series of samples of various lengths were prepared and their ends nickel plated so that contact was made to the core. A "least squares" analysis of the data results in the following expression for the sample resistance R and the total sample length ℓ (including the nickel sheaths)

$$R = 31.3\ell + 1.13 \tag{9}$$

where R is in ohms and ℓ is in cm. This indicates that the contact resistance is approximately 3% of the total measured resistance for a sample of 1 cm. length and decreases for samples of greater length. Contact resistance may thus be safely neglected.

The value for boron conductivity derived above is two to three orders of magnitude greater than that reported by other investigators for pure, single crystal boron. This discrepancy is not alarming in view of the large differences between the fibers and the materials used by other investigators. In particular, the boron of which the fibers are made is not single crystal and the impurity content is not known.

For a fiber of 0.01 cm. diameter, it is possible to define an effective conductivity σ_{eff} for current along the fiber. The fiber conductance G is written

$$G = \frac{\sigma_{eff} A}{L} \tag{10}$$

where A is the fiber cross-sectional area and L is the fiber length. This conductance is the sum of the conductances of the core G_W and the boron layer G_B.

$$G = G_W + G_B \tag{11}$$

$$= \frac{\sigma_W A_W}{L} + \frac{\sigma_B A_B}{L} \tag{12}$$

where A_W and A_B denote the core cross sectional area and the boron sheath cross sectional area respectively.

The effective fiber conductivity can be written as

$$\sigma_{eff} = \sigma_W(A_W/A) + \sigma_B(A_B/A) \tag{13}$$

where $A = A_W + A_B$ is the total cross sectional area of the fiber.

All three areas and σ_B are known. The core conductivity can be readily calculated from the known value of resistance/length, i.e.,

$$R_W = 1/\sigma_W A_W \quad \text{or} \quad \sigma_W = 1/R_W A_W \tag{14}$$

The core diameter is $\sim$0.0018 cm, R_W = 32 ohms/cm and the core conductivity is calculated as

$$\sigma_W = 3(10^5)\text{mhos/m}.$$

The effective fiber conductivity is then determined.

$$\sigma_{eff} = 2.3(10^3)\ \text{mhos/m}.$$

3.5 Temperature Dependence of the Conductivity of Boron Fibers

CVD boron is a material with a highly disordered lattice as indicated by the x-ray diffraction data described in the last chapter. A disordered lattice does not display ideal long-range order. In the case

of an amorphous solid, distortion of the lattice appears when the geometric arrangement of the atoms is statistically disturbed.

In order to examine electrical conductivity in disordered lattices, the usual initial approach is to look at the different conduction mechanisms involved for "extended states" and "localized states" [12]. An extended state is defined in analogy to the well-known Kronig-Penney model for the linear chain of potential energy "impulses". The extended state appears in this model when the absolute value of the wave function becomes periodic with lattice constant a. This of course happens only when all lattice potentials V_i are equal and have the same separation constant a, and when the electron energy E lies within the allowed bands given by the model. Localized states appear when the potential barriers are statistically distributed and/or their heights are not uniform. This leads to wave functions that either diverge or approach zero. All physically allowed (nondiverging) wave functions for the one-dimensional chain with statistically distributed potential barriers represent "localized states". In simple semiconductor theory, extended states determine the basic shape of the energy band diagram. Localized states are usually observed in crystalline semiconductors in conjunction with impurity levels in the band structure of the material. In heavily doped semiconductors these localized states are responsible for trapping mechanisms.

The energy band structure of amorphous semiconductors is made up of extended states as well as localized states. Fig. 3.3 shows a possible simple configuration of an energy band diagram for a highly disordered material.

In the light of what was discussed above, it is possible to separate

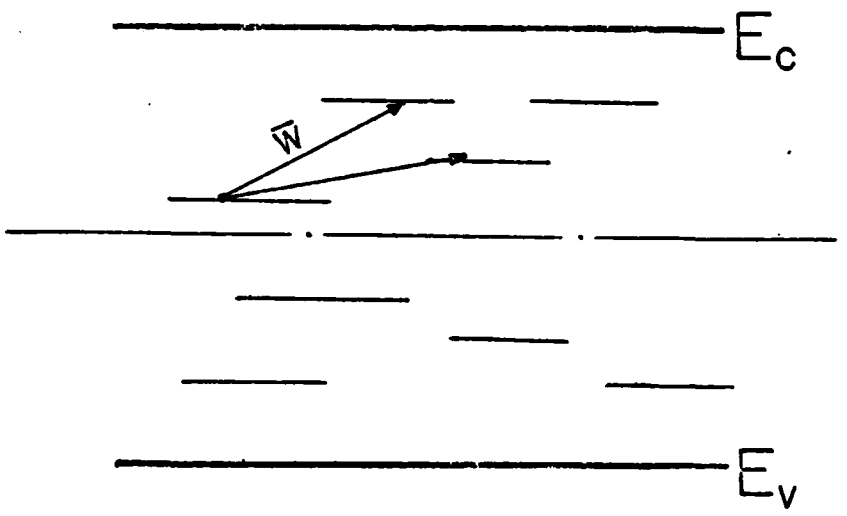

FIG. 3.3

HOPPING ENERGY OF LOCALIZED LEVELS WITHIN THE BAND GAP

the different contributions to the conductivity of the material and relate these theoretical results to the experimental data found for boron fibers.

In crystalline materials with a small amount of impurities, it is possible to relate the conductivity to the temperature in the intrinsic region by the simple formula

$$\sigma(T) = Ke^{-E_g/2k_BT} \tag{15}$$

where K is a constant, $E_g = E_c - E_v$ (the energy gap of the extended states), k_B is Boltzmann's constant and T is the temperature.

This simple model does not describe amorphous or heavily doped semiconductors. It may be argued that, at moderately high temperatures, the contributions to the conductivity of the material is dominated by the extended states. The Fermi level (E_F) then lines up between the conduction band and the valence band in a manner analogous to intrinsic conduction. This is certainly true for moderately doped semiconductors and even polycrystalline materials. In the amorphous semiconductor and the heavily doped semiconductor case, although the experimental data may lead to graphs of similar functional behavior (e.g., $\ln\sigma$ vs. $1/T$), the use of this formula for all temperature ranges may be misleading.

Specifically, conductivity in impurity bands and in amorphous semiconductor receive four major contributions from different mechanisms. Therefore, the conductivity σ is the sum $\sigma_1 + \sigma_2 + \sigma_3 + \sigma_4$ of all possible $\sigma(T)$ dependencies. These contributions appear in the experimental data by slight modifications of the functional form of $\sigma(T)$ for different temperatures. These contributions are as follows [12]:

(1) The contribution due to extended states, $E_F - E_V \ll E_C - E_V$

$$\sigma_1(T) = \sigma_{E_C} \exp[-(E_C - E_F)/K_B T] \qquad (16)$$

where E_C is the bottom of the conduction band and σ_{E_C} is the conductivity of electrons in the bottom of the band (exactly at E_C). Also, E_V is taken as the reference level, where E_V is the top of the valence band.

(2) The contribution due to localized states near the conduction band ($E_C > E_i >> E_F$). This conductivity results from hopping processes between the conduction band and localized states within a fixed distance from E_C. This is called "fixed range hopping" and it is theoretically possible to define a mean hopping energy ($\bar{W}$). This contribution has the functional form

$$\sigma_2(T) = \sigma_{02} \exp[-(E_i - E_F + \bar{W})/k_B T] \qquad (17)$$

where σ_{02} is a proportionality constant.

(3) For localized states near the Fermi energy at high temperature (fixed range hopping) we have the contribution

$$\sigma_3(T) = \sigma_{03} \exp(-\bar{W}/k_B T) \qquad (18)$$

where σ_{03} is a proportionality constant.

(4) Localized states near the Fermi energy at low temperature (variable hopping) contribute

$$\sigma_4(T) = \sigma_{04} \exp[-(To/T)^{1/4}] \qquad (19)$$

where σ_{04} is a proportionality constant and T_o is a constant for different materials [12]. The last equation is known as the Mott's law and describes conduction in amorphous semiconductors in the low temperature range.

In the literature of amorphous materials, plots of $\ln\sigma_1$ vs. T^{-1} and $\ln\sigma_4$ vs. $T^{-1/4}$ are used to classify the amorphous nature ($T^{-1/4}$ -plots) and to find the gap between extended states. The former refers to the activated conductivity of extended states and the latter refers to hopping in the localized states near E_F at low temperatures.

The theory described in the discussion above is helpful in understanding the conductivity data as a function of temperature for the boron fibers.

To clarify the use of resistance rather than conductivity in the graphs of Figures 3.4 and 3.5 recall that these curves have the same slope and therefore within a constant, the same basic functional form. That is, if R is the resistance, then

$$\frac{\partial \ln R}{\partial(1/T)} = \frac{-\partial \ln\sigma}{\partial(1/T)} \tag{20}$$

for the high temperature range and

$$\frac{\partial \ln(R)}{\partial(T^{-1/4})} = \frac{-\partial \ln\sigma}{\partial(T^{-1/4})} \tag{21}$$

for the low temperature range.

Figure 3.4 is a plot of $\ln R$ vs. T^{-1} for the activated conductivity of the extended states ($\sigma_1(T)$). While Figure 3.5 plots the $T^{-1/4}$ law.

Figure 3.5 clearly shows that the conductivity temperature data does not fit Mott's law. Therefore, we look for evidence of other types of contributions.

The graph shown in Figure 3.4 can be reproduced by two terms with different activation energies. For the intrinsic conduction region we assume that $E_i = E_F$ and $E_g/2 = E_C - E_F$ and use the fact that

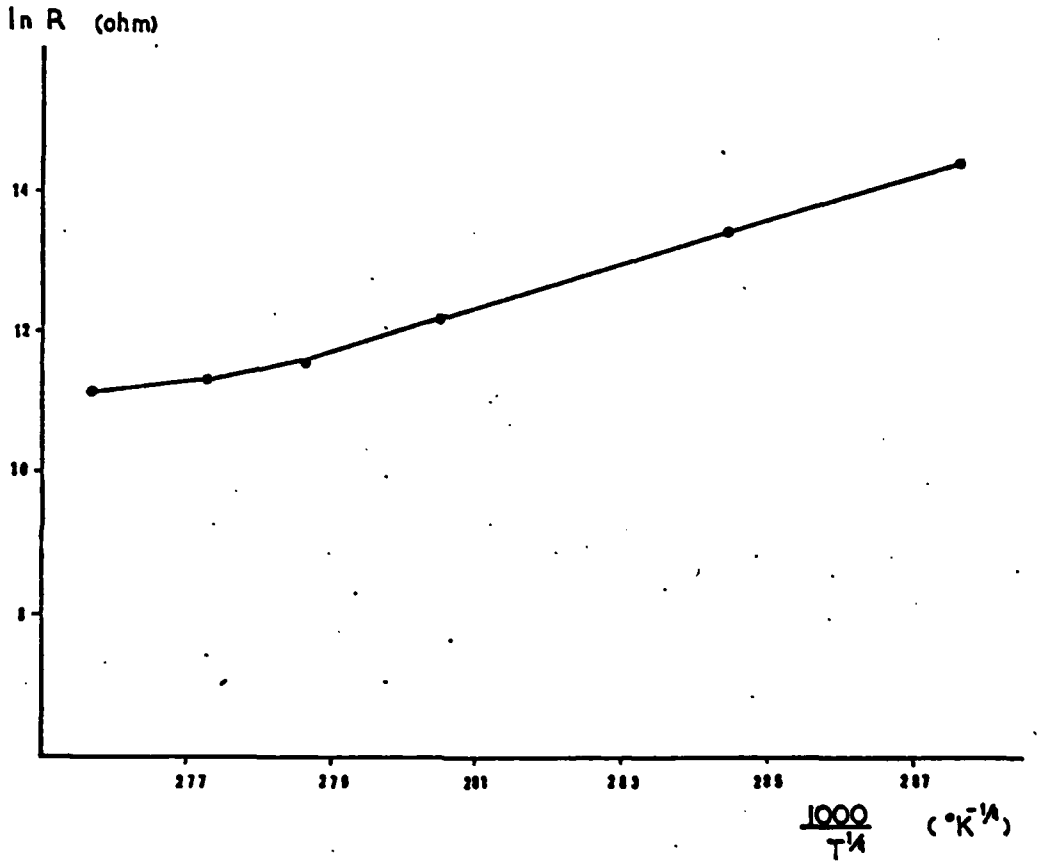

FIG. 3.5

MOTT'S LAW

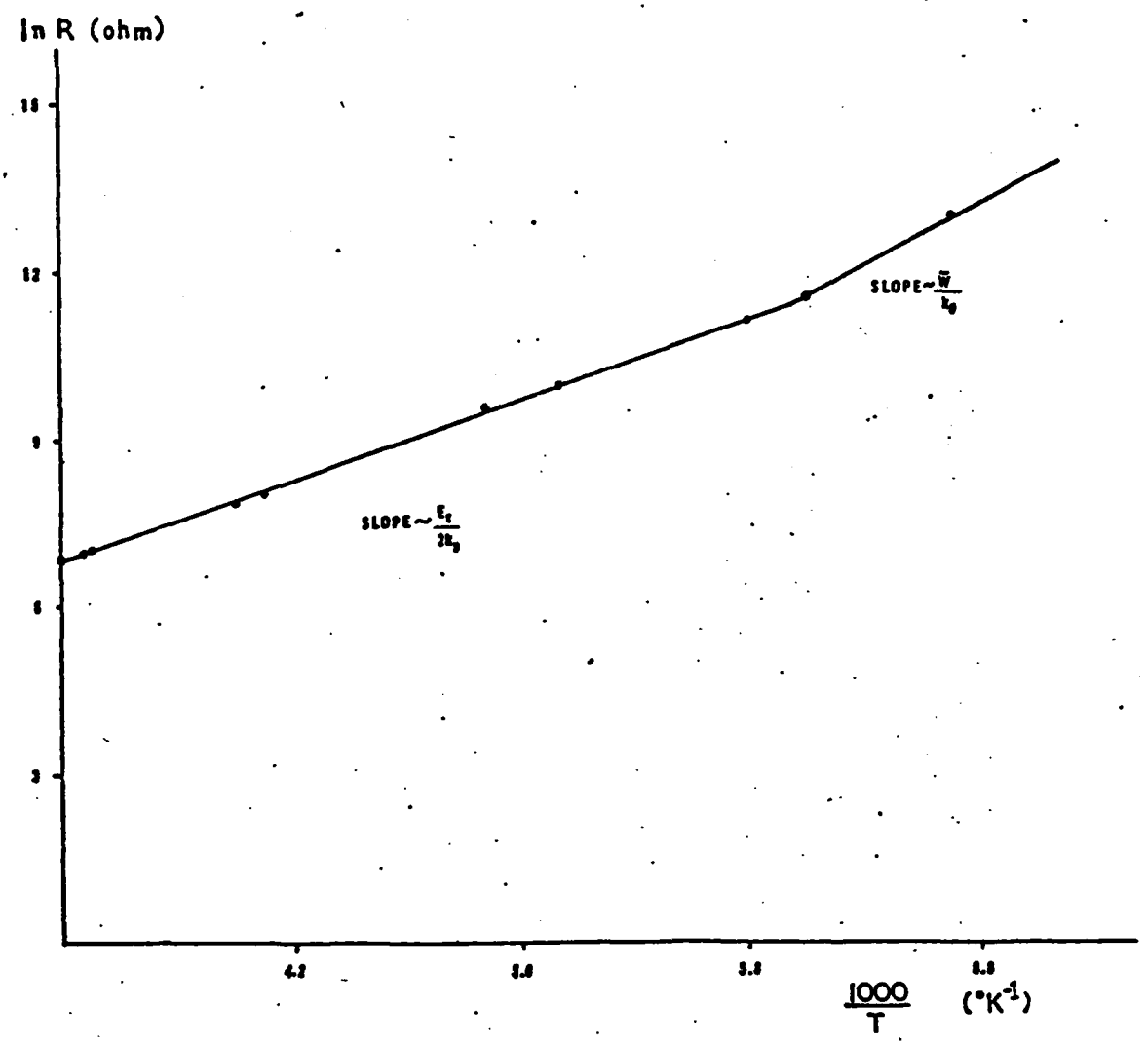

FIG. 3.4

TEMPERATURE DEPENDENCE OF THE CONDUCTIVITY

$$\frac{\partial \ln R}{\partial (1/T)} = \frac{-\partial \ln \sigma_1(T)}{\partial (1/T)} \tag{22}$$

to arrive at a thermal gap $E_g = 0.22eV$ for boron in the fiber configuration.

Since boron fibers grown on tungsten wires have borides near the core which are n-type, it is reasonable to assume that the second contribution to the conductivity arises from localized states near the conduction band: E_C . Therefore, the slope of the graph shown in Figure 3.5 may be related to

$$E_i - E_F + \overline{W} \tag{23}$$

where $E_C > E_i >> E_F$ and we may write

$$E_i - E_F + \overline{W} \simeq E_i + \overline{W} \tag{24}$$

Assuming that E_i is at the center of the thermal gap, we write $E_i = E_g/2$ and the mean value of the hopping energy ($\overline{W}$) may be found to be 0.142eV.

Of course, this is a very rough estimate and there is no sure way to quantitatively describe the current mechanisms in this material.

A final comment can be made in the light of Berezin's paper [13] which Mott's law is used to justify the "amorphous concept" of β-rhombohedral boron. The reverse may be applied here. Since Mott's law is not followed by boron fibers, it may be said that the polycrystalline structure does not have the β-rhombohedral form. This is in agreement with Otte and Lipsitt's paper [4].

CHAPTER IV

ETCHING STUDIES OF 8 MILS DIAMETER FIBERS

4.1 Importance of Surface Etching

As it will be seen later in Chapter V, the strength of boron fibers decreases rapidly if the material is subjected to temperatures above 850°C. This phenomena is primarily due to surface recrystallization and makes high temperature doping of boron fibers (cf. Chapter VI) a very difficult task. The deterioration of the mechanical properties that make boron fibers attractive is a negative aspect for the potential use of these fibers in advanced composite materials. For this reason, it is important to find methods of increasing the fiber tensile strength before and after heat treatment. One way of increasing the fiber tensile strength is the chemical etching of the surface of the fiber. This method has been used [14,15] to show an increase in the fiber tensile strength before and after heat treatment.

Wawner [14] used early boron fiber samples that were formed by vapor deposition of massive amorphous boron of the Talley type [8]. Those early fibers had tensile strengths and Young's modulus as shown in Chapter II. Smith [15], used AVCO boron fibers which have a much higher tensile strength due to better control of the growth process parameters. The average tensile strength of AVCO boron fibers is between 500 and 550 ksi. This high tensile strength however, has a coefficient of variation of 15%. Smith showed that this large coefficient of variation of tensile strength can be reduced to ~5% if an 8 mil diameter fiber is etched down to 6.5 mils diameter. This result is explained in terms of etching effects on surface flaws and the residual stress pattern

of as received fibers. Since no readily observable surface flaws appear on an as received boron fiber, Wawner concluded that the boundaries of the nodules ("orange-peel") are these flaws. These are boundaries of areas of preferred growth on the surface of the filament. The influence of these flaws is not noticeable until ∿0.5 mil of the surface is removed. Thus, the tensile strength increases with radial reduction. After etching, the surface of the fiber no longer has the "orange-peel" appearance of as received fibers but is shiny and uniform.

The need for near ideal surface in contacting boron fibers was discussed in Chapter III. The same need occurs for heat treatment and diffusion experiments. The effects of etching and radial reduction on fiber conduction are useful for an overall understanding of the material. It should be noted that surface flaws are not solely responsible for the strength of the fibers. After surface flaws have been essentially eliminated, the core flaws were observed to be the source of fiber fracture [16].

In this chapter, two types of etchants are studied. The focus is on the sample preparation rather than improvement of mechanical qualities. As will be seen in Chapter VI, etching did not play a significant role in strengthening the fiber so that it would retain its mechanical properties during heat treatment.

4.2 Sulfuric Acid Etching

Sulfuric acid is a very slow etchant of boron but is useful because it leaves effectively no oxide layers for low etching temperatures (80°-90°C) and it "polishes" the surface of boron.

For higher etching temperatures around 300°C, H_2SO_4 leaves thin oxide layers of different thicknesses [17]. Fibers etched this way for 10 minutes no longer displayed surface nodules. This indicates that those fibers were etched more than 0.5 mils. In our experiments, the fibers were "cleaned" in hot H_2SO_4 (cf. Appendix A). The etchant temperature was between 95° - 105°C, and the etching time was kept at 10 minutes so that 3-5μm were removed. Nodules were clearly seen under the optical microscope after etching but foreign particles were absent. H_2SO_4 also removes boron oxides which are easily grown on the surface of the boron fiber due to environmental conditions. This makes H_2SO_4 ideal for sample preparation for conductivity measurements.

The difference in conductance between a fiber that has been "cleaned" in H_2SO_4 and an "as received" fiber is that the latter exhibit non-linear v-i characteristics. Unless specified otherwise, all samples were "cleaned" in 98% H_2SO_4 in the manner described in Appendix A.

4.3 Nitric Acid Etching

Nitric acid is a vigorous etchant of boron and has not been studied in detail [2,14,17].

Because the "attack" on boron by HNO_3 is very rapid and vigorous, the surface of the fiber is non-uniformly etched [17] resulting in a rough, irregular appearance. This characteristic is inherent because etching only occurs after the nitric acid starts to boil (changing into a reddish color). So that reduction in the etching temperature is not possible. A significant increase in the resistance and, in some instances non-linear effects, were observed for the HNO_3 etched samples. To assure that oxides were not created that in turn caused this effect, some samples

were cleaned in H_2SO_4 after HNO_3 etching and no change in their resistances occurred.

Figure 4.1 shows the etching apparatus which allowed agitation of the solution and batch processing. Usually, seven fibers etched at a time. The temperature was kept between 93° - 96°C and the solution was HNO_3 and water (2:1).

The results of three different runs are shown below:

Table 4.3.1

Run No. 1

Sample No.	Etching time (min.)	Diameter(μm)
NE2-4	10	166.67
NE2-5	15	156.19
NE2-6	20	145.24
NE2-7	25	134.29
NE2-8	30	123.81
NE2-9	35	114.29
NE2-10	40	104.76

Initial diameter of an average as received fiber for this batch: 202.38μm (∿8 mils).

Table 4.3.2

Run No. 2

Sample No.	Etching time (min.)	Diameter(μm)
NE2-11	3	180.95
NE2-12	5	176.19
NE2-13	7	171.43
NE2-14	10	161.90
NE2-15	20	128.57
NE2-16	30	95.24
NE2-17	40	78.57

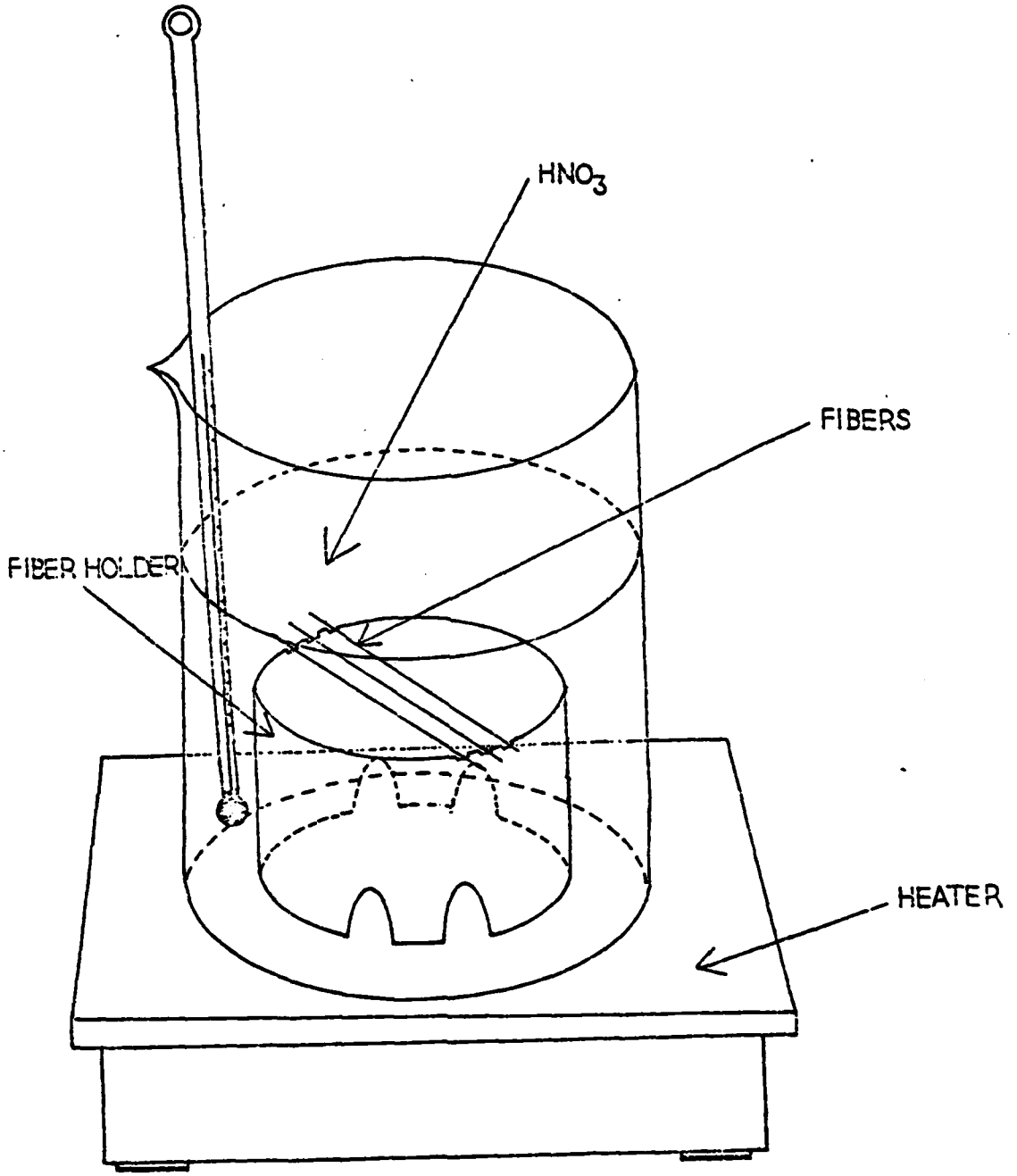

FIG. 4.1

APPARATUS USED FOR HNO_3 ETCHING

Initial diameter of an average as received fiber in this batch: 190.48μm (∿8 mils)

Table 4.3.3

Run No. 3

Sample No.	Etching time (min.)	Diameter (μm)
NE2-18	2	190.48
NE2-19	6	176.19
NE2-20	10	154.76
NE2-21	14	142.85
NE2-22	18	140.48
NE2-23	22	121.43
NE2-24	70	47.62

Initial diameter of an average as received fiber in this batch: 190.48μm (∿8 mils)

The microscope used to measure the diameter of the etched fiber was a Leitz-Wetzlar (20X objective, 10X eye piece). The measurement error for the diameter was found to be +3μm. Figure 4.2 shows a graph of diameter vs. time of etching for all four runs. The etching rate calculated from the slope of this graph is 2μm/min.

The changes in the conductance are summarized below:

Table 4.3.4

Sample No.	Radius (μm)	G(mhos)
NE2-12	88.10	342.46 (10^{-6})
NE2-27	75.0	363.63 (10^{-6})
NE2-22	69.05	466.48 (10^{-6})
NE2-28	57.15	600 (10^{-3})
NE2-16	47.52	1.39 (10^{-3})
NE2-13	85.71	600 (10^{-6})
NE2-20	77.38	NON LINEAR
NE2-17	39.28	666.67 (10^{-6})

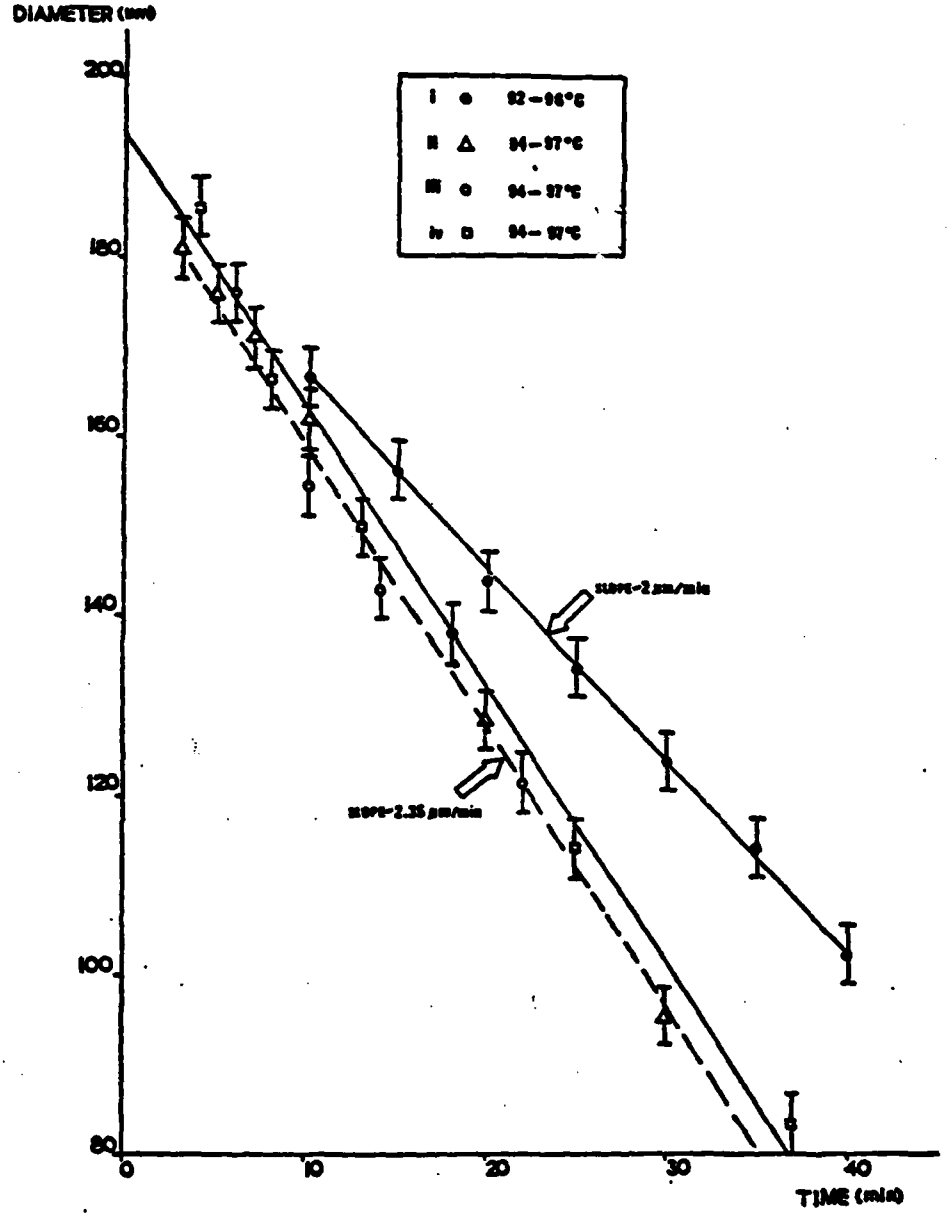

FIGURE 4.2

NITRIC ACID ETCHING

Table 4.3.4 (cont.)

Sample No.	Radius (μm)	G(mhos)
NE2-22	60.71	NON LINEAR
NE2-15	64.28	NON LINEAR

In the data shown above, hysterisis and rectification were the main types of non-linearities. The conductance of the fibers etched in HNO_3 is 70% less than that of samples cleaned in H_2SO_4 (samples with the same diameter). Another set of samples was etched for 10 minutes to an average diameter, of 166.67μm. Then one sample was etched in H_2SO_4 to see if this would remove possible oxides and surface roughness that would have developed during the HNO_3 etching. The average conductance measured was 520×10^{-6} mhos. Comparison with a sample of 198.48μm diameter "cleaned" in H_2SO_4 ($G = 1.25 \times 10^{-3}$ mhos) shows a difference of about 40%.

CHAPTER V

RECRYSTALLIZATION AND NICKEL ALLOYING OF BORON

5.1 Introduction

This chapter describes changes produced on boron fibers by heat treatments under reduced pressures. Some heat treated fibers were later electroplated and electrical measurements taken. Other samples were nickel plated and then heat treated with the nickel sheath on the fiber. Variations of these two main techniques were used to confirm trends in the development of this study.

Two mechanisms affect the conductivity of heat treated fibers. The first is the surface recrystallization of the fibers as observed by several researchers (particularly Gillepsie [6]), which accounts for deterioration of mechanical properties. Second, boron fibers covered with nickel displayed several alloying processes that resulted in an increase in fiber conductivity.

Scanning Electron Microscope analysis accompanied by conductivity measurements afforded step-by-step tracking of the recrystallization and alloying mechanisms mentioned above. These techniques allowed an understanding of the irreversible conversion of amorphous or microcrystalline boron into one of its two rhombohedral forms. (α or β-rhombohedral). No attempt was made to determine the crystal structure of the recrystallized boron. Most researchers report only the presence of the α-rhombohedral form if either the preparation temperature or the temperature of heat treating "as grown" fibers is below 1100°C [3,4,8]. This is based on experimental data or by arguments such as those given by [3] on the thermodynamical stability of this polymorph below the 1100°C range.

Gillepsie [8] reports conversion to the β-rhombohedral modification after heat treatments at temperatures below 1100°C. The boron samples used by Gillepsie were grown in a hydrogen trichloride atmosphere on a tungsten substrate (similar in process to AVCO's fibers). These samples showed areas of dendritic crystal growth after 15 seconds of heat treatment at a temperature of 1050°C and 6.5×10^{-6} torr pressure. After longer periods of heat treatment, complete conversion of the surface to the β-rhombohedral form was observed. This result is in partial agreement with our experimental data. Although we did not attempt to classify the crystalline form, recrystallization of boron in the same range of pressures and temperatures given by Gillepsie was observed. The evidence in Gillepsie's work that recrystallization is mainly at the surface was that x-ray diffraction showed the presence of amorphous material although the "orange-peel" surface associated with amorphous boron disappeared after heat treatment. In our SEM analysis below, results agree with this claim at least partially.

Changes in the conductivity enabled us to follow the extent of surface recrystallization for a standard run of heat treated fibers. This indicated recrystallization below 950°C which conflicts with Gillepsie's result that no surface recrystallization occurs at temperatures around 900°C. This discrepancy may be explained by the duration of our heat treatment process around that temperature being six times that of Gillepsie's cycle.

Nickel-boron alloying and recrystallization of nickel-boron systems is discussed later in this chapter. Complete descriptions of experimental apparatus and techniques is included in Appendix B. All samples were 8 mils in diameter and 6 cm in length. The nickel plated length

was maintained at 1 cm on each end of the fiber and the tungsten core was isolated from the nickel by the method described in Chapter III. Electrical measurements were taken before and after the heat cycle in the manner described in Appendix B. The temperature range used in this work was from 558°C to 1112°C and the durations of all heat treatments were 6 hours.

5.2 Heat Treatment at 558°C

Fibers exposed to temperatures in this range showed no apparent change of surface characteristics. The "orange-peel" aspect of the surface of the fiber was maintained. The interaction of the fiber with the nickel sheath in the absence of dramatic boron recrystallization is of interest. In other words, the fiber maintains its strength and the most important changes are the thermal expansion of the nickel sheath and the reaction of the nickel with the boron.

The coefficient of thermal expansion of nickel is 13.3×10^{6} cm/cm-°C and that of boron is 8.3×10^{6} cm/cm-°C [18]. The nickel sheath that was electroplated on the boron fiber expands more than the boron fibers as the temperature is increased. As the SEM micrograph shows, the nickel sheath moves away from the surface of the fiber leaving evidence of strong interaction between the two materials where they were in contact. Figure 5.1 shows this unfolding of the nickel sheath after heat treatment at 558°C under the average pressure of 1.5×10^{-5} torrs for 6 hours.

Higher magnification (Fig. 5.2) reveals areas where the nickel sheath was contacting the boron and then moved away after heat treatment (Region B in the picture). It is also clearly seen that the "orange-peel" aspect of the boron surface remains the same as that of "as rec-

Fig. 5.1 - Nickel sheath moving away from the surface of the fiber after heat treating at 558°C for 6 hrs. at 1.5×10^{-5} torrs. (200X, 61° angle).

Fig. 5.2 - Region A shows the uncontacted fiber retaining its surface characteristics. Region B shows places where the nickel originally contacted the fiber. Region C is magnified and showed in Fig. 5.3. (500X, 57° angle)

eived" fibers. There is no evidence of apparent recrystallization of the boron at this temperature (558°C) and pressure (1.5×10^{-5} torrs).

It should be noted here that the average value for the pressure for all experiments is 1.4×10^{-5} torrs. Exact measurements showed pressures as low as 8×10^{-6} torrs but over the six hour period of heat treatment starting at pressures $\sim 4 \times 10^{-5}$ torrs the average value of the pressure was $\sim 2.0 \times 10^{-5}$ for the first three hours and $\sim 9 \times 10^{-6}$ for the second three hours.

Figure 5.2 also shows that the entire nickel sheath appears to be "floating" on the surface of the fiber. Region C of Fig. 5.2 is shown in Fig. 5.3 with increased magnification (5000X). It clearly shows this "floating" effect of the nickel sheath. The surface of the boron (Region A of Fig. 5.3) no longer displays the "orange peel" appearance familiar to the boron fiber. Clearly strong reactions with the nickel occurred on the surface of the massive amorphous boron. The roughness of the surface at these reaction sites may be indicative of small crystallite growth of nickel-boron compounds.

That the nickel sheath is no longer in intimate contact with the boron surface shows up in the electrical measurements. Although there is still a linear voltage-current characteristic, the measured value of the conductance is about 1/2 lower than that of an "as grown" fiber. This may be explained because fewer places underneath the nickel sheath are actually making contact with the boron surface. The experimental value of the conductance for these samples is 6.896×10^{-4} mhos.

5.3 Heat Treatment at 687°C

The mechanisms of nickel expansion and nickel-boron reaction des-

Fig. 5.3 - Region C of Fig. 5.2 magnified to 5000X (57° angle). The nickel sheath "floats" on the surface of the fiber. Reaction of nickel with boron is seen by the absence of nodules on the surface of the fiber.

cribed above are significantly more dramatic if the temperature is raised by 129°C. Figure 5.4 shows four regions of different behavior. Region A shows part of the nickel sheath moved up away from the surface of the fiber. This region appears to retain the original qualities of the plated nickel. It is shining and smooth without traces of crystallites. Region C is quite the contrary; the nickel sheath is not moved away from the surface of the boron fiber but the sheath here is quite different. There is a roughness due to small crystallites on the surface. The boundary between regions A and C is significant. The boundary (Region B), starts right where the nickel sheath begins to make intimate contact with the boron surface. This could indicate that region C is no longer just pure nickel but some form of nickel-boron borides. As we move away from the interface and go deep into region C, the size of these crystals diminish as it is shown in Figure 5.6 which has the same magnification as picture 5.5a.

Places that were covered with nickel that broke away and fell off the surface of the fiber are shown in regions D-1 and D-2 of Fig. 5.4. Here, as it was discussed before, reaction of the nickel with the boron occurred but the nickel sheath "fell-off" the surface of the fiber. Figures 5.7a and 5.7b show these reaction sites. Figures 5.7b shows aspects of this "attack" on the surface of the fiber. This particular site is the region D-2 of Figure 5.4. Figure 5.7a shows region D-1. Both regions appear to have the same characteristics.

Another phenomena that occurs at this temperature is shown in Fig. 5.8. In certain places the nickel erupts and creeps up. This part of the nickel sheath clearly is not as much in contact with the boron as in other areas. The areas where the nickel is touching the surface

Fig. 5.4 - Four distinct regions can be identified where different phenomena occurred in the nickel-boron system at 678°C. (200X, 65° angle).

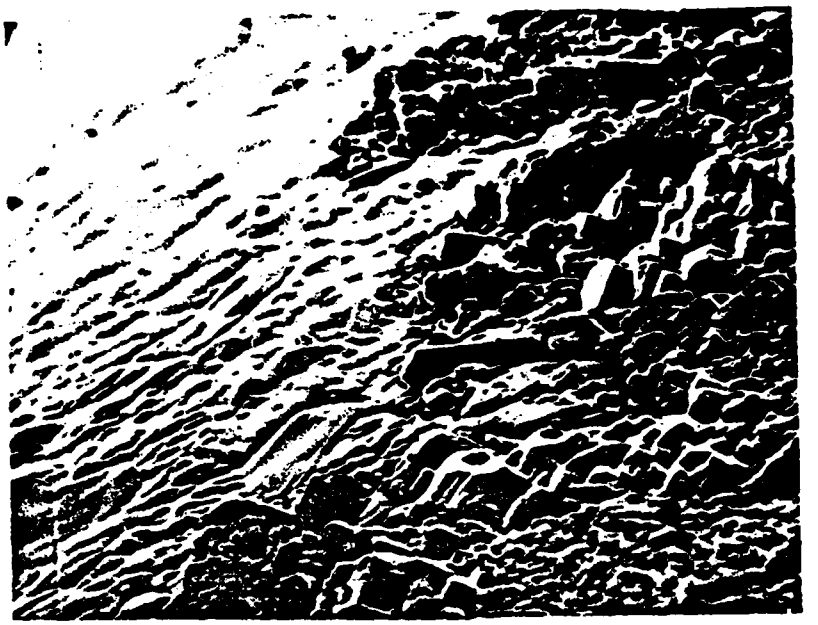

Fig. 5.5(a) - shows the interface (region B of Fig. 5.4) between pure nickel (on the left) and large nickel rich nickel-boride crystals (2000X, 65° angle).

Fig. 5.5(b) - Same crystals shown in 5.5(a) at higher magnification (5000X, 65° angle).

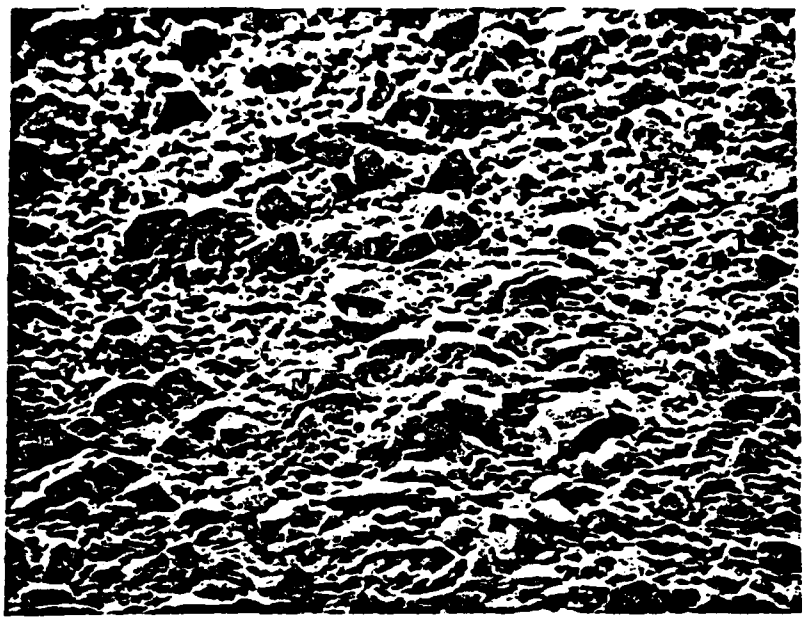

Fig. 5.6 - Region C of Fig. 5.4 showing crystallites of nickel-boron compounds. (2000X, 65° angle).

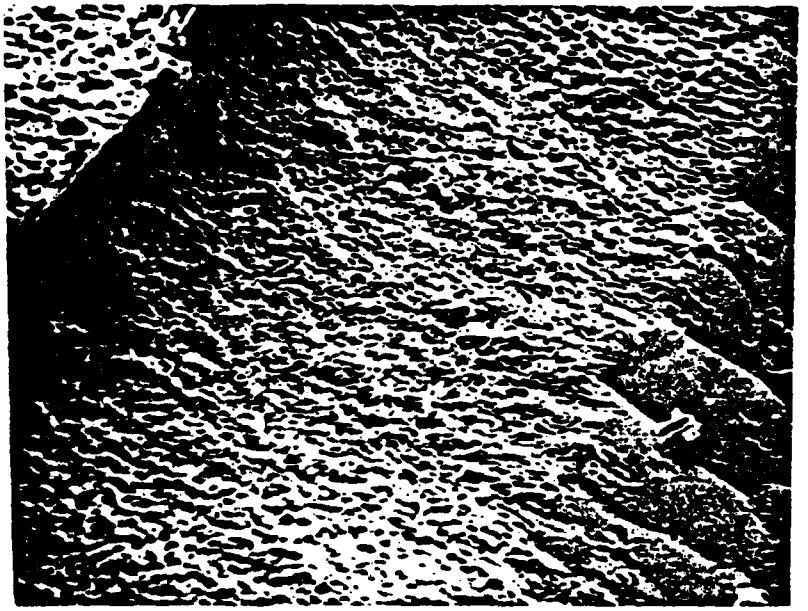

Fig. 5.7(a) - shows region D-1 of Fig. ~~5.5(a)~~ 5.4 (2000X, 65° angle).

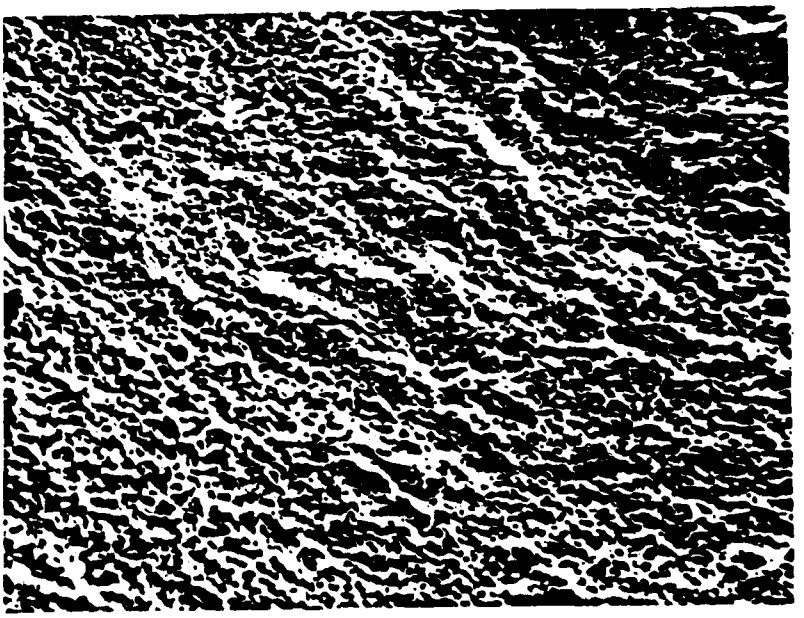

Fig. 5.7(b) - region D-2 (2000X, 65° angle).

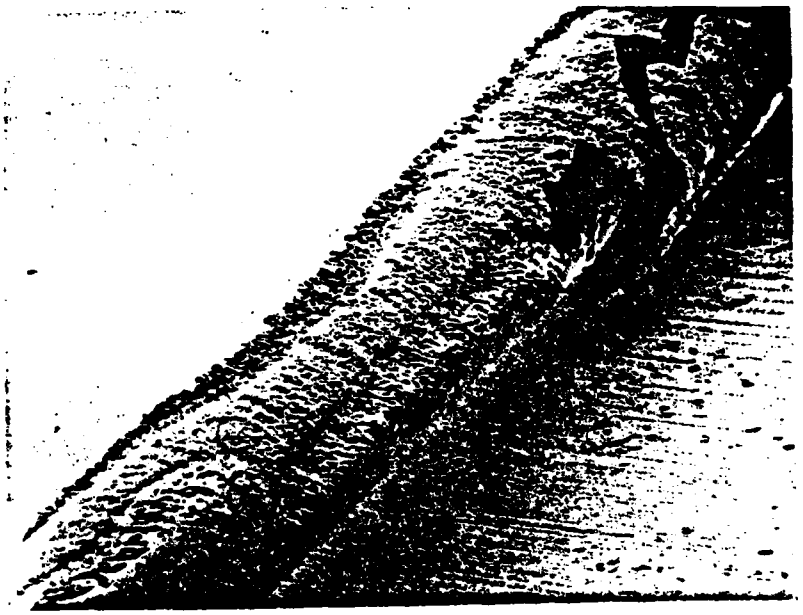

Fig. 5.8 - Creeping up nickel rich crystallites on places where the nickel sheath is not directly contacting the boron surface. (100X, 65° angle).

of the fiber appear as those shown before in Fig. 5.6. Here, crystallites of Ni-B compounds are clearly detected.

This compound formation of certain areas of the nickel sheath (where nickel is in intimate contact with the boron surface) shows up in the electrical measurements. The nickel sheath is no longer "floating" on the surface of the fiber as in the 558°C case. Significant increase in the conductance of these fibers occurred. The measured average value of conductance in this case is 2.1×10^{-3} mhos or 68% larger than the 558°C case. It is also 40% larger than the conductance of "as grown" fibers.

5.4 Heat Treatment at 738°C

The effects of nickel reaction with the boron surface were investigated this time with a thinner nickel sheath of approximately 6μm of thickness. This was accomplished by plating the boron fiber for only 3 minutes and keeping all other parameters of the plating process the same as before. With a thinner nickel sheath, it was expected that the effects of thermal expansions would be less. Therefore, the nickel would stay in contact with the boron surface. It was further expected that the boron fiber would still maintain its original surface characteristics in places where it was not nickel plated. Since this temperature is still below the temperature of surface recrystallization of boron, the fiber would not completely lose its mechanical properties. Figure 5.9a shows that these expectations are for the most part fulfilled. The thinner pure nickel sheath is almost completely converted to nickel-boron compounds. It is also shown that the surface of the boron was severely "attacked" and in some places the boron "caved in". Figure 5.9b shows region A of Figure 5.9a at a higher magnification. There is no

Fig. 5.9(a) - shows complete conversion of the thin (6μm) nickel sheath (200X, 68° angle).

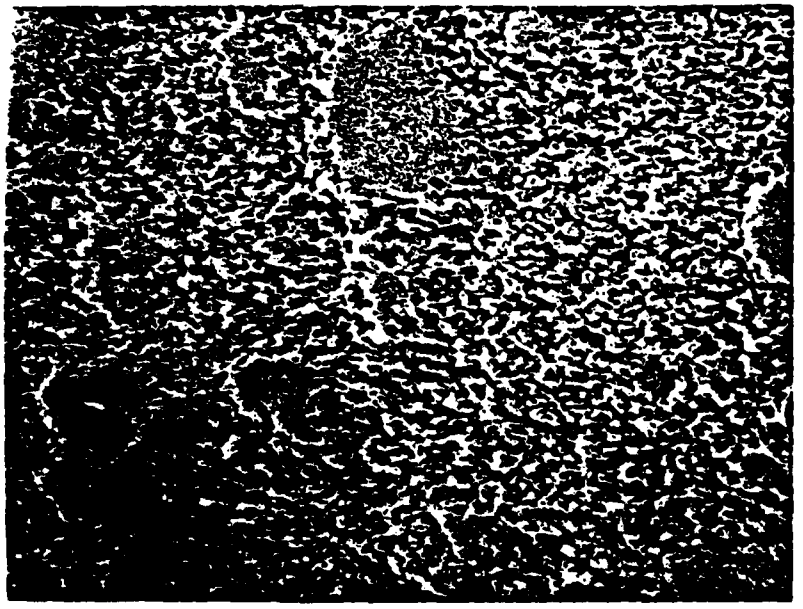

Fig. 5.9(b) - Region A of 5.9(a) magnified to 2000X (68° angle).

longer a smooth nickel sheath. It is now a rough boron-nickel surface made up of small crystallites though not nickel rich enough to grow as large as those shown before in Figure 5.5b. Figure 5.10 shows a reaction site where some of the nickel was converted but did not completely flash away as in the case of Figure 5.9b. Nodules are also present where the fiber was not plated.

This complete conversion of nickel and severe transformation of the boron surface influenced the conductance of the sample. Here, the effect of a completely spread-out nickel-boron sheath is intimate contact. The measured conductance was 5.88×10^{-3} mhos. This is an increase of 470% over the value measured for "as grown" fibers. It is also 853% higher than the conduction of the 538°C case where the nickel expanded and moved away from the surface of the fiber reducing the areas of contact to the surface. Surface recrystallization of boron did not occur during this low time-temperature cycle.

5.5 Heat Treatment at 804°C

We now return to the thicker nickel sheath (~12μm for 6 min. plating). Here, as in all experiments that will follow, the thickness of the nickel sheath is triple that of the 738°C case. Complete conversion is not easily attained. As the fiber heats up, the nickel sheath expands and moves away from the surface of the boron in a more dramatic manner. Figure 5.11a shows the pure nickel sheath "floating" on the surface of the fiber. Region A is magnified and showed in Figure 5.11b. Here, the nickel stayed on the surface of the boron. Compound formation occurred but, due to the large concentration of nickel, there are large crystals of the nickel-rich type described above. Notice on the right side of the

Fig. 5.10 - Reaction site with higher concentration of the nickel. (500X, 30° angle)

picture that the nickel sheath is not completely converted. These are probably places where the nickel has moved up away from the surface of the boron.

As could be expected, these samples have higher conductance than those that were heat treated at 678°C. However, due to incomplete conversion and "floating" effects of the nickel sheath, the conductance of these samples is less than that of the 738°C case. The average conductance of these samples is 3.876×10^{-3} mhos.

Figure 5.11c shows a higher magnification of Region B of Figure 5.11a. Large crystallites of the nickel-rich, nickel-boron compound are visible. Notice that, under the nickel sheath, the aspect of the surface is that of Figure 5.7a and 5.7b. These are reaction sites that did not have enough nickel to "cave-in". That is, the boron surface is as encountered in Figure 5.10, where the concentration of nickel was just enough to create compounds but not high enough to grow the large crystals common to the nickel-rich compound. It is also clearly seen that the nickel expansion before compound formation was more severe. In this particular case, the nickel "floats" 15-20μm away from the surface.

5.6 Heat Treatment at 914°C

At temperatures above 900°C, recrystallization of the pure boron on the surface of the fiber becomes more evident. This mechanism has several important side-effects. The deterioration of the mechanical properties of the fiber is immediate. The material becomes brittle and easily shattered with handling in the laboratory. Figures 5.12a and 5.12b shows complete formation of compounds and only a nickel-boron sheath appears with an even distribution of small crystallites.

Fig. 5.11(a) - Transformation of the nickel sheath at 804°C (100X, 11° angle).

Fig. 5.11(b) - Region A of 5.11(a) magnified to 1000X (11° angle).

Fig. 5.11(c) - Region B of Fig. 5.9a at 1000X magnification (same angle of view: 11°)

Fig. 5.12(a) - Nickel-boron sheath (500X, 67°).

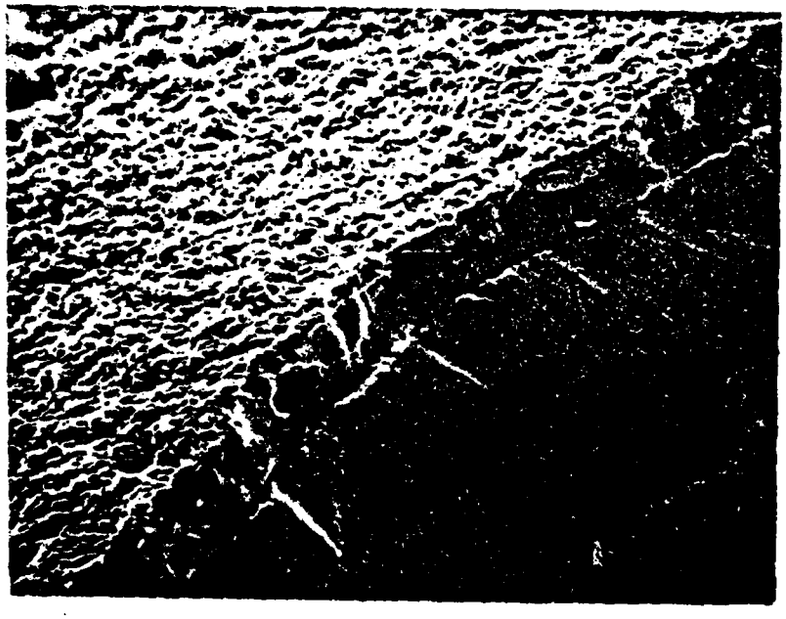

Fig. 5.12(b) - Larger magnification of (a) showing aspects of the even distribution of crystallites (2000X, 67° angle).

Along the unplated length of the fiber, two families of pure boron crystals grow evenly spread out all over the fiber surface. Figure 5.13a shows this phenomena and Figure 5.13b shows region A of Figure 5.11a at a higher magnification where the two types of crystallites are easily distinguishable. Notice, however that nodules are still present where the fiber was not plated.

Figures 5.12a and 5.12b showed the nickel-boron sheath where only one form of crystallite is found evenly spread over the fiber. As expected, this complete conversion of the nickel plus the recrystallization of boron further increased the conductance of the fiber. The average values of the conductance of these samples is 6.536×10^{-3} mhos. This is the largest value measured. This is an increase of 523% over the conductance of "as grown" fibers.

5.7 Heat Treatment at 1011°C and 1112°C

What was a region of an even distribution of small crystallites of nickel-boron compounds is now a region of crystal growth. These highly geometrical shaped crystals are very different from the so-called "nickel-rich" crystals shown in Fig. 5.5b. They are not as symmetrical and smooth. There is a clear hint here that the recrystallization of the boron surface created a new species of boron-nickel compound which is richer in boron then the compound shown in Figure 5.5b. Figure 5.14a shows this distribution of crystallites in samples heat treated at 1011°C. Larger magnification (Figure 5.14b) clearly shows the amount of transformation on the nickel-boron surface. Deep dips of about 1.5μm clearly show severe attacks on the fiber surface which are necessary for the boron to form Ni-B compounds of large crystallites. This "caving-in"

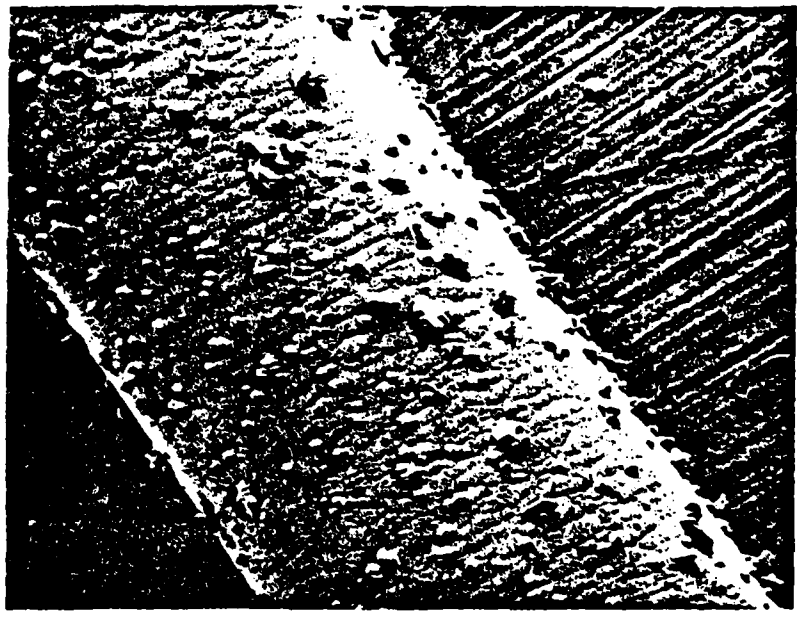

Fig. 5.13(a) - Sparce distribution of two families of recrystallized pure boron (200X, 3° angle).

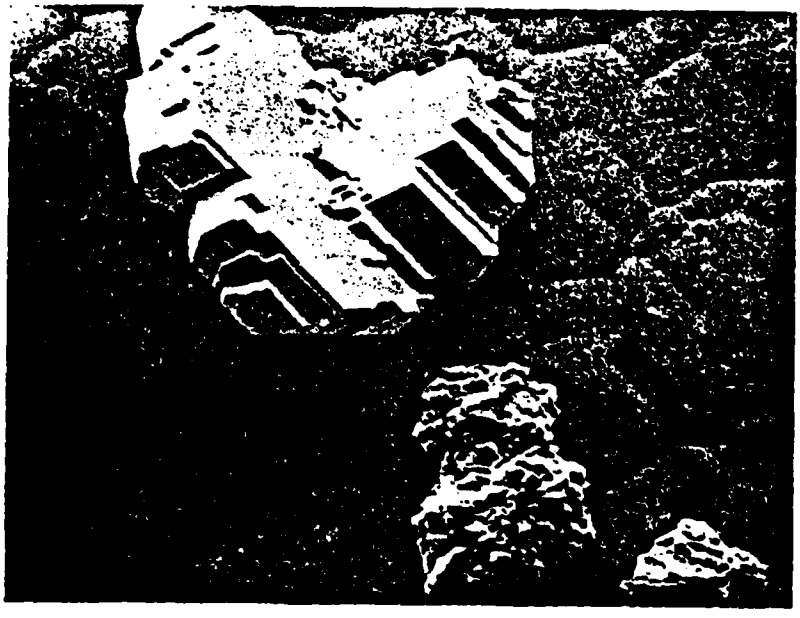

Fig. 5.13(b) - Region A of 5.5(a) showing members of these two families (2000X, 3° angle).

Fig. 5.14(a) - Nickel-boron crystallites grown on the surface of the fiber with high degree symmetry after heat treatment at 1011°C (500X, 3° angle).

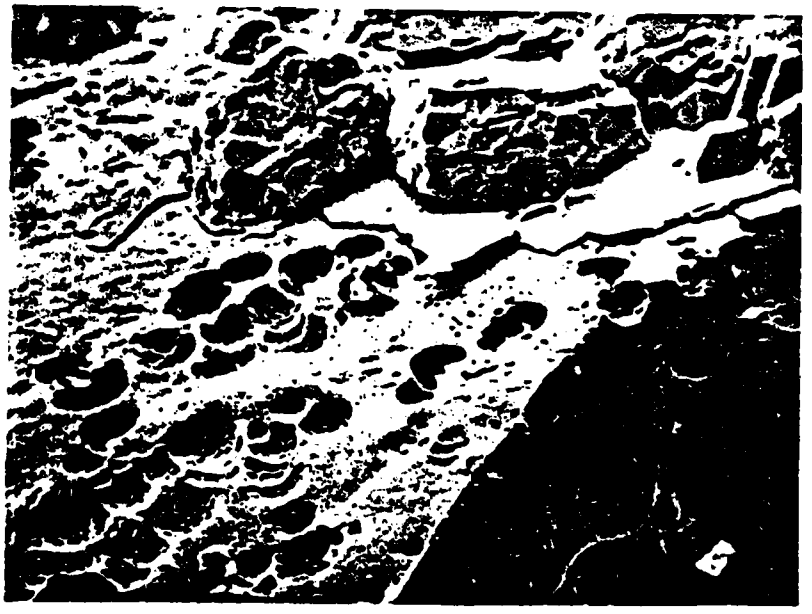

Fig. 5.14(b) - Dips and crystallites of the nickel-boron sheath (2000X, 61° angle).

effect was observed before at lower temperatures but to a much lesser degree. There is clearly a "loss" of boron from the surface of the fiber.

What happens to the unplated part of the sample is shown for a slightly higher temperature (1112°C) in Figures 5.15a and 5.15b. These pictures are to be compared with Figures 5.16a and 5.16b. In the first set of pictures we see crystallites of pure boron recrystallized on the surface of the fiber. The crystallites are nickel borides grown due to the nickel-boron reaction as discussed above. Clearly surface recrystallization helped to form compounds richer in both nickel and boron than before.

Figure 5.12a shows the bulk of the fiber untouched by any kind of crystal growth. In Figure 5.17, the cross-section of one of the three fibers shows vigorous crystal growth of the pure boron type. The fiber shown in Figure 5.12a was cut in order to expose the bulk boron. The fiber in Figure 5.17 shows surface recrystallization on the cross section exposed during the heat treatment. These two pictures agree with the early assumption that recrystallization is a surface phenomena. Figure 5.17 also reveals that surface nodules are not necessary for the recrystallization mechanism since nodules do not appear on the cross section of the fiber.

Figure 5.18a and 5.18b shows other interesting phenomena. Cracks on the nickel-boron sheath reveal dips which are evidence of boron diffusion from the original surface. Crystal growth across two different fibers is evident.

Because of the fragility of the samples heat treated above 1000°C, electrical conductivity data are not available.

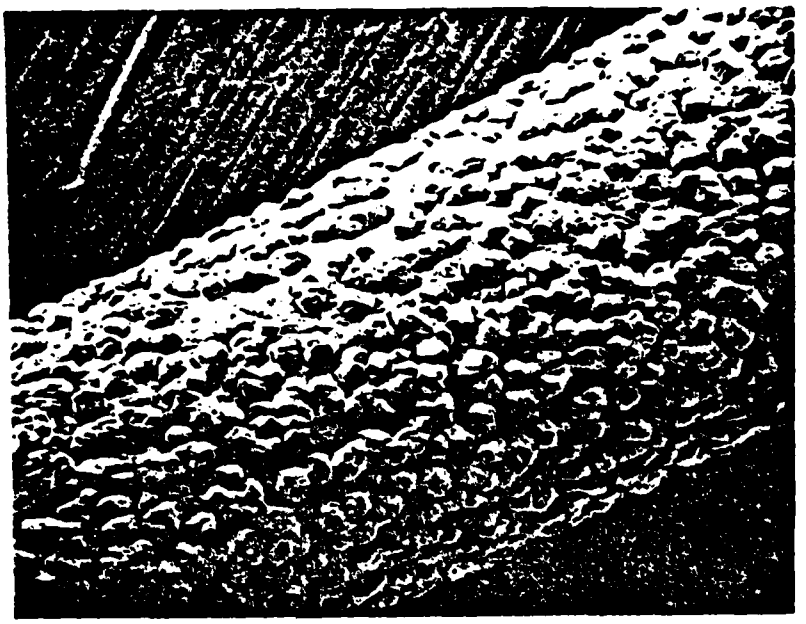

Fig. 5.16(a) - Nickel-boron sheath showing large crystallites of different form from the pure boron crystals shown in Fig. 5.14a. (200X, 41° angle).

Fig. 5.16(b) - Same as (a) at higher magnification (2000X, 41°).

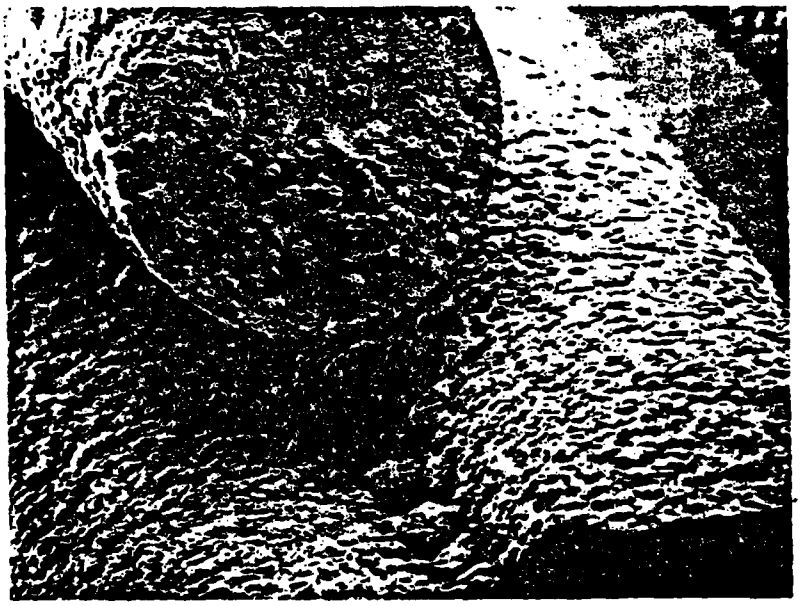

Fig. 5.17 - Boron recrystallization on the cross-section of one of the three fibers shown. (200X, 75° angle)

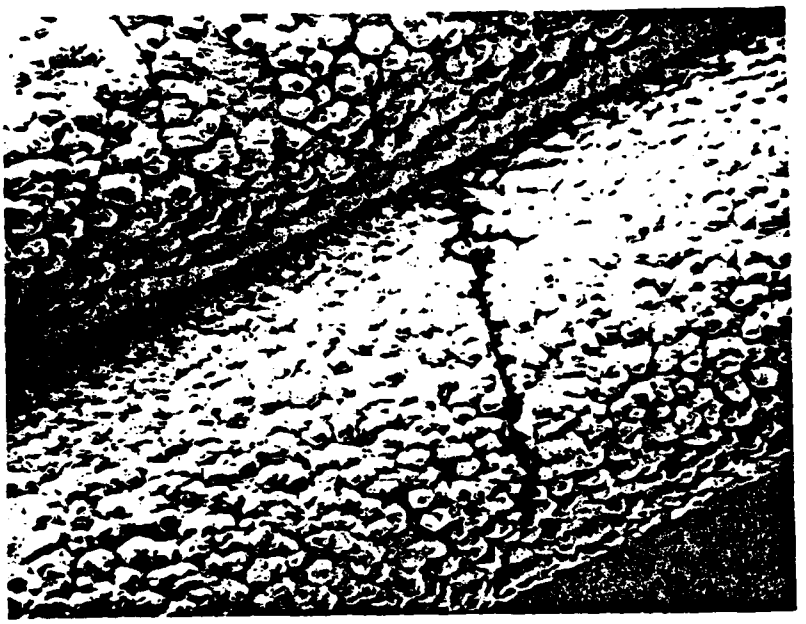

Fig. 5.18(a) - Cracks in the nickel-boron sheath and sintering from one fiber to another (200X, 41° angle).

Fig. 5.18(b) - Deep into the cracks of the Ni-B sheath we can see the surface of the fiber with dips due to diffusion of boron (2000X, 41° angle).

5.8 Summary of Electrical Measurements Data

The conductance of the samples discussed above are summarized below:

Table 5.8.1

Temperature(°C)	time of heat treatment(hrs)	G(mhos)
558°	6	6.896×10^{-4}
678°	6	2.100×10^{-3}
738°(*)	6	5.88×10^{-3}
804°	6	3.508×10^{-3}
914°	6	6.536×10^{-3}

(*) Different thickness of nickel was plated (6μm). All other samples have a thickness of 12μm.

For those samples where complete conversion of the nickel sheath occurred and a nickel-boron sheath appeared instead, it is sensible to find the conductivity of this transformed boron fiber. These calculated values are shown below:

Table 5.8.2

Temperature	σ(mhos/m)
804°C	0.257
914°C	0.479

5.9 Comments on the Results

The data thus far examined clearly show the irreversible process of surface recrystallization of massive amorphous boron. This phenomena accounts for significant reduction of the strength of boron fibers. Fibers heated above 850° - 900°C were so brittle that slight tension

would destroy the sample. Fibers heated above 1000°C were sometimes shattered inside the evacuated chamber without direct application of stress. Attempts were made to measure the conductivity of the recrystallized boron fibers. Fibers without a nickel sheath were heat treated and plated for electrical measurements. Several difficulties on plating were encountered for the heat treated fibers. The results were inconsistent and inconclusive.

Examination of the nickel-boron phase diagram indicated a nickel-boron eutectic at 1050°C. The SEM and electrical measurement analysis included here show formation of compounds well below 1050°C. It is not clear if a new nickel-boron eutectic was found. To check its existence would require further study and is beyond the scope of this thesis.

The conduction of the samples was measured first as the samples came out of the furnace and later after they were replated with extra nickel. The results in both cases were the same. Some samples were also dipped in a 1:1 solution of HF and HNO_3 to remove excess nickel after heat treatment. Later, these samples were replated and remeasured and the results were the same as before. The results presented here detail the recrystallization mechanism and its relation to fiber deterioration. The migration of nickel into boron and vice-versa and the creation of compounds are useful to show that there is still much to be understood about the nickel-boron system. As far as the possibility of conductivity modification while maintaining original mechanical properties, the experiments in the 700°C - 750°C temperature range suggest the possibility of improvement of fiber conductivity with small concentration of plated nickel and shorter time of heat treatment.

CHAPTER VI

EXPERIMENTS ON CARBON DIFFUSION IN BORON FIBERS

6.1 Introduction

Doping of polycrystalline boron with carbon at temperatures around 2300°C was reported by Hagenlocker [19] using samples grown on a tantalum substrate from boron tribromide. After removal of the Ta filament, the material was heat treated by a floating zone technique and impurities such as C, Si and Be were introduced in the melt. Samples doped with carbon showed a change in conductivity up to nearly three orders of magnitude (at 300K). The impurity concentration for samples doped with carbon was 0.1%. The temperature of the molten zone during the introduction of the impurities was 2300°C.

Those results were encouraging for the prospect of doping boron fibers with carbon to increase its conductivity. A series of experiments were performed for carbon diffusion in boron fibers. Before we discuss the results of these experiments, let us compare Hagenlocker samples with our boron fibers. The samples grown by Hagenlocker were 400 - 500μm in diameter. They did not have the inner core filament (Ta). After the floating-zone process, the material was polycrystalline with crystallites between 0.2 - 2.0 mm in size. The material, although of cylindrical geometry was 24 times larger in diameter than a boron fiber (203μm diameter). The conductivity at room temperature (300K) was very low compared to the boron fiber conductivity ($\sim 2.5 \times 10^{-7}$ mhos/cm compared to 8.17×10^{-4} mhos/cm for the 8 mils diameter boron fiber). The energy gap calculated from the Hall constant data was found to be 1.6eV, while the thermal energy gap for the fibers was much smaller (.19eV) as shown

in Chapter III. These differences plus the different methods employed for diffusion will be used later in this chapter to explain our results.

6.2 Experimental Section

The temperatures for the diffusion experiments with carbon was limited within the range where the fiber still maintained its mechanical properties. This was necessary because the intent of this work was to increase the conductivity of the fiber without changing the properties of the fiber. Also, the deterioration of the mechanical properties would make it difficult to do electrical measurements.

Two different types of carbon sources were used. Some samples were covered by a mixture of powdered graphite and water (then the samples were dried to remove the water). Other samples were coated with PELCO's colloidal graphite (aqueous base), #1603-15.

After the heat treatment, the fibers were cleaned in an ultrasonic cleaner and nickel plated. There was no difference in the electrical measurements between fibers that were coated with different carbon sources.

As explained in Chapter V, fibers that were heat treated then nickel plated, gave inconsistent and inconclusive values for the measurements of electrical conductivity. We can use these values here to compare with the fibers that were coated with graphite and undergone heat treatment. Although, as it will be shown below, the scatter of the data is large, it is still the only basis for comparison since it may be argued that plating after heat treatment is not a good technique and obscures any information that could be gathered from the diffusion experiments.

The resistance measurements for 8 mils diameter, 8 cm long fibers with a plated length of 1 cm per end of the sample is summarized below

(all fibers with isolated tungsten core)

Table 6.2.1

Temperature(°C)	Condition	R(ohms)
800	uncoated, just heat treated	2083.33
800	coated with graphite	1660.0
850	uncoated, just heat treated	1000.0
850	coated with graphite	1785.0
900	uncoated, just heat treated	2000.0
900	coated with graphite	1923
950	uncoated, just heat treated	1162.8
950	coated with graphite	1315.8

The heat treatment time was 24 hours for all samples. Fibers that were cleaned with H_2SO_4 after heat treatment (all samples were cleaned before heat treatment with the standard techniques described in Appendix A) showed a small increase in the resistance. The standard resistance measured for 8 mils samples of as received fibers was 892.85 ohms which agrees to the values used to calculate the conductivities described in Chapter VII.

The data are inconclusive. After several experiments, this technique was replaced by the nickel doping described in Chapter V. On the basis of the results above, and the inconsistent measurements of heated-

then-plated fibers, the conductivity modification due to carbon diffusion may not be explained.

The trend of the heat treatment was to double the resistance of a fiber whether it was coated or not with graphite. This doubling the resistance trend was also noticed in samples that were etched by HNO_3 without heat treatment.

In conclusion, carbon diffusion in boron fibers was not successful at this temperature range. In comparison with the Hagenlocher experiments, the difference in temperatures used was nearly 1400°C. Even at high temperatures, Hagenlocher samples showed very small solute concentration. Our data could not be fully analyzed because the "just heated" samples used for comparison with "coated samples" had inconsistencies in their electrical measurements. Also, as described in Chapter V, recrystallization mechanisms on the surface could have influenced the plating after heat treatment. Because of the need for high temperatures for carbon diffusion, the intrinsic properties of the fiber prevent successful conductivity modification while maintaining the original mechanical properties.

AD-A091 025 NOTRE DAME UNIV IN DEPT OF ELECTRICAL ENGINEERING F/G 11/4
MODELING AND MODIFICATION OF THE ELECTROMAGNETIC PROPERTIES OF --ETC(U)
1980 W J GAJDA, P K AJMERA, W C STRIEDER AFOSR-77-3453
UNCLASSIFIED AFOSR-TR-80-1071 NL

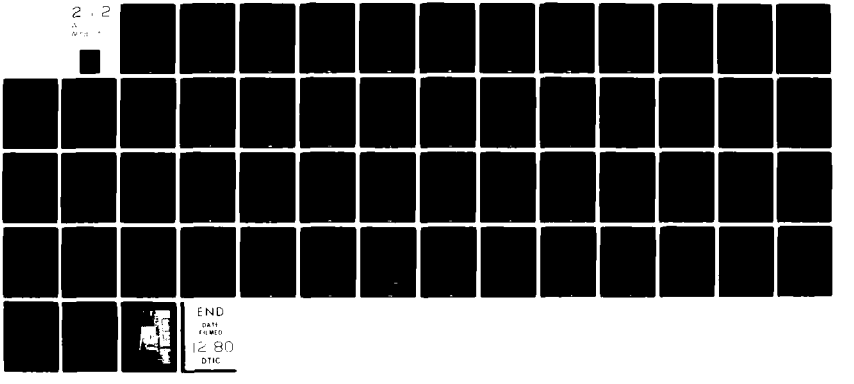

END
DATE FILMED
12 80
DTIC

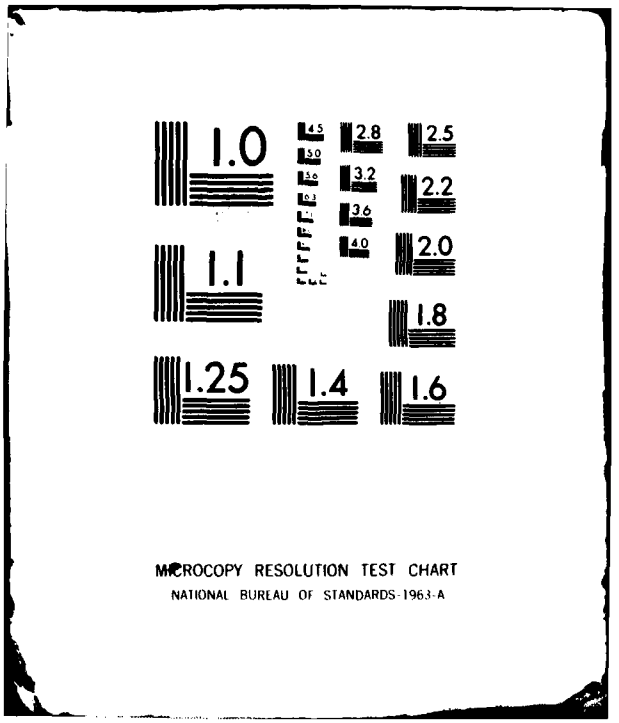
1.0
1.1
1.25
1.4
1.6
1.8
2.0
2.2
2.5
2.8
3.2
3.6
4.0
4.5
5.0
MICROCOPY RESOLUTION TEST CHART
NATIONAL BUREAU OF STANDARDS-1963-A

CHAPTER TWO - SIX REFERENCES

[1] Franklin E. Wawner, Jr., "Modern Composite Materials", edited by Broutman and Krock, Addison-Wesley, 1969.

[2] W. Gajda, Jr., "A Fundamental Study of the Electromagnetic Properties of Advanced Composite Materials," RADC-TR-78-158 Phase Report, July, 1978.

[3] J.L. Hoard and R.E. Hughes, "Elemental Boron and Compounds of High Boron Content: Structure, properties and polymorphism", The Chemistry of Boron and its Compounds, edited by E.L. Muetterties, John-Wiley and Sons, New York, 1967.

[4] H.M. Otte and H.A. Lipsitt, "On the Interpretation of Electron Diffraction Patterns from "Amorphous Boron," Phys. Stat. Sol. 13, 439 (1966).

[5] P.F Lindquist, M.L. Hammond, and R.H. Bragg, "Crystal Structure of Vapor-Deposited Boron Filaments", Journal of Applied Physics, Vol. 39, No. 11, pp. 5152, 1968.

[6] J.S. Gillespie, "Crystallization of Massive Amorphous Boron", Journal Amer. Chem. Soc., Vol. 88, pp. 2423-2425, 1966.

[7] H.M. Otte, H.A. Lipsitt, P.F. Lindquist, M.L. Hammond and R.M. Bragg, "Further Comments on the paper "On the Interpretation of Electron Diffraction Patterns from 'Amorphous' Boron", short notes, Phys. Stat. Sol. 19, 99, (1967).

[8] C.P. Talley, "Preparation and Properties of Massive Amorphous Elemental Boron", Boron Synthesis, Structure and Properties, edited by Gaule et al., Plenum Press, New York, 1960.

[9] S.M. Sze, "Physics of Semiconductor Devices", Wiley-Interscience, New York, 1969.

[10] Raymond Thomson, "The Chemistry of Metal Borides and Related Compounds", "Progress in Boron Chemistry", Vol. 2, edited by R.J. Brotherton and H. Steinberg, Pergamon Press, London, 1970.

[11] W.J. Gajda, Jr., R. Kwor and C. Araujo, "Low Frequency Electrical Conductivity of Boron Fibers", in preparation (1979).

[12] D. Madelung, "Introduction to Solid-State Theory", Chapter 10, Springer-Verlag, Berlin, New York, 1978.

[13] A.A. Berezin, "Electrical and Optical Properties of Amorphous Boron and Amorphous Concept for β-rhombohedral Boron", Journal of Non-Crystalline Solids, Vol. 16, pp. 237-346, 1974.

[14] F.E. Wawner, Jr., "The Effects of Chemical Polishing on the Strength and Fracture Characteristics of Amorphous Boron Filaments", "Boron II", edited by G.K. Gaule, Plenum Press, New York 1965.

[15] R.J. Smith, "Changes in Boron Fiber Strength Due to Surface Removal by Chemical Etching," NASA TN D-8219, Lewis Research Center, Cleveland, 1976.

[16] J.A. DiCarlo, "Techniques for Increasing Boron Fiber Fracture Strain" NASA TMX-73627, Lewis Research Center, Cleveland, 1977.

[17] R.C. Ellis, Jr., "Some Etching Studies on Boron", "Boron, Synthesis, Structure, and Properteis", edited by Gaule et al., Plenum Press, New York, 1965.

[18] C.R. Barrett, "The Principles of Engineering Materials", Prentice-Hall, New Jersey, 1973.

[19] A.K. Hagenlocker, "Halbleitereigenschaften von Bor", doctoral dissertation, Technische Hochschule, Stuttgart, 1958.

7. MODELING OF THE ELECTRICAL CONDUCTIVITY OF ADVANCED COMPOSITE MATERIALS

7.1 Unidirectional Plies - Infinitely Thick Case

A goal of this research is to derive the functional relationship between the electrical conductivity of a fiber reinforced composite with highly conductive fibers and an insulating matrix, and the fiber volume fraction, fiber conductivity, and the contact resistance between the fibers. A sound model for the composite as well as a clear understanding of the relevant phenomena are a prerequisite to the successful completion of such a task. Such a relationship will be useful for the correlation of electrical conductivity data and would eliminate the necessity of expensive experimental measurements. Also, a reliable model may allow us to relate electrical conductivity to interfacial contact areas and to the presence of fiber to fiber contact paths across the individual unidirectional composite plies and these properties in turn may effect the mechanical properties of the composite.

A very simple model of the single unidirectional ply of a fiber reinforced composite was suggested by Adams and Tsai[7-1,7-2]. In their square lattice model, Figure 7-1, the circular fiber cross sections are packed one into each square element of a Cartesian two-dimensional space. To introduce randomness, fibers are removed from the perfect square packing according to a random procedure that satisfies a fixed fiber square fraction x.

Since the fibers must touch as they do in Figure 7-1a, the fiber volume fraction x_f and fiber square fraction x are related by

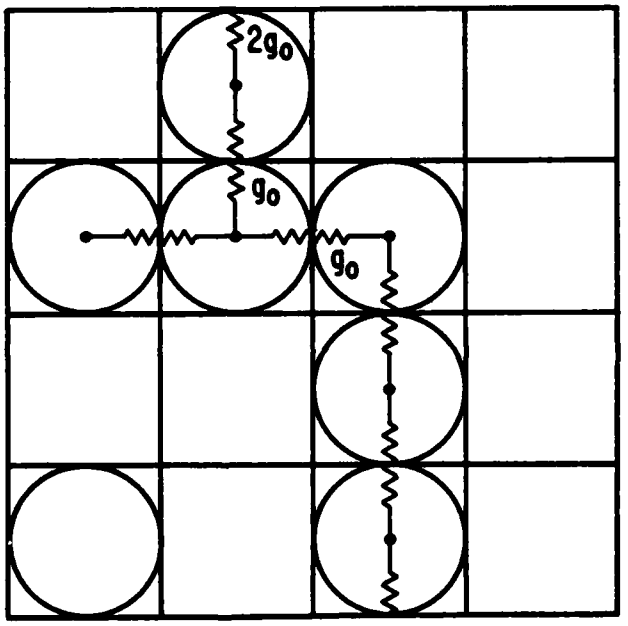

Random Square Lattice

FIGURE 7-1

$$x_f = \pi x/4 \tag{7-1}$$

for the square lattice. The only non-physical restriction of this model is to confine the fibers to rows or columns. Adams and Tsai[7-2] assert that this constraint is secondary to the importance of the introduction of randomness.

One improvement is suggested by the examination of photomicrographs in which fiber cross sections appear to be nearly close packed circles. Figures 7-2 and 7-3 introduce two types of two dimensional close packed structures - the simple close packed and honeycomb close packed models. Again, the randomness characteristic of the real physical system is introduced by removing the fibers by a random number procedure to satisfy a certain fiber hexagon fraction x. Note that x is the fraction of fibers compared to the total that complete packing can accommodate and is related to the fiber volume fraction by

$$x_f = \frac{\pi}{2\sqrt{3}}\, x \tag{7-2}$$

for the simple close packed structure and

$$x_f = \frac{\pi}{3\sqrt{3}}\, x \tag{7-3}$$

for the honeycomb close packed structure. The resistance wires of Figure 7-3 form a honeycomb for the fully packed honeycomb structure and the network can accommodate one-third less fibers than the simple close packed structure.

The electrical conductivity of a single ply of unidirectional composite where the fiber is highly conductive and the matrix is insulating is dominated by the passing of electrical current through the small contact

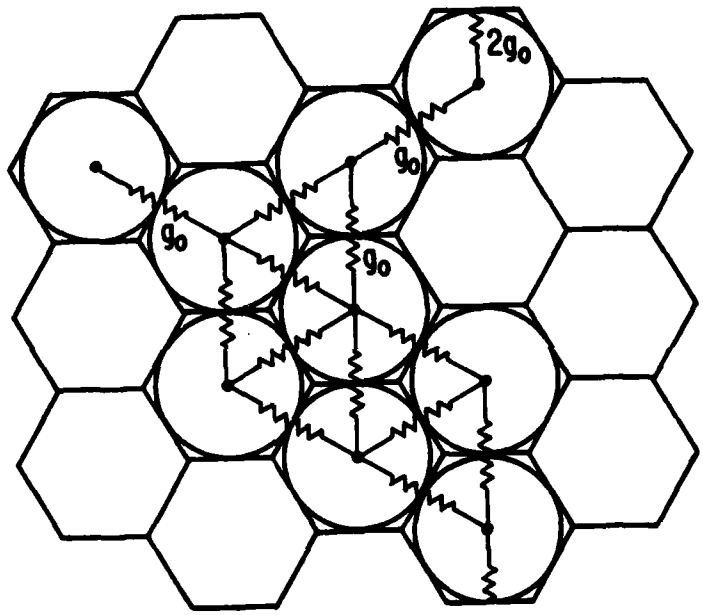

Random Simple Close Packed
or Triangular Lattice

FIGURE 7-2

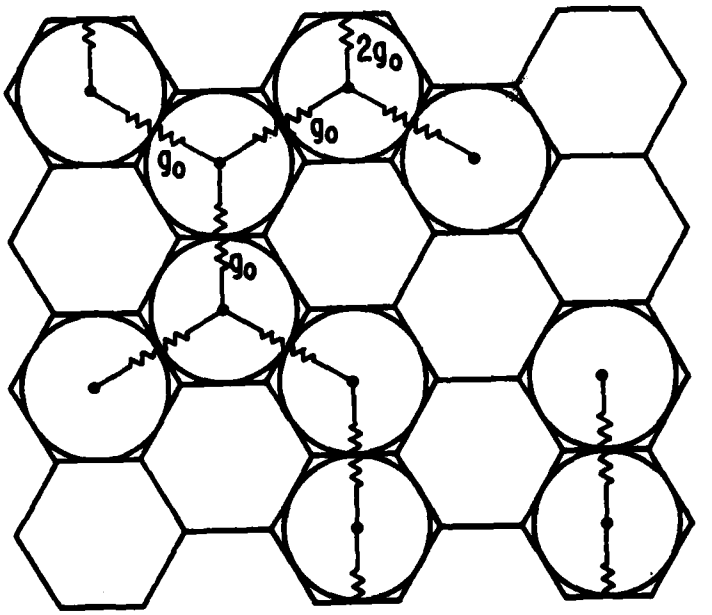

Random Honeycomb
Close Packed Lattice

FIGURE 7-3

points between the fibers. The conductance g_o between two adjacent fibers will be substantially less than the fiber conductivity. Both ideal contact conductance and surface roughness conductance contribute significantly to g_o and the experimental contact conductance g is a measure of both conductances in series. Hence, drawn in on Figure 7-1, 7-2, and 7-3, between any two circles in contact is a conductance g_o and the problem becomes one of the conductivity of a network of conductances g_o with sites (all the conductances g_o about a single junction set to zero) or fiber cross sections removed at random.

The random conductivity of an infinite lattice of resistors with sites removed at random may be obtained from the effective medium theory of random lattices as introduced by Kirkpatrick[7-3] and extended by Watson and Leath[7-4]. In effective medium theory, the conducting and non-conducting sites are introduced as perturbations in a lattice of effective resistances. The method is attractive both for its simplicity and the apparent accuracy of its results when compared with simulations[7-3,7-4]. A complete outline of the theory is presented in several of the attached publications.

Watson and Leath[7-4] calculated with effective medium theory, the conductivity of the random site square lattice of conductances g_o, a model for a unidirectional single ply of composite, in terms of the fiber volume fraction x_f

$$\sigma = g_o[1 - \frac{\pi}{2} + \frac{8}{\pi} x_f^2] \qquad (7\text{-}4)$$

They compared this equation to the simulation of a random site square lattice of conductances by removing, at random, wire crossing sites from a conducting screen and obtained excellent agreement. When the fibers are highly conductive and the matrix is an insulator, lattice conductivity

must depend on paths across the slab (see Figures 7-1, 7-2, and 7-3) made up of contacting fiber cross sections. At lower fiber concentrations due to the random fiber placement such paths will not exist, only isolated small clusters or groups of fibers will be found, and the conductivity will remain zero even though x_f is finite. Eventually, at a critical fiber fraction x_{fc}, when a sufficient number of fiber cross sections are present, such paths will appear in significant numbers and the lattice will conduct. This critical phenomena is called percolation. Equation (7-4) reflects this in the sense that

$$\sigma \leq 0 \quad \text{for} \quad x_f \leq 0.47 \tag{7-5}$$

or, in other words, percolation occurs at the critical fiber fraction

$$x_{fc} = 0.47 \tag{7-6}$$

We have derived the effective medium equations of several improved models of the ply cross section of a unidirectional composite. In the close packed or triangular lattice[7-7] we present (in the attached publications) the solution for the electrical potential of a perfect infinite triangular network of resistors with a point current source. This result is used with effective medium theory to obtain a lattice conductivity for a simple close packed random fiber lattice. Figure 7-2

$$\sigma = g_o \sqrt{3} \left[1 - \frac{6\pi}{\pi + 6\sqrt{3}} + \frac{72}{\pi(\pi + 6\sqrt{3})} x_f^2\right] \tag{7-7}$$

which percolates at $\sigma(x_{fc}) = 0$

$$x_{fc} = 0.48 \tag{7-8}$$

An additional model for a composite of close packed fibers[7-8] is the honeycomb lattice and our results of this case (in the attached preprints) are

$$\sigma = \frac{g_o}{\sqrt{3}} \left[\frac{54}{\pi^2} x_f^2 - 1\right] \qquad (7\text{-}9)$$

which percolates at

$$x_{fc} = 0.43 \qquad (7\text{-}10)$$

Yuge[7-9] has presented another approach of the effective medium theory based on the concept of an average bond. Yuge's calculations are less rigorous than those which led to equations (7-5 to 7-10). In fact, Yuge used random bonds to calculate the conductivity of a random <u>site</u> lattice and 7-7, we point out, is one of the enclosed preprints that his final results are in error. Yuge's conductivity is

$$\sigma = \frac{9}{\pi} x_f \left[\frac{2\sqrt{3}}{\pi} x_f - \frac{1}{3}\right] \qquad (7\text{-}11)$$

which percolates at

$$x_{fc} = 0.30 \qquad (7\text{-}12)$$

All four theories are compared in Figure 7-4 with available conductivity data [7-10]. The constants g_o obtained with a least squares fit of the data (see Appendix 7-1) are listed in Table 7-1 along with the conductivity values for the fiber and epoxy matrix. If we consider only x_f - 0.6 and 0.7, the square and triangular lattice gives best fits. For the three largest points x_f - 0.5, 0.6, and 0.7, the honeycomb lattice gives the best fit. For all four parts, Yuges' "average" bond theory gives the best overall fit, but it is based on the poorest theory.

Table 7-1

Fiber to Fiber Contact Conductives

Lattice	Conductivity (mhos/m)
Triangular	465
Square	299
Honeycomb	201
Yuge	209
Epoxy	10^{-4}
Graphite Fibers	10^{4}

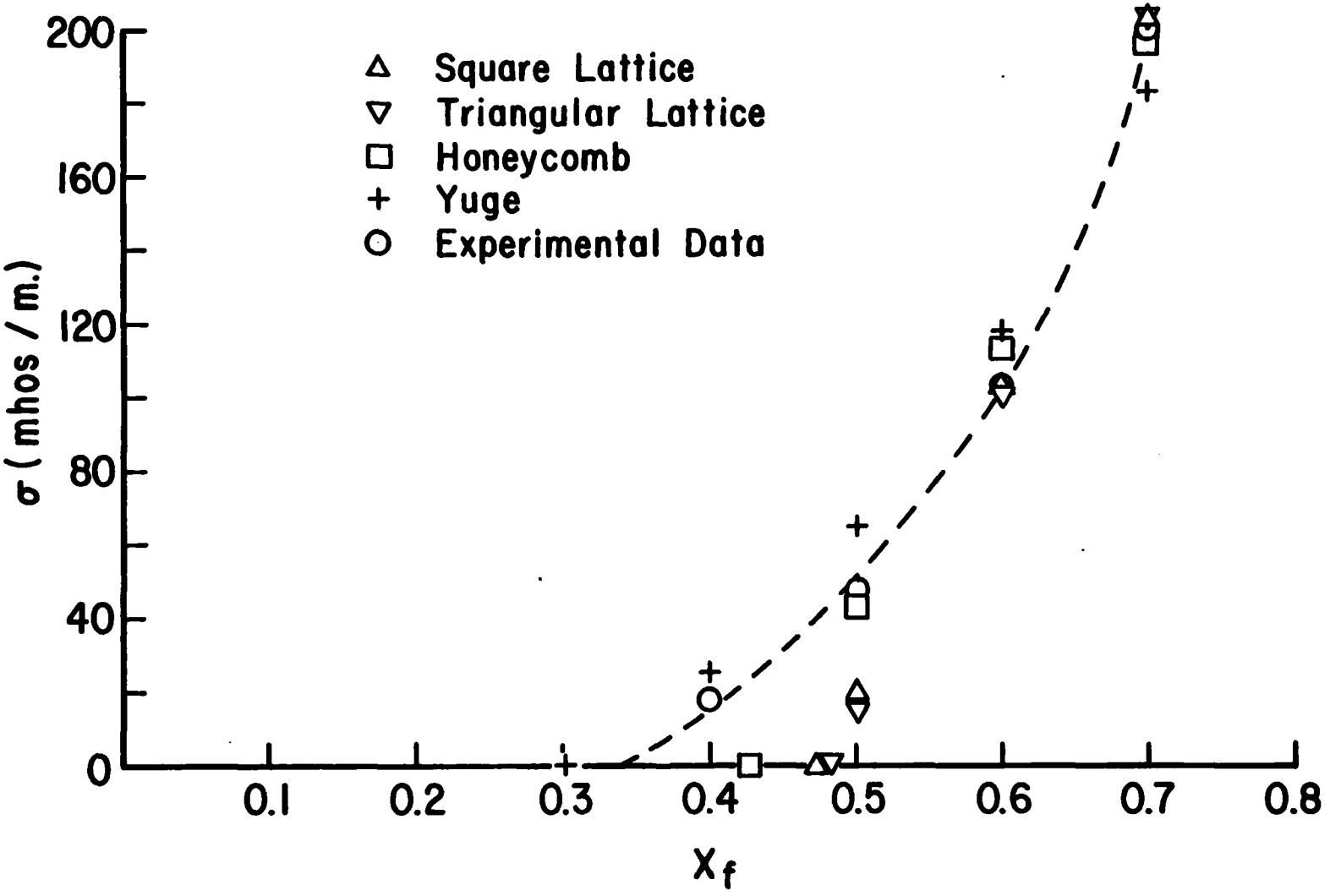

FIG. 7-4 - Conductivity Versus Fiber Volume Fraction

Hertzian [7-5, 7-6] ideal contact resistances, i.e. the resistance to conduction of two perfectly smooth cylinders in contact, account for about half of the conductivity reductions from the fiber value observed in the fiber to fiber contact conductances of Table 7-1. The rest of the reduction is due to a number of factors, not the least of which is surface roughness which requires an experimental parameter to describe the surface geometry. As a result, the contact resistance depends upon the details of fiber preparation.

7.2 Unidirectional Plies - Slabs of Finite Thickness

The experimental conductivities of Figure 7-2 are measured transversely across a single ply slab of graphite/epoxy. Deviations of theory from experiment in Figure 7-4 are most probably due in large part to the finite thickness of the single ply slab. We have shown from square lattice studies[7-11] that a slab must be about 150 fiber diameters thick before it can be regarded as infinitely thick. Commercial pre-preg tapes were only about 20 fiber diameters thick, the transverse conductivity through the ply is that of a finite slab. The theoretical analysis of the conductivity of a finite ply divides itself into two parts: the lattice statistics of percolation, i.e. the probability of path formation across in a very wide slab of finite thickness, and the computer solution of Kirchoffs equation in a ply cross section of infinite width and finite thickness.

We have begun our studies of the effects of finite thickness on the onset of percolation with the random square lattice problem. When fibers are placed at random in a square lattice, clusters of fibers of varying sizes form. Not until a critical fiber fraction x_{fc} is reached are there significant numbers of fiber clusters of sufficient size that equal or exceed the ply thickness. Hence, for composites of conducting fibers and insulating matrix, electrical conduction begins only a critical fiber fraction x_{fc}.

By counting fiber to fiber contact paths across a computer simulation of a single ply, we were able to determine values of the critical fiber fraction x_{fc} for various single ply thicknesses λ, expressed as integer multiples of the fiber diameter. The critical fiber fraction for a ply of $\lambda = 20$ fiber diameters is

$$x_{fc} \ (\lambda = 20) = 0.34$$

and is shifted to the left compared to the value for percolation in an infinite slab;

$$x_{fc} \ (\lambda = \infty) = 0.46$$

From our numerical results in the random square lattice, we can sketch the conductivity curve for a $\lambda = 20$ fiber diameter sample and it is shown as the dashed line in Figure 7-4. From our lattice statistics calculations [7-10] we can conjecture that the points of the random square lattice curve of Figure 7-4 at higher x_f, i.e., 0.6 and 0.7, will not be strongly affected by the finite thickness. Furthermore, points at lower fiber fractions x_f will shift to the left and, for the square lattice, will percolate at 0.34. Using these facts, we propose that the square lattice curve will probably look like the dashed line of Figure 7-2 and should agree very well the experimental data. Only the square lattice x_{fc} has been done, calculations of the critical fiber fraction of a simple close packed lattice, Figure 7-2, are presently underway.

More accurate curves will require an iterative computer solution of Kirchoffs equations in the square and simple close packed lattices, part of our present efforts. From the infinite lattice equations (7-4 to 7-12), we can already place approximate upper and lower limits on the results of the variation of conductivity with thickness λ for fixed fiber fractions

x_f. These limits are given in Table 7-2.

Table 7-2

Limit on Conductivity Variation with Thickness

x_f	Random Square Lattice $\sigma_{\lambda=\infty}/g_o$ Lower Limit	Random Close Packed Lattice $\sigma_{\lambda=\infty}/g_o$ Lower Limit	$\sigma_{\lambda=1}/g_o$ Upper Limit
0.7	0.677	0.437	.891
0.6	0.346	0.217	.764
0.5	0.066	0.031	.637
0.4	0	0	.509

Percolation certainly effects the electrical and thermal conductivities of important fiber reinforced composites e.g., graphite/epoxy. But percolation guarantees that clusters of fibers will run completely across the ply and may also affect mechanical properties. Such percolation related phenomena may not be easy to include in model calculations of mechanical properties but may arise in mechanical experiments on composite materials at these critical fiber fractions. Lattice statistics and calculations of critical fiber fractions for percolation, and their variation with ply thickness, are important to the general area of composite materials and not just to the understanding and modeling of electrical conduction.

J. Phys. C: Solid State Phys., Vol. 11, 1978. Printed in Great Britain. © 1978

LETTER TO THE EDITOR

Effective medium theory of site percolation in a random simple triangular conductance network

Thomas Joy† and William Strieder‡

† Department of Electrical Engineering, University of Notre Dame, Notre Dame, Indiana 46556, USA

‡ Department of Chemical Engineering, University of Notre Dame, Notre Dame, Indiana 46556, USA

Received 14 August 1978

Abstract. An effective medium theory, which includes the overlap of adjacent removed sites, is formulated for a percolating, two-dimensional triangular lattice. The critical concentration $x_c = 0.531$ is compared with Yuge's value $x_c = 0.333$, and the exact value $x_c = 0.500$.

The effective medium theory of a random lattice of resistors has received considerable attention in the recent literature (Kirkpatrick 1973, Watson and Leath 1974, Butcher 1975) largely because of its simplicity and the fact that it exhibits conductive percolation. Watson and Leath (1974) and Watson (1975) have developed the effective medium theory equations for the site model of a percolating, random, two-dimensional square lattice of resistors. In their percolating site model, a fraction $1 - x$ of the nodes (sites) were selected at random from an infinite lattice of conductances g_i, and the entire cluster of conductances about each site were changed to zero. As Butcher (1975) points out, these clusters must overlap, so that the fraction of insulating clusters is given by $1 - b = 1 - x^2$ and the fraction of conducting clusters by the bond probability b

$$b = x^2. \tag{1}$$

The close packed structure is common in certain experimental materials such as granular packed beds or fibre reinforced composites, and the corresponding lattice structure in two dimensions is triangular. There is some interest in exploring the form of the effective medium equations for the site model of a simple triangular lattice.

We proceed to apply simple effective medium theory to the site percolation problem in a triangular lattice (figure 1) and observe that for effective medium theory:

(i) The net effect of the random conductances is represented by a homogeneous effective medium with equal conductances g_m connecting all the nearest-neighbour sites of the triangular lattice.

(ii) The average field inside the medium is equal to the externally applied field, which increases by a constant amount V_m per each row of nodes, and:

(iii) Local fluctuations in the voltage ΔV induced when g_m is replaced by g_0 or by a vanishing conductance should average to zero.

Consider the site S selected at random in the lattice (figure 1(*a*)) and change the cluster of conductances about S from g_m to g_0 (or zero). The uniform solution V_m fails to

0022-3719/78/0021-9867 $01.00

For a single current source i_0 injected at the centre (0, 0) of an infinite triangular lattice

$$\phi(x, y) - \phi(0, 0) = \frac{i_0}{2\pi g_m}\int_{-1}^{1} du(1-u^2)^{-1/2}(2+2u)^{-1/2} I^{-1/2} \times \{T_x(u)[(3-u)(2+2u)^{-1/2} - I^{1/2}(u)]^{2|y|/\sqrt{3}} - 1\}, \quad (5)$$

where

$$I(u) = [(3-u)(2+2u)^{-1/2}]^2 - 1$$

and

$$\times\ T_x(u) = \cos(x \cos^{-1} u).$$

Lattice site coordinates are defined by the possible pairs (x, y) from

$$x = 0, \pm 1, \pm 2, \ldots$$
$$y = 0, \pm\sqrt{3}, \pm 2\sqrt{3}, \ldots, \quad (6)$$

or from the possible pairs (x, y) of

$$x = \pm\tfrac{1}{2}, \pm\tfrac{3}{2}, \ldots$$
$$y = \pm\sqrt{3}/2, \pm 3\sqrt{3}/2, \ldots. \quad (7)$$

The difference in potential between F and D for the infinite effective lattice of figure 1(*a*) is obtained by superposition of the potential differences from each current i_0; the conductance G_{FD} is determined to be

$$G_{FD} = (\tfrac{4}{3} - 2\sqrt{3}/\pi)^{-1} g_m. \quad (8)$$

The extra voltage ΔV across FS of figure 1(*b*) due to the presence of the conductances g_0 from equations (2), (3), (4), and (8) is written

$$\Delta V = V_m(g_m - g_0)/[g_0 - g_m + 2(\tfrac{4}{3} - 2\sqrt{3}/\pi)^{-1} g_m]. \quad (9)$$

But it follows from condition (iii) for an effective medium that the average $\langle \Delta V \rangle$ from the conducting and non-conducting clusters must vanish,

$$\langle \Delta V \rangle = (1-b)\, V_m/[2(\tfrac{4}{3} - 2\sqrt{3}/\pi)^{-1} - 1] + bV_m(g_m - g_0)/[g_0 - g_m + 2(\tfrac{4}{3} - 2\sqrt{3}/\pi)^{-1} g_m] = 0. \quad (10)$$

Butcher (1975) has presented an alternative derivation to the effective medium equations of a random lattice. Though his discussions are restricted to square lattices, they can be easily generalised to the triangular case, and equations (9) and (10) are of the same form as Butcher's equations (1), (4*a*), and (4*b*). In this Letter, we have identified the constant λ that Butcher discusses, for a percolating triangular lattice to be

$$\lambda = \tfrac{4}{3} - \sqrt{3}/\pi. \quad (11)$$

In addition we must include a factor of 2 in the net conductivity

$$\sigma = \sqrt{3}\, g_m \quad (12)$$

for our triangular lattice, since there are two wires that carry current, rather than one as in Butcher's square lattice.

Solving for g_m from (10), substituting into (12), and relating the bond probability b

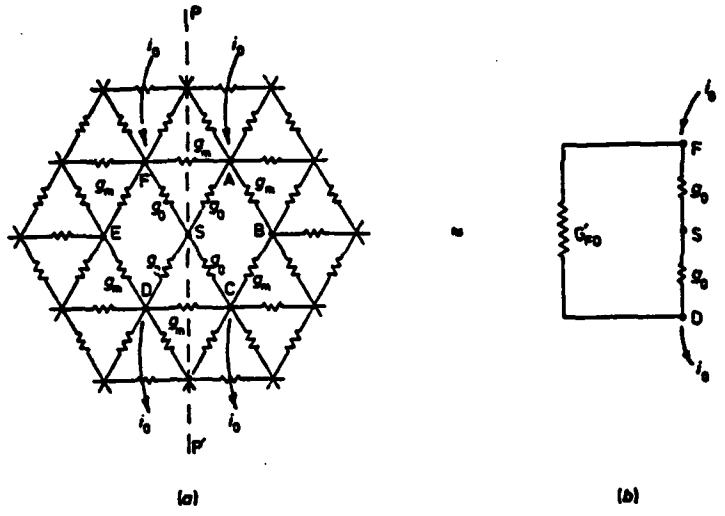

Figure 1. Single site S of a triangular lattice. Conductances g_0 around S within an effective network of conductances. Conductances g_{ES} and g_{BS} can be ignored.

satisfy current conservation at sites A, C, D and F; the magnitude of the current i_0, introduced or extracted at A, C, F and D, is chosen to correct for this

$$i_0 = V_m(g_m - g_0). \tag{2}$$

The external potential is applied vertically, furthermore the lattice and the site currents i_0 are symmetric with respect to the line EB. This symmetry is sufficient to suppress any transverse currents in g_{ES} and g_{BS} and these conductances may be ignored.

A second symmetry of the lattice and the site currents i_0 about the line PP' of figure 1(*a*), implies that current cannot flow across any point on this line. Then we can regard the equivalent problem of a semi-infinite lattice insulated along the line PP' (see figure 1(*b*)). The extra voltage ΔV across FS can be calculated, if we know the conductance G'_{FD} between the points F and D on the semi-infinite lattice when g_{FD} is absent,

$$\Delta V = i_0/(g_0 + 2G'_{FD}). \tag{3}$$

The conductance G'_{FD} can be obtained directly from the conductance G_{FD} between F and D in the uniform semi-infinite effective medium, i.e., figure 1(*b*) with g_0 replaced by the effective value g_m

$$G_{FD} = \tfrac{1}{2}g_m + G'_{FD}. \tag{4}$$

The current to potential difference ratio G_{FD} across FD is then calculated from the equivalent problem of four symmetric currents introduced into the effective infinite lattice, i.e., figure 1(*a*) with $g_0 = g_m$. The electrical potential $\phi(x, y)$ at the various sites of the infinite triangular lattice have been derived through a straightforward though tedious extension of Van Der Pol and Bremmer's calculations (1950) on a square lattice.

to the site fraction x by (1), we obtain the variation of the random lattice conductivity with site fraction

$$\sigma = \sqrt{3}\left(1 - \frac{6\pi}{\pi + 6\sqrt{3}}(1 - x^2)\right)g_0. \tag{13}$$

Percolation occurs when the conductivity vanishes [$\sigma(x_c) = 0$],

$$x_c = \left(1 - \frac{\pi + 6\sqrt{3}}{6\pi}\right)^{1/2}, \tag{14}$$

or

$$= 0.531. \tag{15}$$

It is known that the greatest inaccuracies of the effective medium theory occur near percolation. From exact lattice calculations (Sykes and Essam 1964) percolation in a triangular, random site lattice is observed at $x_c = \frac{1}{2}$; at percolation equation (13) is in an error by only 6%. On the other hand Yuge (1977) has proposed a modified effective medium theory based on 'average bonds,' which would predict

$$\sigma = \frac{3\sqrt{3}}{2}g_0 x(x - \tfrac{1}{3}) \tag{16}$$

and percolate at $x_c = \frac{1}{3}$ in error by 33%.

The authors wish to thank the Air Force Office of Scientific Research who provided the financial support for the research under grant number AFOSR 77-3453.

References

Butcher P N 1975 *J. Phys. C.: Solid St. Phys.* 8 L324–7
Kirkpatrick S 1973 *Rev. Mod. Phys.* 45 574–88
Sykes M F and Essam J W 1964 *Phys. Rev.* 133 A310–5
Van der Pol B and Bremmer H 1950 *Operational Calculus* (Cambridge: University Press) pp 371
Watson B P 1975 *Phys. Rev.* C 12 498
Watson B P and Leath P L 1974 *Phys. Rev.* B 9 4893–6
Yuge Y 1977 *J. Statist. Phys.* 16 339–48

Percolation in a Thin Ply Of Unidirectional Composite

THOMAS JOY

Department of Electrical Engineering
University of Notre Dame
Notre Dame, Indiana 46556

AND

WILLIAM STRIEDER

Department of Chemical Engineering
University of Notre Dame
Notre Dame, Indiana 46556

(Received October 2, 1978)

ABSTRACT

A unidirectional composite is modeled as a two-dimensional cartesian square lattice of infinite width and finite thickness. Circular fiber cross sections, each contained completely within a lattice square and touching on all four sides, are placed at random within the lattice according to the fiber volume fraction. Percolation, in this system, is shown to be very sensitive to the lattice thickness. To be regarded as infinitely thick a lattice must be at least 150 fiber diameters across, and for a typical ply thickness of 20 fiber diameters the critical fiber fraction for percolation is shifted by 26% from the infinite lattice value of 0.46 to a smaller value of 0.34.

SCOPE

ADAMS AND TSAI [1,2] have suggested the random lattice model as an appropriate physical model for the effective transport properties of a unidirectional composite material. In their square lattice model each square element of a Cartesian lattice (Figure 1) is assigned either a complete fiber cross section or only matrix material according to a random number procedure and the fiber volume fraction. The fiber fraction x_f must be distinguished from the fraction x of fiber squares. If

Reprinted from Journal of COMPOSITE MATERIALS, Vol. 13 (January, 1979)

0021-9983/79/01 0072-07 $04.50/0

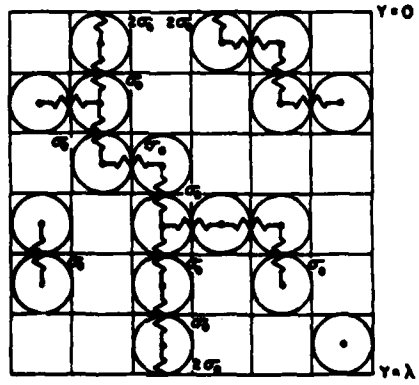

Figure 1. Random square lattice model six fiber diameters thick. Fiber to fiber conductance σ_0 is indicated on the current paths shown. Thickness λ is measured in fiber diameters.

the fibers touch as they do in Figure 1 the fiber fraction and fiber square fraction are related by

$$x_f = \frac{\pi x}{4} = 0.785x \tag{1}$$

for a square lattice. The only unphysical restriction of this model is to confine the fibers to rows or columns. Adams and Tsai [2] have pointed out that this constraint is secondary to the importance of the introduction of randomness.

Many papers [2–6] and reviews [7–9] have discussed the probabilities and statistical properties of an infinite random square lattice, largely because the infinite, random square lattice problem relates directly to the Ising model of statistical physics. The size of clusters of fibers and the cluster probabilities have been calculated, but the central and most physically relevant result of these studies is the prediction of a lattice phase condensation or the formation of infinite fiber clusters at a certain minimum critical fiber fraction x_{fc}. Infinite clusters do not occur within the infinite square lattice until a certain critical fiber block fraction [4]

$$x_c = 0.59 \quad . \tag{2}$$

Percolation will occur in unidirectional composites with a very highly conductive fiber phase and an insulating matrix phase. The prediction of the effective electrical (thermal) conductivity of such a medium, one of the more difficult problems of random media theory, can be modeled from the random lattice, if we insist that the

fibers touch, and represent the conduction between two adjacent fiber centers (Figure 1) by a conductivity σ_o. The matrix center to matrix center or matrix center to fiber center links have zero conductivity, present no path for the current, and can be omitted from Figure 1. Then the square lattice model predicts that, due to the absence of infinite clusters of fibers, the conductivity of a thick unidirectional composite slab (or infinite lattice) of highly conducting fibers in an insulating matrix will vanish below the critical fiber concentration and this phenomena is called percolation. The composite conductivity will vanish below the percolation concentration [4]

$$x_{fc} = 0.59 \times 0.785 = 0.46 \tag{3}$$

(the fiber square fraction times the fiber fraction per block).

A major difficulty with using the literature values for percolation of single ply unidirectional composites is that previous theory is addressed to the infinite limit. Results only apply to a single ply very large in both width and thickness, whereas in many cases the single ply is only a few fiber diameters thick. The conductivity of a single ply slab of composite will depend on the existence of unbroken paths that travel completely across the slab. To pose the question of existence of percolation in a thin ply, and to determine how the critical percolation concentration x_{fc} changes with ply thickness λ(in fiber diameters), we define the probability $P(x,\lambda)$ that a block on the edge of the ply will contain a fiber and connect with one or more paths across the composite. The variation of this probability with thickness will give some idea of when a slab is statistically thick, and its vanishing will provide a test for percolation.

CONCLUSIONS AND SIGNIFICANCE

From this study, the following conclusions can be drawn:

1. For fiber square fractions above 0.59 a significant number of paths exist across even an infinitely thick ply; below this critical concentration the conductivity of the infinitely thick ply must vanish.
2. A ply may be regarded as infinite if it is at least 150 fiber diameters thick.
3. For a typical single ply thickness of $\lambda = 20$ fiber diameters, the slab is not infinite, and the critical fiber square fraction at percolation is decreased from the infinite ply value of 0.59 to 0.43. The infinite medium result is in error by 27%. The corresponding critical fiber volume fraction is

$$x_{fc} = 0.785 \times 0.43 = 0.34 \tag{4}$$

at $\lambda = 20$ fiber diameters.

SUPPLEMENTARY INFORMATION

The calculations of the probability $P(x,\lambda)$ that an edge site at $y = 0$ will contain a fiber (Figure 1) which connects to an unbroken conduction path across the thickness of ply were performed on an IBM 370/158 computer. The composite was modeled as a two-dimensional cartesian lattice of infinite width and finite thickness, λ fiber diameters. The random fiber lattice was generated by placing circular fiber cross sections, all of the same diameter d, by a modular multiplication random number routine onto the squares (Figure 1) of the lattice with the additional constraint that on the average the fibers satisfy the fiber square fraction x (or fiber volume fraction $x_f = .785x$). For conductive percolation the fibers must be very good conductors and the matrix must be an insulator. The necessary conduction paths are simulated from fiber to fiber by insisting that each fiber, contained completely within the lattice square, touch the square edges on all four sides. The random structure occurs from the absence of fibers or clusters of fibers within the lattice.

To count the paths across the ply we addressed each square at the edge of the lattice. Algorithms to mark a conductance path starting from the edge square, to properly backtrack when the path was blocked, and avoid closed loops, located those cases where a path from the edge square completely crossed the slab. The ratio of edge squares that began such a path to the total number of edge squares considered gave us the probabilities $P(x,\lambda)$.

To assure statistical stability the probabilities calculated were calculated for a very wide slab but finite slab thickness, λ fiber diameters. Samples were taken 700 elements wide with specified thickness λ. On each side of the sample 100 edge squares were deleted from the path counting procedure to avoid end effect errors. Then 25 such samples were run. The cumulative sample average of $P(x,\lambda)$ was stable enough to provide sufficient accuracy for Figures 2 and 3.

Figure 2 contains the calculated path probabilities $P(x,\lambda)$ versus the ply thickness, λ fiber diameters, for various fiber square fractions x. The curves are clearly asymptotic at non zero values for $x > 0.59$, hence significant numbers of paths are found even at infinite thickness. Asymptotes form on the λ-axis for $x < 0.58$, we expect no conduction across an infinite slab for x below 0.58. For the infinitely thick lattice, asymptotic values of $P(x,\lambda)$ when divided by the fiber fraction always lie below the percolation probability [3–5] and either probability can be used to indicate percolation, however, the calculation of $P(x,\lambda)$ requires less computer time.

From Figure 2, asymptotes are most rapidly formed at high and low x. Asymptotes form at $\lambda_a = 6$ for $x = 0.7$; and at $\lambda_a = 14$ for $x = 0.4$. Asymptotes do not readily form near percolation, the $x = 0.58$ curve is not yet completely asymptotic at $\lambda = 150$. While these curves regard the problem from the point of view of the path probability, this model suggests that slab conductivity will increase with decreasing ply thickness in a thin ply of fiber reinforced composite, and that this effect will be most important near the percolation concentrations.

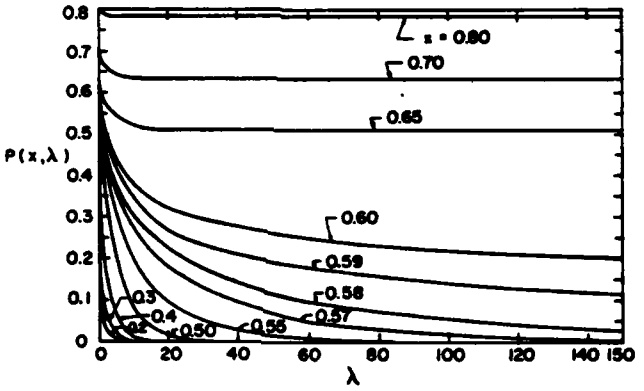

Figure 2. Path probability P(x,λ) of a random square lattice of conducting fibers plotted versus the ply thickness λ in fiber diameters for various fiber block fractions.

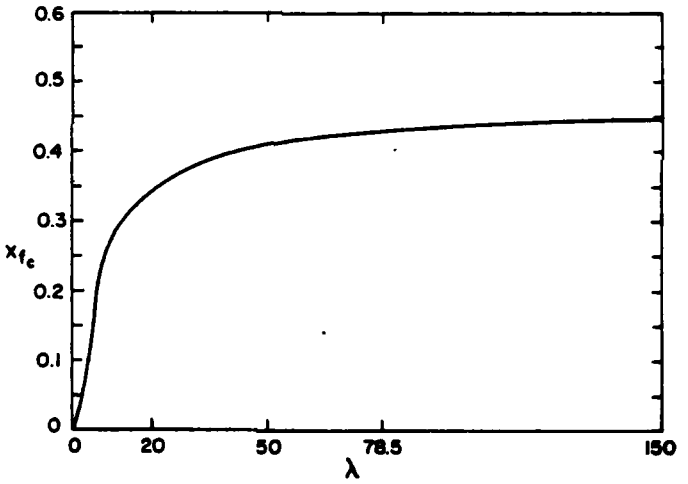

Figure 3. Critical fiber volume fraction x_{fc} for percolation versus the ply thickness λ in fiber diameters for a random square lattice of conducting fibers.

For a finite lattice we can extrapolate out the critical fiber square concentrations for percolation from a vertical line in Figure 2 drawn through the various $P(x,\lambda)$ curves at constant λ. These values are converted to fiber volume fractions upon multiplication by .785 and plotted versus the ply thickness in Figure 3. For a typical single ply thickness λ = 20 fiber diameters we find the slab is not infinite at percolation, and the fiber square fraction at percolation is decreased from the infinite medium result of 0.59, to 0.43. The infinite medium result is in error by

27%. The critical fiber fraction is

$$x_{fc}(\lambda = 20) = 0.785 \times 0.43 = 0.34 \tag{5}$$

This same slab appears to be sufficiently thick to be considered infinite at higher values of x, and conductivity will probably deviate from infinite medium results [11] only as it moves towards percolation.

Since thinness tends to shift conduction versus fiber fraction curves to the left, we can regard the formation of the asymptote in Figure 3 as a measure of the limit of infinite ply thickness for conduction processes. Ply thickness λ above

$$\lambda_{\infty} = 150 \tag{6}$$

may be regarded as infinite for the random fiber square lattice model. Above λ_{∞} the x_{fc} values are asymptotic, very slowly varying, and lie within 4% of the infinite limit 0.46.

Computer calculations of the conductivity of a two-dimensional square random lattice would be of both theoretical and practical interest. Computational difficulties in two-dimensions arising from the slow convergence of the iteration of Kirchoff's equations in a large lattice have been discussed by several authors [10, 12], and the problem has not yet been successfully done on a computer. We feel that computing in a thin slab and studying the thickness curves may simplify the calculations at least at large x where the λ asymptote is readily formed. Research on both the computational and the corresponding experimental problem of single ply conductivity variation with thickness are presently underway. Adams and Tsai [2] point out that a random close packed lattice gives even better results than the square lattice, this more difficult problem is also under consideration.

ACKNOWLEDGEMENTS

The authors wish to thank the United States Air Force Office of Scientific Research who provided the financial support for this study under grant number AFOSR 77-3453.

REFERENCES

1. G. S. Springer and S. W. Tsai, "Thermal Conductivities of Unidirectional Materials," *J. Composite Materials*, Vol. 1 (1967), p. 166.
2. D. F. Adams and S. W. Tsai, "Influence of Random Packing on Transverse Stiffness of Unidirectional Composites," *J. Composite Materials*, Vol. 3 (1969), p. 368.
3. H. L. Frisch, J. M. Hammersley and D. J. A. Welsh, "Monte Carlo Estimates of Percolation Probabilities for Various Lattices," *Phys. Rev.*, Vol. 126 (1962), p. 949.
4. M. F. Sykes and J. W. Essam, "Critical Percolation Probabilities by Series Methods," *Phys. Rev.*, Vol. 133 (1964), p. A310.

5. J. Roussenq, J. Clerc, G. Girand, E. Guyon and H. Ottavi, "Size Dependence of Percolation Threshold of Square and Triangular Networks," *Journal de Physique Letters*, Vol. 37 (1976), p. L-99.
6. C. Mitescu and J. Roussenq, "Une Fourmi dans un Labyrinthe Diffusion dans in Systeme de Percolation," Vol. 283, C. R. Acad. Sc. Paris (1976), p. A999.
7. V. K. S. Shante and S. Kirkpatrick, "An Introduction to Percolation Theory," *Adv. in Phys.*, Vol. 20 (1971) p. 325.
8. H. L. Frisch and J. M. Hammersley, "Percolation Processes and Related Topics," *J. Soc. Indust. Appl. Math.*, Vol. 11 (1963), p. 894.
9. J. W. Essam, "Percolation and Cluster Size," *Phase Transition and Critical Phenomena*, ed. C. Domb and M. S. Green, Academic Press, N.Y. (1972), Vol. 2, p. 197.
10. S. Kirkpatrick, "Percolation and Conduction," *Rev. Mod. Phys.*, Vol. 45 (1973), p. 574.
11. B. P. Watson and P. L. Leath, "Conductivity in the Two-Dimensional Site Percolation Problem," Vol. 9 (1974), p. 4893.
12. J. P. Straley, "Critical Exponents for the Conductivity of Random Resistor Lattices," *Phys. Rev. B.*, Vol. 15 (1977), p. 5733.

J. Phys. C: Solid State Phys., Vol. 12, 1979. Printed in Great Britain.

LETTER TO THE EDITOR

Effective-medium theory of the conductivity for a random-site honeycomb lattice

Thomas Joy† and William Strieder‡

†Department of Electrical Engineering, University of Notre Dame, Notre Dame, Indiana 46556, USA

‡Department of Chemical Engineering, University of Notre Dame, Notre Dame, Indiana 46556, USA

Received 9 January 1979

Abstract. The effective-medium theory for the random-site model of a percolating honeycomb lattice is formulated. The value of the critical site concentration obtained, $x_c = 0.707$, is compared with the series value $x_c = 0.70 \pm 0.01$ and the Monte Carlo value $x_c = 0.688 \pm 0.015$.

In this paper, we present the effective-medium calculation (Kirkpatrick 1973, Watson and Leath 1974, Watson 1975) of the conductivity for the percolating, random-site, honeycomb lattice. To generate our model, a fraction $(1 - x)$ of the nodes (sites) of the lattice is selected at random from an infinite honeycomb lattice of conductances g_0 and the entire cluster of three conductances about each selected site is changed from g_0 to zero. These clusters will overlap, and as Butcher (1975) has pointed out, the fraction of insulating cluster sites is given not by $(1 - x)$, but by one minus the fraction p of bonds present:

$$1 - p = 1 - x^2. \tag{1}$$

For effective-medium theory, the potential at the sites of the random conductance network, across which a vertical voltage has been applied, is the sum of an 'external field' and a fluctuating 'local field.' The average of the local field over a sufficiently large region of the lattice must vanish. The random lattice of conductances g_0 and zero is regarded as an effective medium of equal conductances g_m, defined such that the average field inside the lattice is equal to the external field. To perform the calculations, all the conductances about certain randomly selected sites in the effective medium are changed from g_m to g_0 (or zero) and as a criterion to fix g_m, we require that the extra voltages induced to maintain the external field must average to zero.

In figure 1(*a*), a honeycomb lattice is placed on its side and a vertical voltage is applied to obtain the lattice longitudinal conductivity σ. The external, average effective-medium potential increases by a constant amount V_m for each row of nodes. Suppose a site S is selected at random in the effective-medium lattice and the cluster of conductances about S are changed from g_m to g_0. The uniform solution V_m fails to satisfy current conservation at sites A and C. The magnitude of the current i_0 introduced at A and extracted at C in figure 1(*a*) is chosen to correct for this:

$$i_0 = V_m(g_m - g_0). \tag{2}$$

0022-3719/79/070279+03 $01.00

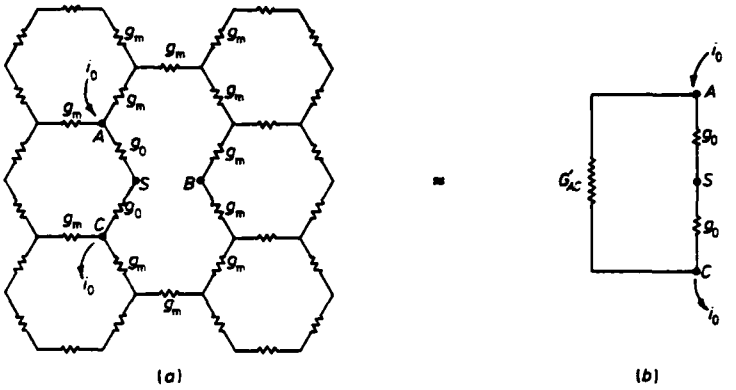

Figure 1. Single site S of a honeycomb lattice for the calculation of the longitudinal conductivity. The cluster of three conductances g_0 around S are located within an effective network of conductances g_m. From symmetry the conductance g_{SB} can be ignored.

The external voltage applied vertically will produce no potential difference between S and B and furthermore, the site currents i_0 are symmetric about SB. This symmetry is sufficient to suppress any currents in g_{SB} and this conductance may be left out of figure 1(a). The extra voltage ΔV_{AC} induced between A and C can be calculated from the equivalent circuit of figure 1(b), if we know the conductance G'_{AC} of the network between points A and C when the g_0 conductances are absent (figure 1b):

$$\Delta V_{AC} = i_0/(\tfrac{1}{2}g_0 + G'_{AC}). \tag{3}$$

Calculation of the conductance G_{AC} between A and C in a uniform effective medium provides the conductance G'_{AC} from the equality

$$G_{AC} = G'_{AC} + \tfrac{1}{2}g_m. \tag{4}$$

We seek the current distribution for the circuit of figure 1(a) for the special case $g_0 = g_m$. These currents can be expressed as the superposition of two contributions, a current i_0 introduced at A and extracted at very large distances in all directions and an equal current introduced at infinity and extracted at C. Unlike the square or triangular lattice (Joy and Strieder 1978), both the current distribution for a single source in an infinite effective-medium honeycomb lattice and G_{AC} can be obtained without recourse to an infinite set of simultaneous equations, i.e. Kirchoff's law for all the sites. The current i_0 introduced at A flows through three equivalent bonds and hence each bond carries $\frac{1}{3}i_0$. At the sites immediately adjacent to A, by symmetry again, the current must split to follow two equal paths and each of these currents is $\frac{1}{6}i_0$. This determines that the voltage developed across the sites A and C will be $i_0(2g_m)^{-1}$ for the current i_0 at A and for the superposition of the current injected at A and extracted at C

$$G_{AC} = g_m \tag{5}$$

or

$$G'_{AC} = \tfrac{1}{2}g_m. \tag{6}$$

From equations (2), (3) and (6) we obtain for ΔV_{AC}

$$\Delta V_{AC} = 2V_m(g_m - g_0)/(g_m + g_0). \tag{7}$$

Note that there are two kinds of clusters in the honeycomb lattice. The horizontal member in figure 1(*a*) can go either to the right or to the left, but from arguments the same as those above, we can show that the same ΔV_{AC} applies to both cases. There is no need to differentiate between them.

It follows from the condition for an effective medium that the average $\langle \Delta V \rangle$ from the conducting and non-conducting clusters must vanish, i.e.

$$\langle \Delta V \rangle = (1 - p)2V_m + p2V_m(g_m - g_0)/(g_m + g_0) = 0. \tag{8}$$

The effective-medium conductivity is found to be

$$g_m = g_0(2p - 1). \tag{9}$$

The net longitudinal conductivity σ of the honeycomb lattice in terms of g_m can be obtained by geometrical arguments from the effective-medium lattice:

$$\sigma = g_m/\sqrt{3} \tag{10}$$

and for the longitudinal conductivity in terms of the site fraction x:

$$\sigma = (2g_0/\sqrt{3})(x^2 - \tfrac{1}{2}) \tag{11}$$

from equations (1), (9) and (10). The transverse conductivity, figure 1(*a*) rotated by 90°, is also given by equation (11).

Percolation occurs when the conductivity vanishes, i.e. $\sigma(x_c) = 0$ and effective-medium theory for the honeycomb lattice predicts

$$x_c = 1/\sqrt{2} = 0{\cdot}707. \tag{12}$$

The greatest inaccuracies of the effective-medium theory occur near percolation, hence percolation provides a good test for equation (11). For exact lattice calculations, percolation in a random-site honeycomb lattice was observed at 0·70 ± 0·01 by Sykes and Essam (1964), but equation (12) predicts percolation within these bounds, above the median by 1·0%. Furthermore, from Monte Carlo calculations, Dean (1963) proposed the value 0·688 ± 0·015. Effective-medium theory predicts percolation at a site fraction about 2·8% higher the median. The effective-medium result is again almost within the range of error.

The authors wish to thank the Air Force Office of Scientific Research who provided support for the research under grant number AFOSR 77-3453.

References

Butcher P N 1975 *J. Phys. C: Solid St. Phys.* **8** L324–7
Dean P 1963 *Proc. Camb. Phil. Soc.* **59** 397–410
Joy T and Strieder W 1978 *J. Phys. C: Solid St. Phys.* **11** L867–70
Kirkpatrick S 1973 *Rev. Mod. Phys.* **45** 574–88
Sykes M F and Essam J W 1964 *Phys. Rev.* **133** A310–5
Watson B P 1975 *Phys. Rev.* C **12** 498
Watson B P and Leath P L 1974 *Phys. Rev.* B **9** 4893–6

Effect of Thickness on Single Ply Percolation and Conductivity

Thomas Joy and Pratul Ajmera

Department of Electrical Engineering
University of Notre Dame
Notre Dame, Indiana 46556

and

William Strieder

Department of Chemical Engineering
University of Notre Dame
Notre Dame, Indiana 46556

ABSTRACT

A single ply of unidirectional composite is modeled as a two-dimensional close packed lattice of circular fiber cross sections of infinite width and finite thickness. To introduce randomness fibers are removed at random from the lattice, leaving vacant lattice sites of matrix material, until a certain fiber volume fraction is reached. The effect of lattice thickness on the critical fiber fraction for percolation is calculated for this random, close packed fiber model. For a typical ply thickness of 24 fiber diameters, the critical fiber fraction for percolation is reduced by 20% from the infinite lattice value of 0.45 to a smaller value of 0.36. The percolation versus thickness results of the random square lattice of fibers are compared with those of the random close packed fiber model. Experimental measurements of the increase in electrical conductivity of a single ply of graphite/epoxy composite with decrease in ply thickness predicted by the random close packed fiber model, are presented.

SCOPE

Adams, Springer, and Tsai [1,2] have suggested both the random square and random close packed arrangements of circular fiber cross sections as appropriate physical models for the calculation of effective transport properties across a ply of unidirectional composite material. In a previous publication [3], numerical studies of the percolation of a random square lattice of contacting fibers were presented. In this paper we will investigate the lattice statistics of a random, close packed fiber model of a thin ply of unidirectional composite to determine the existence of percolation, the effect of ply thickness on percolation, and the asymptotic ply thickness beyond which the statistical properties of the ply no longer depend on ply thickness. We will compare the square lattice results of percolation in a thin single ply with those for the random close packed fiber lattice. In addition, the increase of electrical conductivity for thinner plies, predicted from our calculations of lattice statistics, will be presented herein in the form of experimental data points.

In the random, close packed fiber lattice (Figure 1), fiber cross-sections are removed by a random number procedure from a perfect close packed lattice of identical circles. What results is circular fibers placed at random in a triangular lattice of all possible fiber sites. Any fiber site in the triangular lattice is either vacant or occupied by a circular fiber cross-section. A fiber will directly contact only those fibers occupying one of its six nearest neighbor fiber sites. The fiber volume fraction x_f must be distinguished from the fraction x of occupied fiber sites,

$$x_f = (\pi/2\sqrt{3})x = 0.907x \qquad (1)$$

The only unphysical restriction of this model is to confine the fibers to rows or columns. Adams and Tsai [2] have pointed out that this constraint is secondary to the introduction of randomness. Also, fibers in fact tend to close pack in the actual composite.

Suppose that almost all of the fiber sites are vacant and fibers occupy only a few randomly selected sites of the close packed lattice of sites. At this lower volume fraction, the fibers will appear isolated, but as the number of fibers is increased pairs in contact will form. Ultimately, as the fiber fraction is further increased groups or clusters of fibers will form. The statistics of an infinite close packed fiber lattice, for example, the maximum cluster size and cluster probabilities [4-9] for any fiber fraction, have been calculated. The central and most physically relevant result is the prediction of a lattice phase condensation or the formation of infinite fiber clusters at a certain minimum critical fiber fraction x_{fc}. Infinite clusters do not occur within the infinite close packed lattice of fibers until a certain critical fraction [4,5] of the fiber sites are occupied

$$x_{\infty} = 0.500 \qquad (2)$$

Percolation, the vanishing of the conductivity below a certain critical fiber fraction, will occur in a unidirectional composite with a very highly conductive fiber phase and an insulating matrix phase. The prediction of the effective electrical conductivity of such a medium can be modeled from the random, close packed fiber lattice. Fibers occupying adjacent sites in a random close packed fiber lattice will contact at a point (Figure 1), and we represent the conductvity between two adjacent fiber centers by σ_o. Current can pass only from a fiber center to an adjacent fiber center. An

unoccupied fiber site is filled with matrix material of zero conductivity. The current flow between a fiber center and an unoccupied neighboring fiber site or between two adjacent unoccupied fiber sites is zero and their conductivity can be omitted from Figure 1. A random, close packed fiber lattice completely filled with fibers, i.e., $x=1$, forms a triangular lattice of conductances σ_o . If a fiber is removed all six conductances to the unoccupied fiber site will vanish as the matrix is insulating. Sites are filled or unoccupied at random; the lattice of conductances is sometimes called [10] the random site triangular lattice. The random, close packed fiber model predicts, due to the absence of infinite clusters, that the conductivity [10] of a thick unidirectional composite slab (or infinite lattice) of highly conductive fibers in an insulating matrix will vanish below the critical fiber site concentration given by (2) and this phenomenon is called percolation. The composite conductivity for an infinitely thick ply of random, close packed fibers will vanish below the percolation concentration [4,5]

$$x_{fc} = 0.500 \times 0.907 = 0.454 \qquad (3)$$

A major difficulty with comparing random lattice literature values [4-10] for the percolation or conductivity with those of a single ply of unidirectional composite is that the previous theory is addressed solely to understanding the infinite lattice. The previous literature results for the random close packed fiber lattice only apply to a single ply very large in both width and thickness, whereas in practical applications the single ply is sometimes only a few fiber diameters thick. The conductivity of a single ply of composite will depend on the existence of unbroken paths of conductance that travel completely across the slab. In a recent publication

[3], to pose for a random square lattice of fibers, the question of the existence of percolation in a thin ply, we formulated the probability $P(x,\lambda)$ that a block on the edge of the ply will contain a fiber and connect with one or more unbroken resistor paths across the composite. In this paper we will calculate $P(x,\lambda)$ for the random, close packed fiber model and determine how the critical percolation fiber volume fraction x_{fc} changes with ply thickness λ (in fiber diameters). The variation of $P(x,\lambda)$ with thickness for the random close packed fiber model will give some idea of when a ply is statistically thick, and its vanishing will provide a test for percolation. The variation of the critical percolation concentration x_{fc} with ply thickness λ found for the close packed model will be compared with that of the square lattice.

Both the $P(x,\lambda)$ curves [3] for the square lattice of fibers model and for the random, close packed fiber model discussed in this paper, predict that the conductivity of a thin slab will decrease with thickness. When the path probability is plotted versus the ply thickness the number of conductance paths across the ply decreases rapidly with increasing thickness to either a positive, non zero, asymptote for $x_f > x_{fc}$, or for $x_f < x_{fc}$ to an asymptotic value at zero path probability on the abcissa. Beyond these asymptotic thicknesses predicted from the $P(x,\lambda)$ curves, the lattice is effectively infinite i.e., the lattice is statistically thick, and the composite model properties no longer depend on λ. Experimental conductivities of graphite/epoxy fiber reinforced composites measured for plies of thickness currently used in aircraft fabrication, and presented in the last section of this paper, show this same decrease with thickness.

CONCLUSIONS AND SIGNIFICANCE

From this study, the following conclusions can be drawn:

1. If more than 50% of the fiber sites of the closed packed random fiber model are filled a significant number of paths exist across even an infinitely thick ply; below this critical concentration the conductivity of the infinitely thick ply must vanish.
2. The close packed random fiber model of a unidirectional composite material is infinitely thick if it is at least 150 fiber diameters thick.
3. For a typical single ply thickness of λ=24 fiber diameters, the random close packed fiber model of a ply is not infinite, and the critical fiber site fraction at percolation is decreased from the infinitely thick ply value of 0.50 to 0.40. The infinite medium result is in error by 20%. The corresponding critical fiber fraction is:

$$x_{fc}(\lambda=24) = 0.907 \times 0.40 = 0.36 \qquad (3)$$

4. A comparison of the curves of percolating fiber fractions versus λ for the random square lattice of fibers model and the random close packed fiber model shows the difference in x_{fc} for the two lattices to be small, for example, the critical fiber fractions for percolation differ by only 3% for a thickness of 24 fiber diameters. However, due to the asymptotic nature of the curves of the two models, the critical thickness for percolation for a given fiber fraction (below $x_{fc\infty}$) can differ significantly near the asymptotic limits. For example, the square lattice percolates beyond 33 fiber diameters whereas the

random, close packed fiber lattice does not percolate until 40 fiber diameters for a fiber volume fraction of 39%.

5. Both the random square lattice of fibers and the random, close packed fiber models suggest that the electrical conductivity of a thin ply of unidirectional composite should increase with decrease in thickness. Experimental conductivities of graphite/epoxy fiber reinforced composite measured for plies of thicknesses currently used in aircraft fabrication and presented in the last section of this paper do exhibit the predicted increase.

EFFECTS OF PLY THICKNESS ON THE PATH PROBABILITIES AND PERCOLATION FOR THE RANDOM, CLOSE PACKED FIBER MODEL

The calculations of the probability $P(x,\lambda)$ that an edge site at $y=0$ will contain a fiber (Figure 1) which connects to an unbroken fiber path across the thickness of the ply were performed on an IBM 370/168 computer. The composite was modeled as a two-dimensional lattice of close packed circular fiber cross sections all of the same fiber diameter d. The lattice is of infinite width but of finite thickness, λ fiber diameters. Because of the lateral displacement of adjacent rows of circles (Figure 1) a lattice containing N rows of fibers has a thickness

$$\lambda = d + d(N-1)\sqrt{3}/2 \qquad (4)$$

The random close packed fiber lattice was generated by removing fiber cross sections from the lattice (Figure 1) with a modular multiplication random number routine and the additional constraint that on the average the fibers

satisfy an occupied fiber site fraction x (or fiber volume fraction $x_f = 0.907$). The random structure occurs from the absence of fibers or clusters of fibers within the close packed lattice.

For conductive percolation the fibers must be very good conductors and the matrix must be an insulator. The necessary conduction paths across the ply are simulated from fiber to fiber contacts between nearest neighbors. In a close packed lattice, each fiber has at most six nearest neighbors (Figure 1). If a fiber's nearest neighbor site is occupied then the two fibers touch and the sites of the two fiber centers are connected by a conductance σ_o , but if a nearest neighbor fiber has been removed, no contact occurs and no conductance is drawn in. If both adjacent fiber sites are unoccupied, the conductance is also omitted.

To count the unbroken conductance paths across the ply, we addressed each fiber at the edge of the lattice, i.e., $y=0$. Algorithms to mark the conductance path started from the edge fiber, and moved across on occupied sites of the close packed lattice, from site to adjacent site terminating at the opposite side. At each site along the path, the program examined the nearest neighbor sites in a set order, beginning the search at five o'clock and moving clockwise. The search for a path moved to the first nearest neighbor site that was found to be occupied. Each new site on the path was marked with the direction to the previous site from which the path came for backtracking. Each new site was also marked with the starting edge square number to avoid closed loops and paths already essayed. The ratio of edge fibers that begin such a path to the total number of occupied or unoccupied edge sites considered gives the path probability $P(x,\lambda)$.

To assure statistical stability the probabilities calculated were calculated for a very wide slab but finite slab thickness, λ fiber diameters. Samples were taken 900 elements wide with specified thickness λ. On each side of the sample 200 edge squares were deleted from the path counting procedure to avoid end effect errors. Then 25 such samples were run. The cumulative sample average of $P(x, \lambda)$ was stable enough to provide sufficient accuracy for Figures 2 and 3.

Figure 2 contains the calculated path probabilities $P(x, \lambda)$ versus the ply thickness, λ fiber diameters, for various filled fiber site fractions x of a random, close packed fiber lattice. The curves are clearly asymptotic at non zero values for all $x > 0.50$. Significant numbers of paths across the ply are formed even at infinite thickness, and we can speak of a non vanishing effective conductivity of an infinite lattice that does not depend on λ, but does depend on x. Asymptotes form on the λ axis for $x < 0.48$ and we expect no conduction across an infinite lattice for x below 0.48. For the infinitely thick lattice, asymptotic values of $P(x, \lambda)$ when divided by the fiber fraction always lie below the percolation probability [4-6] and either probability can be used to indicate percolation, however, the calculation of $P(x, \lambda)$ requires less computer time.

From Figure 2 asymptotes are most rapidly formed at low and high x. The asymptote forms on the λ-axis at roughly 11 fiber diameters, the maximum fiber cluster size across the lattice for a filled fiber site fraction of 0.30. All, but a few small clusters, of the fibers occupying the first rows of fiber sites in the random close packed fiber lattice belong to an infinite cluster for a filled fiber site fraction of 0.60 and the asymptote is already formed at about 11 fiber diameters. On the other hand, near the fiber site fraction 0.50, the maximum cluster size becomes quite large, approaching

infinity at 0.50, and asymptotes do not readily form. Indeed those of the $x = 0.48$ and $x = 0.49$ curves have yet to form on the λ-axis at $\lambda = 130$ fiber diameters.

The $P(x,\lambda)$ curves of Figure 2 for the random, close packed fiber lattice show the same general trends as those of the random square lattice [3]. The only major exception is that the critical percolation fiber site fraction in the infinite square lattice of fibers [4,5], the $P(x,\lambda)$ curve that splits the zero from the positive asymptotes, occurs at a fiber site fraction of 0.59, whereas in Figure 2 the percolation in an infinitely thick, random close packed lattice of fibers occurs at a filled fiber site fraction of 0.50.

For a finite lattice we can extrapolate out the critical fiber site concentrations for percolation from a vertical line in Figure 2 drawn through the various $P(x,\lambda)$ curves at constant λ. These values are converted to fiber volume fractions upon multiplication by 0.907 and plotted versus the ply thickness as the lower curve in Figure 3. For a typical single ply thickness $\lambda = 24$ fiber diameters we find the fiber square fraction at percolation is decreased from the infinite medium result of 0.50 to 0.40. The infinite medium result is in error by 20%. The critical fiber fraction is

$$x_{fc}(\lambda = 24) = 0.907 \times 0.40 = 0.36 \qquad (5)$$

This same slab appears to be sufficiently thick to be considered infinite at higher values of x, and conductivity will probably deviate from infinite medium results [10] only as it moves towards percolation.

Since thinness tends to shift conduction versus fiber fraction curves to the left, we can regard the formation of the asymptote in Figure 3 as a measure of the limit of infinite ply thickness for conduction processes. Ply

thickness λ above

$$\lambda_\infty = 150 \qquad (6)$$

may be regarded as infinite for the random fiber square lattice model. Above λ_∞ the x_{fc} values are asymptotic, very slowly varying, and lie within 5.8% of the infinite limit 0.45.

We note from Figure 3 that the critical fiber fraction x_{fc} curves for the square lattice (upper curve) and close packed fibers (lower curve) are rather close. At λ=24 the square lattice gives a critical fiber volume fraction of 0.37, only 3% higher than the random close packed fiber lattice value stated previously. If we determine instead the thickness at which the two lattices percolate for a given fiber volume fraction, the square lattice percolates at 33 fiber diameters whereas the close packed lattice percolates at a larger thickness of 40 fiber diameters for a fiber volume fraction of 39%. This difference can of course become larger near the asymptotes.

EFFECTS OF PLY THICKNESS ON THE TRANSVERSE ELECTRICAL CONDUCTIVITY

The curves of the path probability $P(\pi,\lambda)$ versus thickness in Figure 2 suggest that the effective electrical conductivity of a thin ply of unidirectional composite should significantly increase with decreasing thickness due to the additional conduction paths. Furthermore, the model suggests that the increase will not begin until a certain asymptotic thickness, and that this thickness is of the order of a commercial single ply thickness. Experimental measurements of electrical conductivity at several thicknesses were carried out on T-300/Narmco 5208 cured unidirectional, single ply graphite/epoxy composite material to test the validity of these predictions.

Single ply samples of four different thicknesses were prepared. The four specimens were cut from the same strip of single ply material and lapped to the varying thicknesses. Each sample was lapped on both sides to ensure good electrical contacts. The specimen was then bound on both sides to copper plates with the help of silver conducting epoxy. The silver conducting epoxy was cured at 150°C for 30 minutes in air and is known to form a good contact with the graphite/epoxy conducting material [14].

The resistance measurements on these samples were carried out on a General Radio Impedance Bridge type 1608-A at 1kHz test frequency. A sample was connected to the impedance bridge with the help of copper strips held firmly to the top and the bottom copper plates of the sample by a lightly loaded insulating spring clip. Measured values of the resistance are given in Table 1. The thickness of the single ply samples was measured optically under a microscope. While care was taken to keep the sample uniform, some slight scatter in sample thickness was observed and both the thickness and scatter are listed in Table 1. Also listed in Table 1 are the fiber volume fractions, and the areas to which the flux is perpendicular, necessary for the conductivity calculations.

Table 1. PHYSICAL PROPERTIES OF THE SAMPLES

Thickness mm	Area cm^2	Fiber Volume Fraction	Resistance ohms	λ	Conductivity mho/m
0.1616±.0065	0.5146±1%	0.404	9.511	24.7	0.330±.017
0.1313±.0095	0.8835±1%	0.385	4.475	20.1	0.332±.027
0.0955±.0095	0.7046±1%	0.390	3.235	14.6	0.408±.045
0.0516±.0071	0.5695±1%	0.383	1.417	7.9	0.639±.094

Finally, the conductivity values and the uncertainty that arises from its direct proportionality to the thickness are given. The conductivity is plotted versus fiber thickness in Figure 4.

The electrical conductivity values in Figure 4 demonstrate for graphite/epoxy composite systems currently in use that the electrical conductivity of the single ply varies with ply thickness. Further, we find that the expected increase in electrical conductivity with decreasing thickness is significant. The average fiber volume fraction of the four samples from Table 1 is 39%. This value is less than the critical percolation fiber volume fraction for the infinitely thick ply of 45%. Therefore, the models predict that the electrical conductivity will eventually vanish with increasing ply thickness. We have already determined the thickness for percolation at a fiber fraction of 39% from Figure 3 to be 33 and 40 fiber diameters for the random square lattice and random close-packed lattice, respectively. Multiplying both results by the average fiber diameter 6.54μm we find the random square lattice predicts percolation at 0.216mm whereas the random, close packed fiber model predicts the conductivity will vanish at 0.262mm.

Experimental samples, approximately 700 fiber diameters wide, are infinitely wide in the sense that they do not suffer end effects. However, some statistical fluctuation in the conductivity value from the randomness of the fiber distribution can occur from sample to sample. If we include also the experimental uncertainties (Table 1) in the ordinate and abcissa from the thickness variations, it is not difficult to construct a curve that includes the four experimental points as well as the predicted percolation point. The predicted percolation thicknesses do not appear on Figure 4, nor do they influence the very rough curve that we have drawn, for they are not experimental

points but depend on the model simulation that we have performed.

On the other hand, for fiber volume fractions just below percolation (Figure 2) it is very difficult to predict the critical percolation thicknesses exactly for they are very sensitive to small changes in fiber volume fraction x_f. Predictions from the random close packed fiber model should be more successful at higher fiber volume fractions where the fibers close pack, than near percolation. Lattice models will probably tend to underestimate the conductivity near percolation and make the critical percolation thickness at any x_f too small. The real distribution of fibers is not restricted to a lattice and can find more ways to form paths. Suppose we return to Figure 2 calculated for a close packed lattice, and for the moment accept the general shape of the curves for the real composite system, but suppose the infinite lattice would percolate at 0.47 rather than 0.50. This in effect would decrease each fiber site fraction listed on Figure 2 by 0.03. The conductivity data from Figure 4 taken at a fiber volume fraction x_f of 0.39 by Equation (1)

$$x=x_f/0.907 = 0.39/0.907 = 0.43$$

corresponds to a site fraction of 0.43. The rather small decrease in percolation of the infinite lattice by jsut 0.03 would shift our consideration from the 0.43 curve of Figure 2 to the 0.46 curve and this would increase our critical percolation thickness by a factor of about 2-1/2. The effect of a fiber crossing from site to site as it moves down the depth of the composite ply, in addition, while probably a small factor at ordinary concentrations, may also delay percolation and increase the experimental percolation thickness somewhat.

Even with these difficulties, the percolation thickness predicted by the model are of the correct order of magnitude. At these critical thicknesses we do find experimental curves of the shape predicted by the lattice models.

While the path probability curves give insight into the physical processes within a single ply, they may not give the precise shape of the corresponding conductivity curves. For example, in the infinite square [4,13] and random close packed fiber [4,10] lattices the percolation probability and conductivity curves versus fiber volume fraction are quite different in shape. Computer calculations of lattice conductivity [11,12] for both the random square and random close packed fiber models, as well as additional single ply conductivity measurements presently underway will give some idea of the shape of the conductivity versus thickness curve and how the asymptote is formed. However, the experimental data points presented here do verify qualitatively the essential features of the ply conductivity as suggested by the random lattice models.

ACKNOWLEDGEMENTS

The authors wish to thank the United States Air Force Office of Scientific Research who provided the financial support for this study under grant number AFOSR 77-3453.

LIST OF CAPTIONS

Figure 1 Random, close packed fiber lattice 4.46 fiber diameters thick. Fiber to fiber conductance σ_o is indicated on the current paths shown. Thickness λ is measured in fiber diameters.

Figure 2 Path probability $P(x,\lambda)$ of a random close packed fiber lattice versus the ply thickness λ in fiber diameters for various fiber block fractions.

Figure 3 Critical fiber volume fraction x_{fc} for percolation versus the ply thickness in fiber diameters. The lower curve represents critical fiber fractions for the random, close packed fiber lattice and the upper curve is the corresponding result for a random square lattice of conducting fibers from reference [3].

Figure 4 Electrical conductivity σ of single plies of graphite/epoxy composite with fiber volume fraction of 39%, average fiber diameter of 6.54μm and various thicknesses. The conductivity is measured across the thickness of the ply, perpendicular to the central axis of the fibers.

"Effect of Thickness ... and Conductivity"

Fig. 1

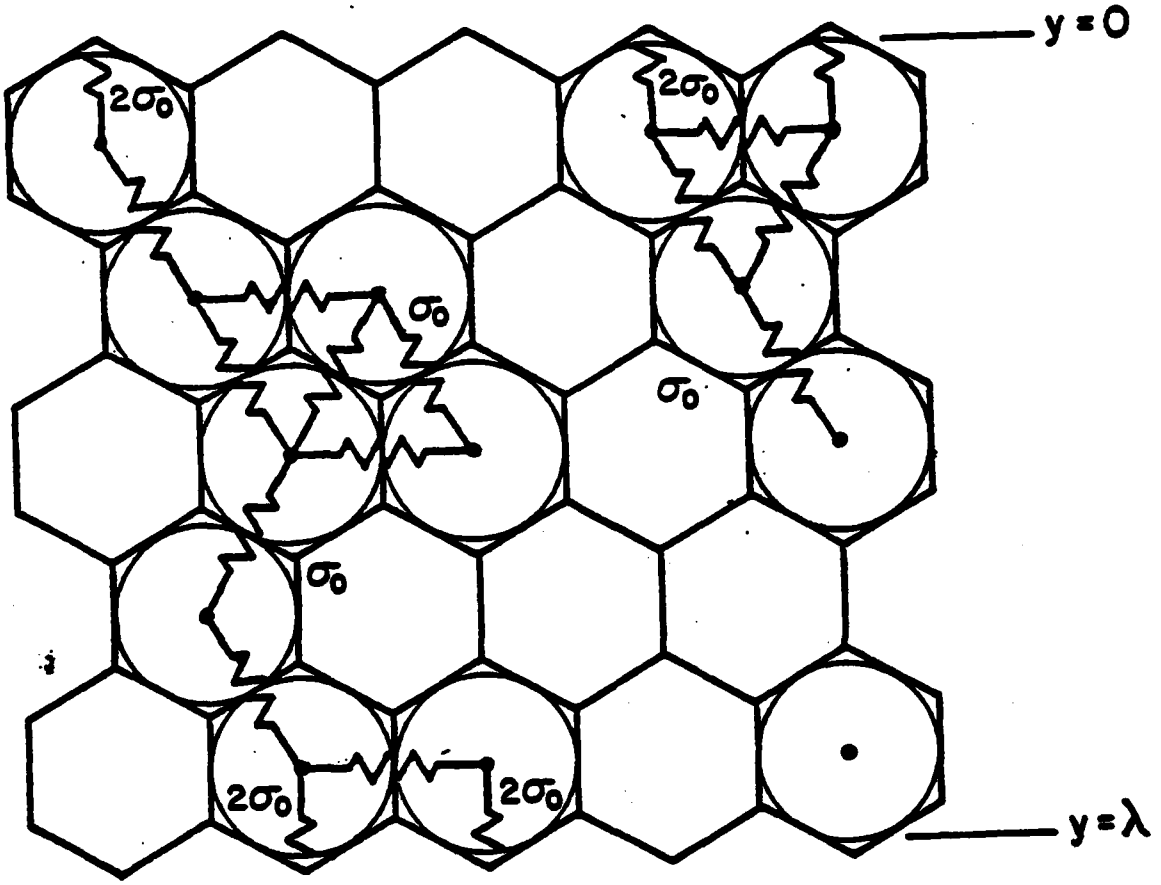

Effect of thickness on ... Fig 2

Jay & Shneider

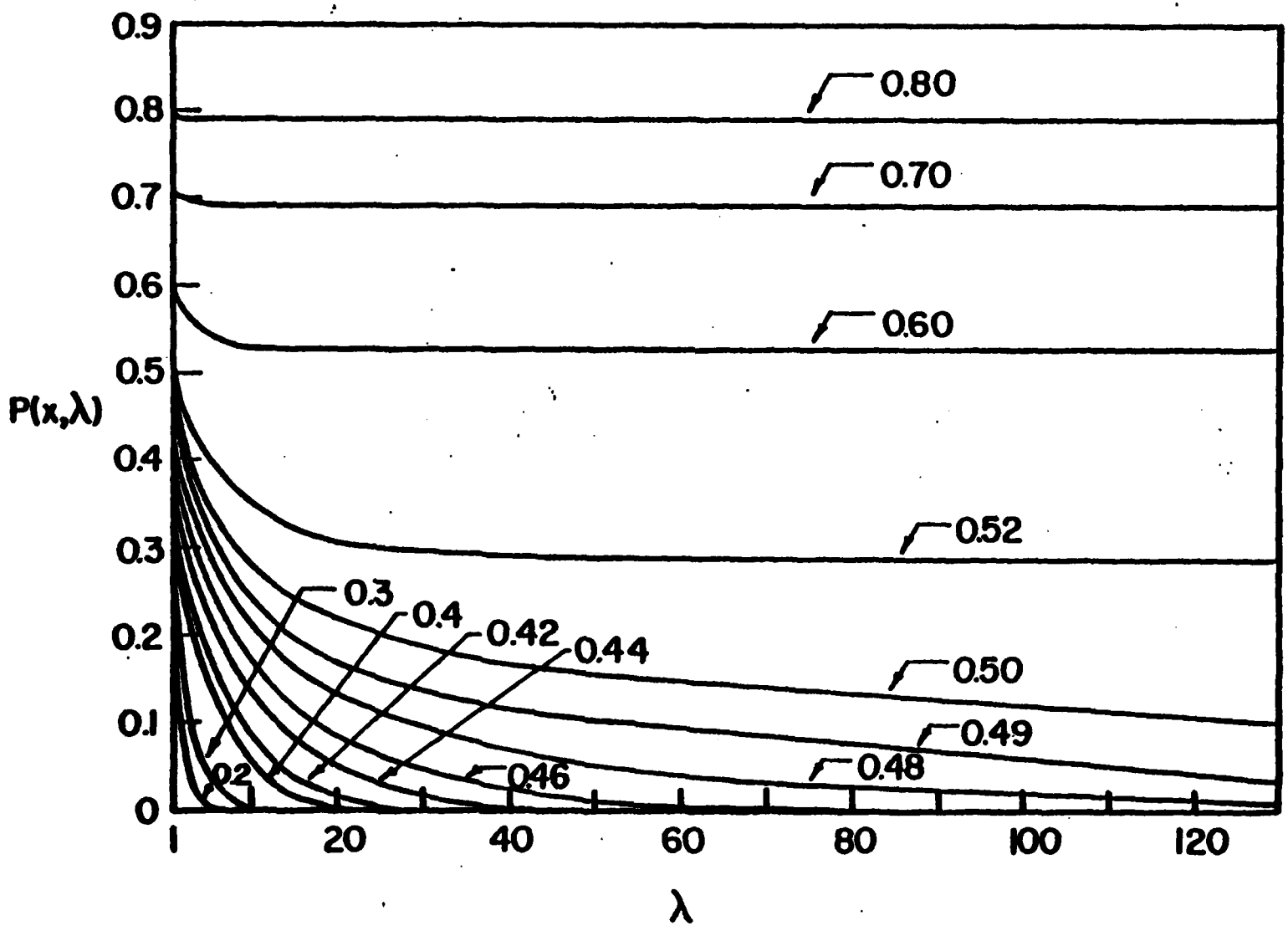

Fig 3
Joy and Shinder

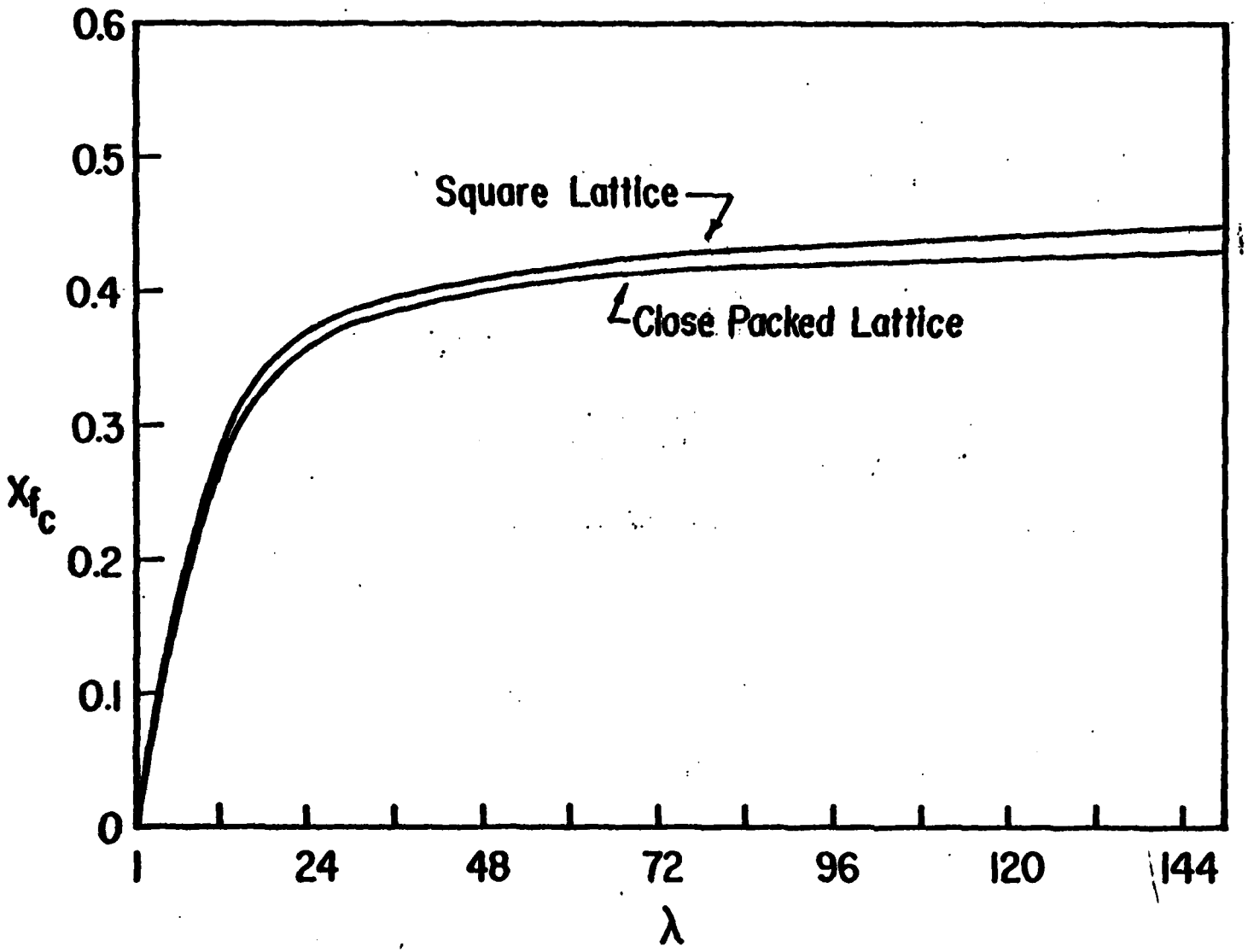

"Effect of Thickness on Single Ag Percolation and Conductivity"

Fig 4
Jay and Shwain

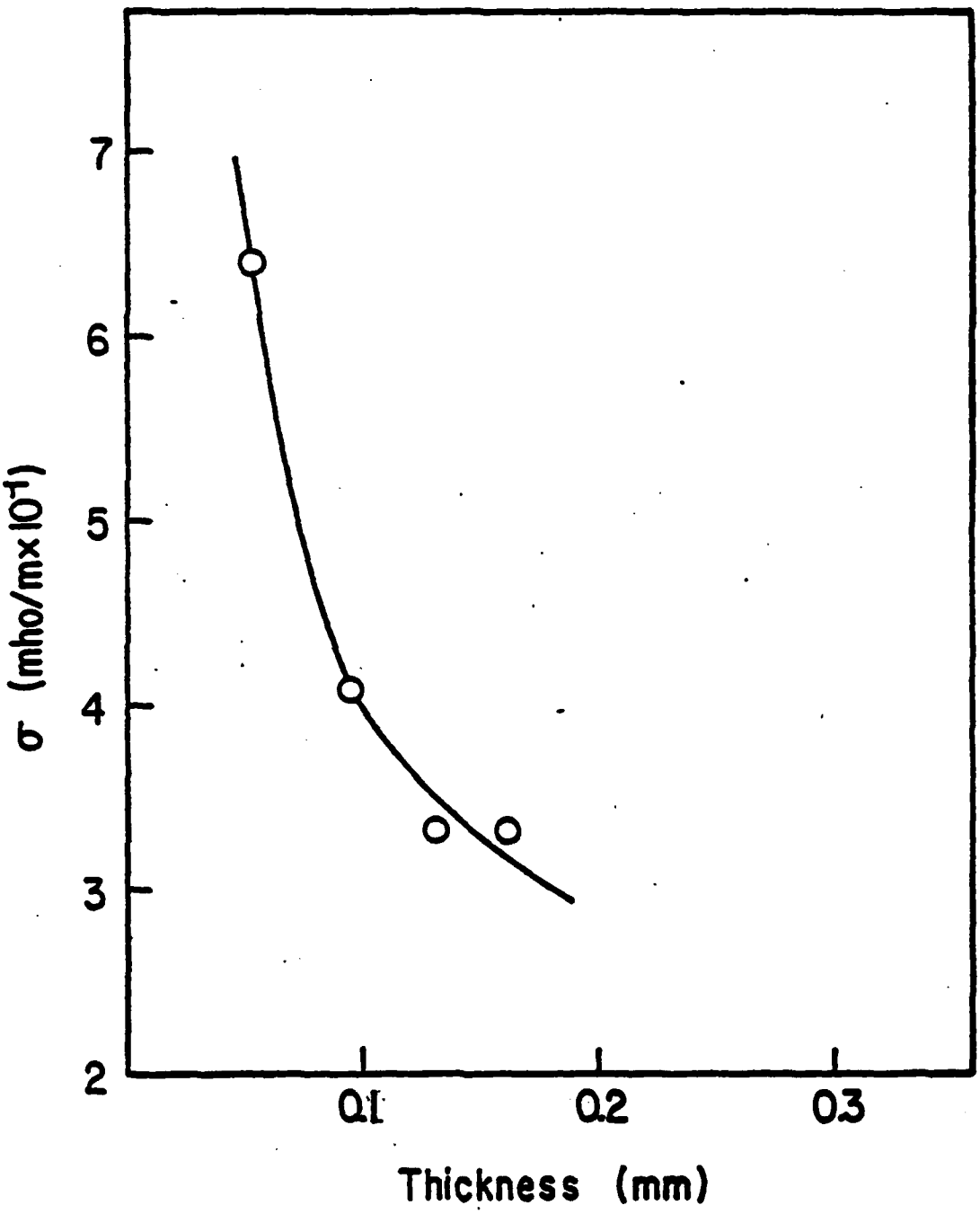

CHAPTER VII REFERENCES

7-1 G.S. Springer and S.W. Tsai, "Thermal Conductivity of Unidirectional Materials," J. Composite Materials Vol. 1 (1967), p. 166.

7-2 D.F. Adams and S.W. Tsai, "Influence of Random Packing on Transverse Stiffness and Unidirectional Composites," J. Composite Materials, Vol. 1, (1969), p. 368.

7-3 S. Kirkpatrick, "Percolation and Conduction", Reviews of Modern Physics, Vol. 11, (1973), p. 574.

7-4 B.P. Watson and P.L. Leath, "Conductivity in the Two-Dimensional-Site Percolation Problem" Phys. Rev. B. Vol. 9, (1974), p. 4893.

7-5 M.M. Yovanovich and J. Coutancian, "Sur la D etermination de la R esistance Thernique Transversale d un Cylindre de R evolution Homogene Isotrope avec des Conditions Aux Limites Mixtes", Comptes Rendus de l'Academie Sciences, Vol. 268 (1969), p. 821.

7-6 B.B. Mikic, "Thermal Contact Conductance; Theoretical Considerations", I.J. Heat Mass Trans., Vol. 17, (1974), p. 205.

7-7 T. Joy and W. Streider, "Effective Medium Theory of Site Percolation in a Random Simple Triangular Conductance Network," J. Phys. C: Solid State Phys., Vol. 11, (1978), p. L867 (reprint enclosed).

7-8 T. Joy and W. Streider, "Effective Medium Theory of the Conductivity for a Random Site Honeycomb Lattice" (in press J. Phys. C. Solid State Phys., preprint enclosed).

7-9 Y. Yuge, "Three-Dimensional Site Percolation Problem and Effective Medium Theory: A Computer Study," J. Statist. Phys., Vol. 16, (1977), p. 339.

7-10 W.J. Gajda, Jr., "Experimental Variation of Electrical Conductivity with Fiber Volume Fraction in Graphite/Epoxy," to be presented at the 1979 IEEE International Symposium on Electromagnetic Compatibility.

7-11 T. Joy and W. Streider, "Percolation in a Thin Ply of Unidirectional Composite", (in press J. Composite Materials, preprint enclosed).

APPENDIX A

PLATING SOLUTION AND SAMPLE PREPARATION

A.1 Introduction

This appendix briefly describes the technique of nickel plating as it was used to electrically contact boron fibers.

In Section A-2 the nickel plating bath used in this particular case is described. Section A-3 summarizes the cleaning and plating procedures and, in the conclusion, the success of this technique is described.

A.2 The Nickel Plating Bath

The nickel plating solution used in this particular experiment is a Watts Bath. The main constituents of this bath are nickel chloride, nickel sulfate and boric acid. Nickel sulfate is the principal source of nickel ion in the Watts Bath. The concentration of the nickel sulfate determines the limiting current density and the plating rate. Consequently, this determines how much current can flow through the cathode (i.e., the boron fiber). Nickel chloride improves anode (i.e., nickel metal) corrosion and conductivity. Increasing conductivity is of practical importance in order to reduce the voltage necessary to produce the desired current density. Boric acid is the solution buffer and helps to produce smoother and more ductile deposits of nickel.

Sound deposition of nickel depends on other parameters besides the chemicals in the solution. Temperature, agitation, controlling of the pH level, anti-pitting reagents, optimal anode-cathode current densities and low contamination are all of importance.

The bath that is used in our particular case has the following composition and operation conditions:

Constituent	Quantity
Nickel Sulfate ($NiSO_4.6H_2O$)	300 g/l
Nickel Chloride ($NiCl_2.6H_2O$)	60 g/l
Boric Acid (H_3BO_3)	42 g/l
4% Sodium Hydroxide Solution (NaOH)	42 g/l
30% Hydrogen Peroxide	2.5 ml/l diluted in 200 ml of H_2O
Activated Charcoal	2.4 g/l

Operating Conditions	Range	Preferred
Temperature	49° to 66°C	60°C
pH	3.5 to 5.0	4.5
Current density of anode	-----	100 amp/m^2
Current density of cathode	-----	530 amp/m^2

The following steps are typical in the preparation of 500 ml of solution:

Day 1: 1. Fill a clean beaker with 500 ml of distilled water. Heat it up to 66°C.

2. Add 150g nickel sulfate and 30g of nickel chloride.

3. Add 4% sodium hydroxide until the pH is approximately

5.2; agitate vigorously.

4. Add 30% hydrogen peroxide - 1.25 ml diluted in 100 ml of H_2O. Stir.
5. Add 1.2g of activated carbon, stir for 2 hours and allow solution to settle overnight.

Day 2: 6. Filter all the carbon out.

7. Add 21g of boric acid (stirring continuously).
8. Adjust pH to 4 with dilute CP graded sulfuric acid.

Finally, for the first plating job using this solution, it is better to use a dummy cathode (e.g. copper wire). Nothing has been said so far about the anode and specific characteristics are given in Section II. For our case, a 100% pure nickel anode is not necessary which makes the technique economically attractive.

A.3 Cleaning and Plating Procedures

In order to attain consistent results for every plating of boron fibers, cleaning of the fiber is of vital importance. Considering the small diameter of these fibers (e.g., 4 to 8 mils) any particle of foreign material at the surface of the fiber will be covered with nickel and give v-i measurements inconsistent with similar samples of boron fiber. In order to avoid this the following procedure is used:

(1) Vapor degrease the sample with trichlorethylene for at least 5 minutes.

(2) Run the fiber through acetone, methanol and distilled water.

(3) Drop fiber in sulfuric acid for 5 minutes.

(4) Run through distilled water.

(5) Blow dry with prepurified nitrogen. (Do not use any paper cleaning).

Before plating, the current densities were calculated using the following relationship:

$$j_A S_A = j_C S_C = I_p \qquad \text{(A.3.1)}$$

where j_A = current density of the anode

S_A = surface area of the anode

j_B = current density of cathode

S_B = surface area of cathode

I_p = plating current

Assuming $j_A = .01 A/cm^2$ (preferred value for best results) and $i_C = .054 A/cm^2$ the relation becomes $S_A = 5.38\ S_c$. This immediately determines the ideal minimum size of the nickel metal anode.

For our case, in the range of different diameters of fibers and up to 20 cm long samples, the anode is immersed 3-4 cm. and the plating current is set to 6 ma.

By setting the temperature at $60° \pm 2°C$, the ph at 4.5, I_p = 6ma and lightly agitating, best results are attained.

A.4 Conclusions

The technique thus far described has proven to be a reliable method of contacting boron fibers. It is also an easy and economic way of depositing uniform sheets of nickel on the boron fibers. Further, controlled

thickness and amount of plating area make it convenient to measure v-i characteristics and verify current flowing predictions on the basis of the sample's geometry.

APPENDIX B

FURNACE AND VACUUM SYSTEM

Boron fibers were heat treated in the high temperature Lindberg furnace shown in Figure B.1 (arrow B). The furnace tube has a two inches diameter. The temperature range is 500° - 1600°C. The quartz tube was evacuated by means of the mercury diffusion pump (arrow A in Figure B.1). The pressure of the diffusion pump was as low as 7×10^{-6} torr. The initial vacuum was attained by means of a mechanical pump in series with the diffusion pump. Pressures were measured by means of two thermocouple gauges and an ion gauge. The entire system is as shown in Figure B.1.

The samples were slid inside the evacuated chamber when the furnace had attained the desired temperature. A quartz boat was used, and because of vitrification of quartz above 1200°C, this was the maximum operating temperature of the system.

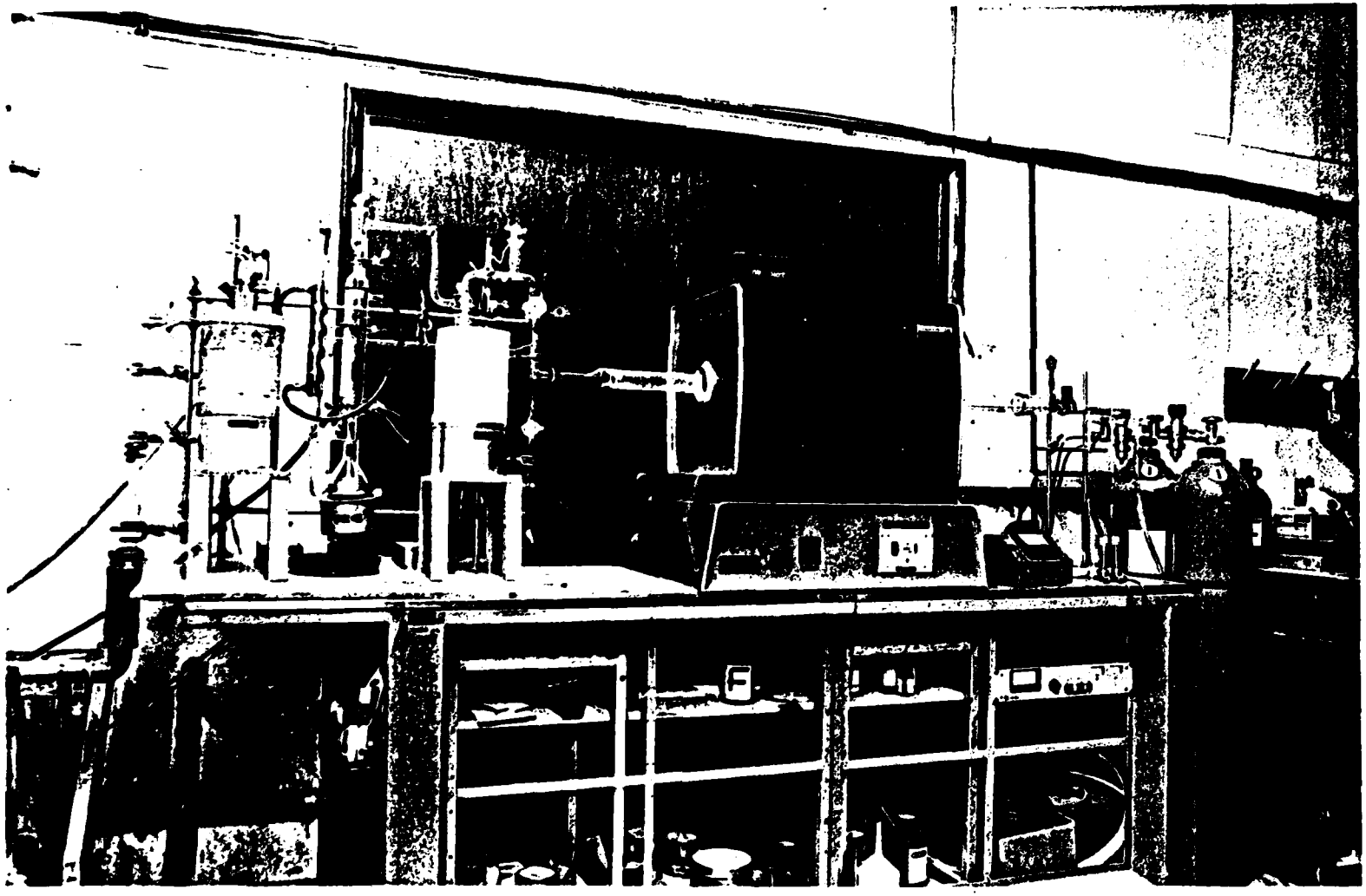

Fig. 8.1.1 - Vacuum System and Diffusion Furnace

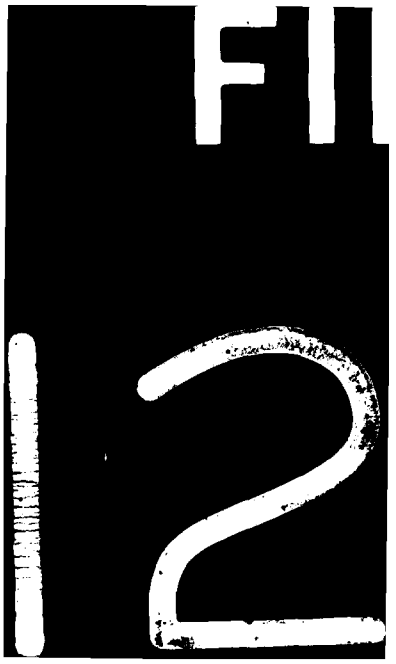
FI
12